Proceedings of

EUROMECH Colloquium 512

Small Scale Turbulence and Related Gradient Statistics

Torino, October 26-29, 2009

Edited by
DANIELA TORDELLA
KATEPALLI R. SREENIVASAN

ACCADEMIA DELLE SCIENZE DI TORINO
2009

This volume is dedicated to the memory of
Robert Kraichnan and Akiva Yaglom

«Atti della Accademia delle Scienze di Torino. Classe di Scienze Fisiche, Matematiche e Naturali», Supplement 2009 − Vol. 142, 2008.

CONTENTS

Foreword

Turbulent flows are known to contain a wide range of scales, with different physics operating in different sub-ranges. For instance, the energy dissipation takes place at small-scales. Yet, the process is linked to the large scales of the system, which carry most of the energy. A general interest clearly exists in the problems just mentioned if only because turbulence is a paradigm for the behaviour of systems with many degrees of freedom. In comparison with other problems of condensed matter and complexity, turbulence is a relatively clean system whose lessons, if based on solid foundation, can be of greater value.

The basis for expecting the near-universal behaviour of small scales is Kolmogorov's theory (1941 and 1962). Nowadays, the gaps in this theory are becoming increasingly certain. To establish possible consensus of the new and post-Kolmogorov ideas, this Euromech Colloquium was organized, to deal primarily with the non-universality of the small scale dynamics.

Given the emphasis on similar topics in geophysics, stellar physics, MHD and plasma dynamics, perhaps even in cosmology, we think that the contents of the Colloquium can be of interest to a number of communities. The question of whether a universal state exists independent of the forcing, or of the aspects in which the latter effects continue to be felt, is the core of research in several of these areas. The advances made in turbulence proper in these directions are significant enough to be able to take stock of the situation with some clarity.

The readership of these Proceedings is expected to be interdisciplinary between physics (general physics, mathematics and statistics, earth and atmospheric sciences, astrophysics, plasma physics), and engineering (fluid dynamics, aerodynamics, environmental engineering, chemical engineering).

September 2009

Torino — Daniela Tordella
Trieste — Katepalli Raju Sreenivasan

PAPERS

The papers have been arranged
in alphabetical order according to the presenters

Dissipation element analysis of scalar fields in wall-bounded turbulent flow

FETTAH ALDUDAK*, MARTIN OBERLACK**

Abstract. *In order to analyze the geometry of turbulent structures in turbulent channel flow, the scalar field obtained by Direct Numerical Simulations (DNS) is subdivided into numerous finite size regions. In each of these regions local extremal points of the fluctuating scalar are determined via gradient trajectory method. Gradient trajectories starting from every material point in the scalar field $\phi(x,y,z,t)$ in the directions of ascending and descending scalar gradients will always reach a minimum and a maximum point where $\nabla\phi = 0$. The ensemble of all material points belonging to the same pair of extremal points defines a dissipation element [2]. They can be characterized statistically by two parameters: namely the linear length connecting the minimum and maximum points and the absolute value of the scalar difference $\Delta\phi$ at these points, respectively. Because material points are space-filling, dissipation elements are also space-filling and unique, which means that the turbulent scalar field can be decomposed into such elements. This allows the reconstruction of certain statistical quantities of small scale turbulence. Here special focus will be given to examine if and how critical points and accordingly dissipation elements are in relationship with the characteristic layers of a turbulent channel flow.*

Keywords: small scale turbulence, dissipation elements.

The analysis is based on 3D direct numerical simulations of a turbulent channel flow at $Re_\tau = 180$ and $Re_\tau = 360$ where $Re_\tau = \frac{hu_\tau}{\nu}$ is the friction based Reynolds number. The code for the DNS was developed at KTH, Stockholm (for details see [1]) using a spectral method to solve the time-dependent incompressible Navier-Stokes equations with Fourier decomposition in the streamwise (x) and spanwise (z) directions and Chebychev decomposition in the wall-normal (y) direction. All quantities are non-dimensionalized by the centerline velocity of the flow field u_{CL} and the channel half-height h. Periodic boundary conditions are employed in the horizontal streamwise and the spanwise direction. At the walls, where $y = \pm 1$, no-slip boundary conditions are used. The

*Chair of Fluid Dynamics, Department of Mechanical Engineering, Darmstadt University of Technology, Petersenstr. 13, 64287 Darmstadt.

E-mail: aldudak@fdy.tu-darmstadt.de

**E-mail: oberlack@fdy.tu-darmstadt.de

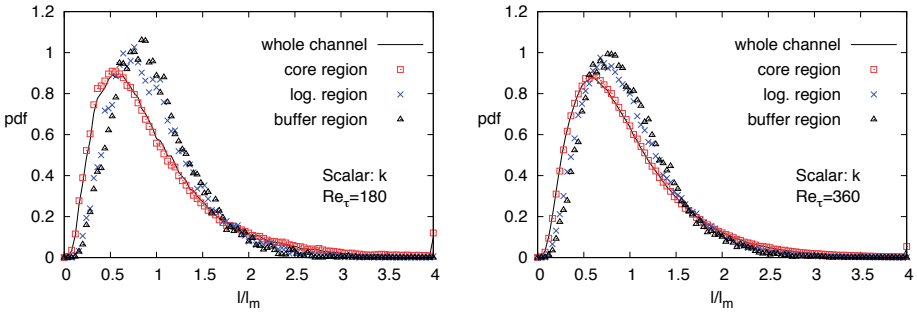

Figure 1: Normalized length scale distribution from 3D DNS.

simulation domain is $L_x \times L_y \times L_z = 2\pi \times 2 \times \pi$ in units of the channel half-height. Both simulations were performed with $512 \times 257 \times 256$ collocation points.

Figure 1 illustrates the marginal probability density function $P_l(l/l_m)$ normalized by the mean dissipation element length l_m for different wall-normal channel layers calculated from 3D DNS. To explore the wall-normal dependency of the pdf we examine its distribution in the classical buffer layer, logarithmic layer and the core region of the channel. It is seen that for the chosen scalar of kinetic energy k there exists a slight deviation between the shapes of the pdfs. We observed the same feature for the fluctuation of the u_1-velocity. The over-all pdf, however, shows no significant dependency on the Re number and the choice of the scalar field in our findings.

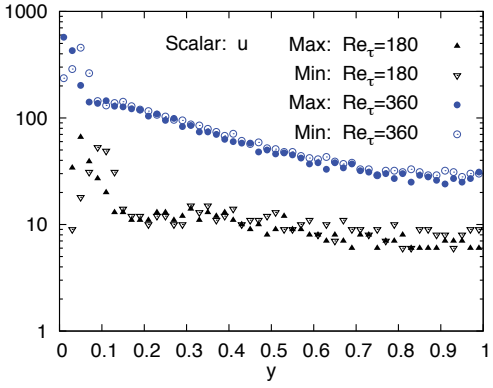

Figure 2: Distribution of extremal points along wall-normal direction.

As pointed out the length of the dissipation element is defined by the linear

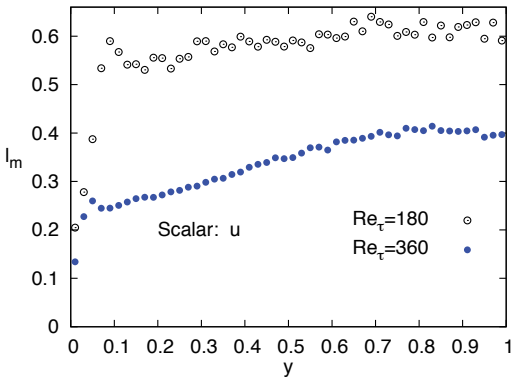

Figure 3: Mean length of dissipation elements along wall-normal direction.

connection of both minimal and maximal points, respectively. Thus, it is interesting to analyze the spatial distribution of the critical points. In figure 2 the number of minimal and maximal points is compared for the two different *Re* numbers as a function of wall-normal direction starting from the wall ($y = 0$) to the channel center ($y = 1$). The plots show that the numbers of minimal and maximal points are of the same order of magnitude. Maximal generation of extremal points appears to occur in the buffer layer. In the higher *Re* number case significantly more extremal points are generated. Beginning from around the logarithmic layer an exponential decay can be seen which extends into the middle of the channel core region. This behavior is more obvious for the higher turbulent case of $Re = 360$.

The mean linear length of the dissipation elements connecting the critical points is plotted in figure 3 against the wall-normal direction. The curves show a linear increase in the same interval where figure 2 exhibits exponential behavior. Apart from a very steep slope in the near-wall region the mean length of elements seems to grow uniformly in this interval until it reaches a constant stage in the middle of the channel. The mean element length is smaller for the high *Re* number. This finding is a consequence of the fact that in this case more critical points are generated. As a result the points have shorter distances to their neighboring points.

References

[1] LUNDBLADH, A., HENNINGSON, D., JOHANSSON, A., *An efficient spectral integration method for the solution of the Navier-Stokes equations*, *Tech. Rep.*, FFA-TN 1992-28, Aeronautical Research Institute of Sweden, Bromma.

[2] PETERS, N., WANG, L. *Dissipation element analysis of scalar fields in turbulence*, C. R. Mechanique, **334** (2006).

Analogy between small-scale velocity and passive scalar fields in a turbulent channel flow

ROBERT ANTHONY ANTONIA*, HIROYUKI ABE**

Abstract. *DNS databases for a turbulent channel flow with a passive scalar at a molecular Prandtl number of 0.71 are used to examine the limiting forms, at zero separation, of the transport equations for the turbulent kinetic energy and scalar variance structure functions. The results support the notion that the limits are identical over a significant portion of the outer region when the Reynolds number is sufficiently large and the normalization is based on Kolmogorov and Batchelor scales.*

Keywords: Velocity and scalar derivatives, Turbulent channel flow.

Recently, the present authors [1,2] examined various properties of small-scale velocity and scalar fields using DNS databases for a fully developed turbulent channel flow at several values of the Karman number h^+ (h is the halfwidth of the channel) with passive scalar transport – the time-averaged heat flux is constant at each wall and the molecular Prandtl number Pr is 0.71. In particular, attention was given to the question of how best to compare properties associated with the two fields. Earlier work, e.g. [3], suggested that an appropriate framework for comparison should be based on the turbulent kinetic energy q^2 and the scalar variance θ^2 , at least when the turbulence is non-decaying. This idea was adopted [4] when comparing results from Kolmogorov's [5] equation for the second-order velocity structure function with those of Yaglom's [6] equation for the second-order scalar structure function. Indeed, it was confirmed in [2] that there is close agreement between spectra corresponding to q^2 and θ^2 in both inner and outer regions of the flow. This agreement extends, with slightly impaired quality, to spectra which correspond to the enstrophy and scalar dissipation rates.

In the present work, we focus on the limiting forms, at zero separation, of the equations, for stationary turbulence, by Kolmogorov and Yaglom, viz.

$$\overline{u_{1,1}^3} = -2\nu\overline{u_{1,11}^2} \tag{1}$$

$$\overline{u_{1,1}\theta_{,1}^2} = -\frac{2}{3}\kappa\overline{\theta_{,11}^2} \tag{2}$$

as well as the generalized form of (1), as given in [4], viz.

*Discipline of Mechanical Engineering, University of Newcastle, NSW 2308, Australia.
E-mail: robert.antonia@newcastle.edu.au
**Japan Aerospace Exploration Agency, Tokyo 182-8522, Japan
E-mail: habe@chofu.jaxa.jp

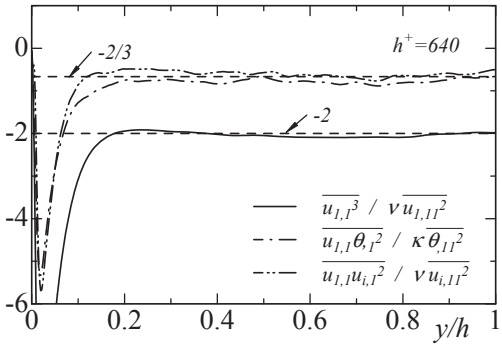

Figure 1: Distributions of the ratios $\overline{u_{1,1}^3}/\nu\overline{u_{1,11}^2}$, $\overline{u_{1,1}\theta_{,1}^2}/\kappa\overline{\theta_{,11}^2}$ and $\overline{u_{1,1}u_{i,1}^2}/\nu\overline{u_{i,11}^2}$ at $h^+ = 640$ normalized by the Kolmogorov and Batchelor scales. Note that the latter two ratios are obtained from one instantaneous realization.

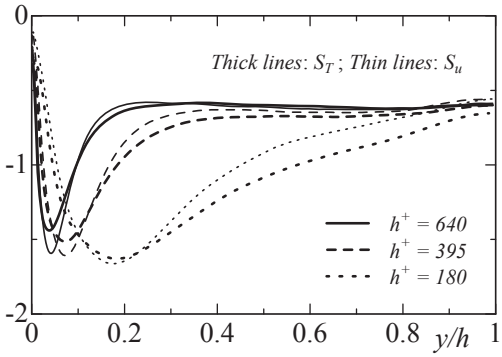

Figure 2: Distributions of S_u and S_T at $h^+ = 180$, 395 and 640.

$$\overline{u_{1,1}u_{i,1}^2} = -\frac{2}{3}\nu\overline{u_{i,11}^2}. \tag{3}$$

Results for (1)–(3), normalized by Kolmogorov and Batchelor scales, are plotted in Fig. 1 for $h^+ = 640$. In the outer region, (1)–(3) are closely satisfied, reflecting the adequacy of local isotropy, while (2) and (3) are essentially identical.

The derivative skewnesses S_u and S_T defined as

$$S_u = \frac{\overline{u_{1,1}^3}}{\left(\overline{u_{1,1}^2}\right)^{3/2}} \tag{4}$$

and

$$S_T = \frac{\overline{u_{1,1}\theta_{,1}^2}}{\left(\overline{u_{1,1}^2}\right)^{1/2}\left(\overline{\theta_{,1}^2}\right)} \tag{5}$$

have attracted special attention since they are closely associated with the production terms in the transport equations of the enstrophy and scalar dissipation rates. Distributions of S_T and S_u are shown in Fig. 2 for $h^+ = 180$, 395 and 640. The two quantities are close to each other over the outer region of the channel at $h^+ = 640$ and in reasonable agreement with values obtained for box turbulence (see [7] and [8] and references therein). This seems consistent with the data of [1] which indicated that the morphology associated with the enstrophy (i.e. tubes) and scalar dissipation rate (i.e. sheets convected by a quasi-uniform random straining field, as considered by Batchelor [9] and Kraichnan [10]) is similar for the outer region of the channel and box turbulence. The relationship between S_T and $S_q \left(= \overline{u_{1,1} u_{i,1}^2} / \left(\overline{u_{1,1}^2} \right)^{3/2} \right)$, which can be inferred from the spectral similarity between q^2 and θ^2, will be discussed at the meeting.

References

[1] ABE H., ANTONIA R.A. AND KAWAMURA H., *Correlation between small-scale velocity and scalar fluctuations in a turbulent channel flow*, J. Fluid Mech. **627** (2009), 1-32.

[2] ANTONIA R.A., ABE H. AND KAWAMURA H., *Analogy between velocity and scalar fields in a turbulent channel flow*, J. Fluid Mech. **628** (2009), 241-268.

[3] FULACHIER L. AND ANTONIA R.A., *Spectral analogy between temperature and velocity fluctuations in several turbulent flows*, Int. J. Heat Mass Transfer **27** (1984), 987-997.

[4] ANTONIA R.A., OULD-ROUIS M., ANSELMET F. AND ZHU Y., *Analogy between predictions of Kolmogorov and Yaglom*, J. Fluid Mech. **332** (1997), 395-409.

[5] KOLMOGOROV A.N. *Dissipation of energy in the locally isotropic turbulence*, Doklady Akad. Nauk SSSR **32** (1941), 19-21.

[6] YAGLOM A.M., *On the local structure of a temperature field in a turbulent flow*, Doklady Akad. Nauk SSSR **69** (1949), 743-746.

[7] SREENIVASAN K.R. AND ANTONIA R.A., *The phenomenology of small-scale turbulence*, Annu. Rev. Fluid Mech. **29** (1997), 435-472.

[8] ANTONIA R.A. AND ORLANDI P., *Effect of Schmidt number on small-scale passive scalar turbulence*, Appl. Mech. Rev. **56** (2003), 615-632.

[9] BATCHELOR G.K., *Small-scale variation of convected quantities like temperature in turbulent fluid Part 1. General discussion and the case of small conductivity*, J. Fluid Mech. **5** (1959), 113-133.

[10] KRAICHNAN R.H., *Convection of a passive scalar by a quasi-uniform random straining field*, J. Fluid Mech. **64** (1974), 737-762.

The Stokes-Ekman layer

STEFANO SALON*, VINCENZO ARMENIO**

Abstract. *A numerical study of an oscillating boundary layer, subjected to rotation at three different latitudes, is here presented. The direct numerical simulation of the laminar problem and the differences in the wall shear stress among the different cases, obtained by large-eddy simulations, are discussed.*

Keywords: Stokes boundary layer, rotation.

The Stokes-Ekman layer is an oscillatory boundary layer subjected to rotation of the frame of reference. The study of the turbulent mixing in a Stokes-Ekman layer has important implications in oceanography since the combined effect of a bottom Ekman layer forced by an oscillating current represents the prototype of a tidal bottom boundary layer ([1, 2, 3]). In the present contribute, we introduce the problem from the physical and the numerical point of view and comment some preliminary results as derived from a series of *resolved* LES (i.e. the near-wall layer is directly resolved without the use of wall functions). This work constitutes the third part of a research aimed at understand the characteristics of the oscillating boundary layers in turbulent regime without and with rotation (for details see [4] and [5]).

The boundary layer under investigation is driven by a harmonic pressure gradient aligned with the x-direction in a rotating frame of reference, that has the x-axis oriented eastward, the y-axis northward and the z-axis upward. The free-stream velocity (u) has a sinusoidal behaviour, and due to the rotation, an oscillating transverse velocity (v) develops in the flow. Two non-dimensional numbers are related to this problem:

- the Reynolds number associated to the Stokes flow, $Re_S = \frac{U_0 \delta_S}{\nu}$, where U_0 is the maximum amplitude of the outer layer velocity and $\delta_S = \sqrt{2\nu/\omega}$ is the thickness of the Stokes boundary layer, with ν the kinematic viscosity of the fluid and ω the angular frequency of the oscillations;
- the Rossby number, defined as the ratio between inertial and Coriolis forces, $Ro = \frac{U_0}{Lf}$, where $L = U_0/\omega$ is the length scale associated to the amplitude of the oscillatory motion and f is the Coriolis parameter.

*Dipartimento OGA, Istituto Nazionale di Oceanografia e di Geofisica Sperimentale - OGS, B.go Grotta Gigante 42/c, 34010 Sgonico, Italy.
E-mail: ssalon@ogs.trieste.it

**Dipartimento di Ingegneria Civile ed Ambientale, Università di Trieste, Piazzale Europa 1, 34127 Trieste, Italy.
E-mail: ARMENIO@dica.units.it

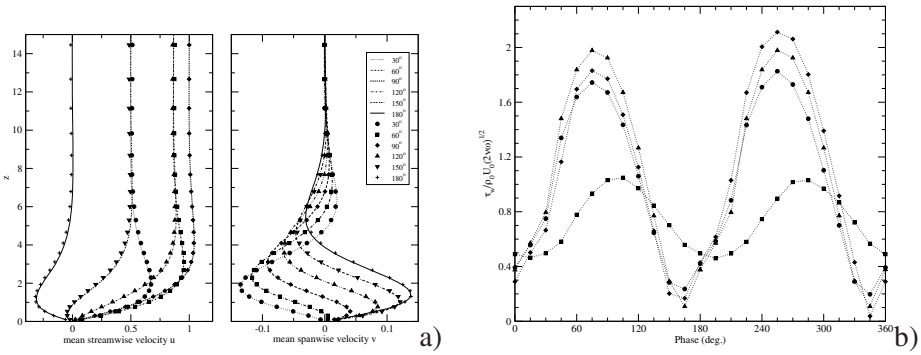

Figure 1: a) Comparison between the vertical profiles of the mean streamwise and spanwise velocity of the laminar Stokes-Ekman layer as obtained from the analytical solution (lines) and the DNS (symbols); see inlet for details of the phases' degrees. b) Non-dimensional ensemble-averaged wall shear stress for the three latitude cases at 15^o interval: ML (solid line); PL (dashed line); QE (dash-dotted line). As a reference, the same quantity evaluated in the purely oscillating case (OF) is shown.

From [4], we chose $Re_S = 1790$ and, considering a tidal current driving the boundary layer with a M2-semidiurnal tidal frequency, we obtain for three significant latitudes ϕ the following values for Ro: 1) polar case (PL, $\phi = 90^o$), $Ro = 0.96$; 2) mid-latitude case (ML, $\phi = 45^o$), $Ro = 1.36$; 3) quasi-equatorial case (QE, $\phi = 5^o$), $Ro = 11.04$. The governing equations, that include the full-component Coriolis acceleration, are solved by means of the *resolved* LES approach, with the subgrid model formulated according to [6] (see also [4]). Free-slip and no-slip boundary conditions are imposed respectively at the top and bottom boundary, while in the horizontal directions, periodic boundary conditions are taken due to homogeneous turbulence in the streamwise and spanwise directions. As initial condition for the three cases we use a turbulent field previously developed for the set of simulations performed in [5]. A domain grid of $96 \times 96 \times 320$ points respectively in the streamwise, spanwise and vertical direction is adopted.

As a first step, we validate our numerical approach by simulating the laminar flow of the Stokes-Ekman layer via DNS (i.e. our LES with the subgrid model switched off), comparing the results obtained with the analytical solution (A. Scotti, personal communication; [1, 3]). In this case, we adopt the f-plane approximation and the governing equations provide the vertical dependence of the horizontal velocity components of the flow (u and v) throughout the cycle of oscillation. The boundary conditions are no-slip at $z = 0$ and no-stress at $z \to \infty$. As shown in Fig.1a, the DNS correctly reproduces the analytical solution.

The second step is the analysis of the LES outputs: Fig.1b shows the non-dimensional ensemble-averaged temporal evolution of the wall shear stress τ_W obtained in simulations ML, PL and QE together with the simulation of the purely oscillating flow (OF, see [4]). The evolution of τ_W along the cycle of oscillation is rather similar among the two non-polar cases and the OF one, while the PL case shows more differences, both in the shape and in magnitude. As widely discussed in [4] for OF, for the value of Re_S here investigated the onset of the turbulent activity is observed in ML and QE cases between 30^o (210^o in the second semi-cycle) and 45^o (225^o), when the behaviour of τ_W rapidly increases from the sinusoidal shape that characterizes the phases between 340^o (160^o) and 30^o (210^o). This is related to the transition to turbulence and the rapid increase of the turbulent kinetic energy (not shown) that is similar to what observed for the non-rotating case. The τ_w in the PL case still presents the sinusoidal shape before the transition to turbulence, but this process starts later than 45^o (225^o) and the maximum value of is found at 90^o (270^o), later and almost halved than that observed in the non-polar and OF cases. A difference in the maximum values of τ_W between the two semi-cycles of oscillation can be seen in the rotating cases, conversely to what observed for OF, and increases towards the equator. Such a difference is an indicator of the asymmetry between the two semi-cycles due to the rotation, as already described in [5], and is related with the increasing value of the horizontal component of the background rotation. The same asymmetry was observed in the DNS study of [7], who related it to the "east/west enhancement/reduction trend" in the turbulence activity. This aspect becomes even more evident in the QE case, in agreement with [7] who noticed as the DNS at $\phi = 10^o$ easterly forced (and corresponding to our second semi-cycle) was the most turbulent case. The non-zero asymmetry observed in the PL case seems to be peculiar of the turbulent oscillatory flow.

References

[1] PRANDLE D., *The vertical structure of tidal currents and other oscillatory flows*, Cont. Shelf Res. **1** (1982), 191-207.

[2] SOULSBY R.L., *The bottom boundary layer of shelf seas*, in Physical Oceanography of Coastal and Shelf Seas, edited by B. Johns, pp. 189-266, Elsevier, Amsterdam (1983).

[3] MAAS L.R.M. AND VAN HAREN J.J.M., *Observations on the vertical structure of tidal and inertial currents in the central North Sea*, J. Mar. Res. **45** (1987), 293-318.

[4] SALON S., ARMENIO V. AND CRISE A. *A numerical investigation of the Stokes boundary layer in the turbulent regime*, J. Fluid Mech. **570** (2007), 253-296.

[5] SALON S., ARMENIO V. AND CRISE A. *A numerical (LES) investigation of a shallow water, mid-latitude, tidally-driven boundary layer*, Env. Fluid Mech. (2009) doi:10.1007/s10652-009-9122-y.

[6] ARMENIO V. AND PIOMELLI U. *A Lagrangian mixed subgrid-scale model in generalized coordinates*, Flow Turb. and Comb. **65** (2000), 51-81.

[7] COLEMAN G.N., FERZIGER J.H. AND SPALART P.R. *A numerical study of the turbulent Ekman layer*, J. Fluid Mech. **213** (1990), 313-348.

Statistical properties of small scale turbulent flows in the dissipation range

ROBERTO BENZI*

Abstract. *Using high resolution numerical simulations and recent experimental data for lagrangian turbulence, we discuss the statistical properties of homogenous and isotropic turbulence in the dissipation range. We compare our results against predictions based on the multifractal theory, which seems to capture the basic mechanism in the dissipation range.*

Keywords : small scale turbulence, dissipation range.

The aim of this paper is to discuss some recent numerical, experimental and experimental results on the statistical properties of turbulent fluctuations in the dissipative range. We deal with the case of homogenous and isotropic turbulence. It is known that, for large Reynolds number $Re \equiv UL/\nu$ (where U is some characteristic velocity at large scale L and ν is the kinematic viscosity of the flow), the statistical properties of turbulent flows show anomalous scaling.

The existence of anomalous scaling in the inertial range is usually referred to as the intermittency problem of fully developed turbulence. There are two main point of view on the intermittency problem and both views require a breaking of scale invariance of the statistical properties of turbulence. The first view is the multifractal theory [1]. The multifractal approach to turbulence is based on the assumption that the statistical properties of turbulent flows do exhibit scaling properties even if there is intermittency. In the multifractal theory, all the correlation functions should be computed by averaging over the propability $P_h(r) = r^{F(h)}$ leading to $S_p(r) \equiv \langle [\delta v(r)]^p \rangle \sim r^{\zeta_p}$, where $\zeta_p = inf_h[ph + F(h)]$ and $\delta v(r) = (u_i(\vec{x}+\vec{r}) - u_i(\vec{x})r_i/r)$.

The second view on intermittency disregards the existence of a scaling properties (if any) in the inertial range and it considers the existence of coherent structures as the main object one needs to study in order to understand the origin and the physical meaning of strong fluctuations in the small scale turbulent velocity field. Some properties of these coherent structures have been discussed in details in careful designed laboratory experiments and in numerical simulations.

It is difficult to imagine two approaches to the same problem as different as the one previously described and, indeed, there has been and still there are a number of discussions where the two views of the problem provide different re-

*Dip. di Fisica, Univ. di Roma "Tor Vergata", via della Ricerca Scientifica 1, 00133, Roma, Italy.
E-mail : roberto.benzi@roma2.infn.it

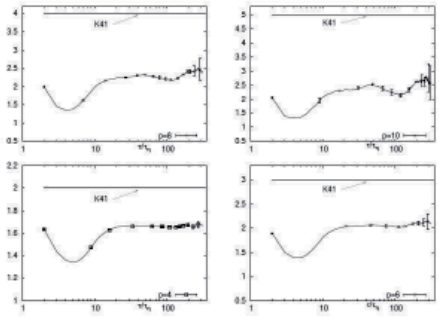

FIG. 1 – Lagrangian local scaling exponents $\kappa(p,\tau)$ for $p = 4,6,,8,10$.

sults and explanations. One particular case, on which we focus our discussion, is related to the turbulent fluctuations in the dissipation range.

To study turbulent fluctuations in the dissipation range we need to measure velocity difference at scale equal or smaller than the Kolmogorov scale $\eta \equiv (\nu/\varepsilon^3)^{1/4}$. Recently, it has been observed that the statistical properties of a lagrangian particle sampled at relatively short times can provide direct informations on the dissipation range. This observation is crucial as soon as one realized that both experimentally and numerically it is very efficient to work with high frequency sampling of lagrangian trajectories with respect to any eulerian measurements [3, 4, 5, 6, 7, 8, 9] (see also [10] for a recent review). Neutrally buoyant particles, advected by a turbulent velocity field $\mathbf{u}(\mathbf{x},\mathbf{t})$, follow the same path of fluid molecules and evolve according to the dynamics $\dot{\mathbf{X}}(t) = \mathbf{v}(\mathbf{t}) \equiv \mathbf{u}(\mathbf{X}(\mathbf{t}),\mathbf{t})$, where the Lagrangian velocity $\mathbf{v}$ equals the Eulerian one $\mathbf{u}$ computed at the particle position $\mathbf{X}$. Such particles constitute a clear-cut indicator of the underlying turbulent fluctuations. Recently, it has been shown, by comparing the different numerical studies and different experimental results [11, 12], that Lagrangian turbulence is universal, intermittent, and well described by a suitable generalization of the Eulerian Multifractal formalism to the Lagrangian domain [13, 14, 15].

Lagrangian Structure Functions (LSF) are defined as :

$$\mathcal{S}_i^{(p)}(\tau) = \langle [v_i(t+\tau) - v_i(t)]^p \rangle = \langle (\delta_\tau v_i)^p \rangle, \tag{1}$$

where $i = x,y,z$ runs over the three velocity components, and the average is defined over the ensemble of particle trajectories evolving in the flow. From now on, we will assume isotropy and therefore drop the dependency from the spatial direction i. The presence of long spatial and temporal correlations suggests, in analogy with critical phenomena, the existence of scaling laws for time scales larger than the dissipative Kolmogorov time and smaller than the

typical large-scale time, $\tau_\eta \ll \tau \ll T_L$:

$$\mathcal{S}^{(p)}(\tau) \sim \tau^{z(p)}. \tag{2}$$

Straightforward dimensional arguments *à la* Kolmogorov predict $z(p) = p/2$, independently of the flow properties. However, it is known that LSF experience strong variations at changing the time lags τ, as highlighted by the more and more non-Gaussian tails characterizing the probability density functions of $\delta_\tau v$ for smaller and smaller τ's [3], leading to a breakdown of the dimensional argument and in the corresponding growth of the Lagrangian flatness by going to higher and higher frequencies. In [11, 12] it has been shown that, at least concerning the scaling exponent, $\kappa(4) = z(4)/z(2)$, entering in the evolution of the fourth order flatness :

$$\frac{\mathcal{S}^{(4)}(\tau)}{(\mathcal{S}^{(2)}(\tau))^2} \sim (\mathcal{S}^{(2)}(\tau))^{\kappa(4)-2} \tag{3}$$

the results do not depend on the experimental or numerical large scale set-up, i.e. the high frequency fluctuations are universal.

It is possible to get a link between Eulerian and Lagrangian MF formalism via the dimensional relation :

$$\tau \sim r/\delta_r u. \tag{4}$$

The validity of (4) is an important result in favor of the multifractal theory of turbulence, since it is based upon the assumption of scaling in the inertial range. In figure (1) we show the local slopes

$$\kappa(p,\tau) \equiv \frac{d\ log(\mathcal{S}^{(p)}(\tau)}{d\ log(\mathcal{S}^{(p)}(\tau))} \tag{5}$$

for $p = 4, 6, 8, 10$ as obtained by a recent high resolution numerical simulation performed at large *Re* and with about 10^6 lagrangian particles. Note that each lines has been shown with the corresponding error bars. Two important points can be highlight by looking at figure (1). The first non trivial point is that *anomalous scaling is observed*. The computation of the error bars rules out any K41 theory. Moreover the anomalous scaling is consistent with the anomalous scaling in the eulerian framework, i.e. with equation (4). This is again a crucial statement on the intermittency problem. The second non trivial point is the "dip" observed at relatively small τ close to the Kolmogorov time τ_η. The dip is increasing with increasing the order p of the local slope $\kappa(p,\tau)$. The crucial point about the dip is that a careful analysis shows that the dip is indeed due to the particle trapping in the coherent structures of the flows [7].

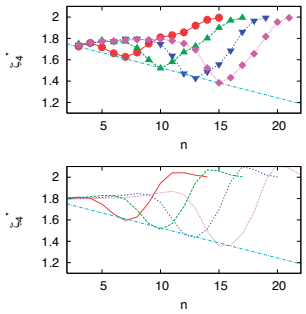

FIG. 2 – Top : local scaling exponents for fourth order structure functions, $\kappa(4,k_n)$, in the Shell Model, versus $log_2(k_n)$. Bottom MF prediction ; the straight line is a fit for the behaviour of the bottleneck (maximum of intermittency), the slope of the line is -0.028.

Thus the results of figure (1) show that coherent structures strike back again no matter how good is the scaling observed in the inertial range ! Recently [11] the existence of the dip in the lagrangian local slopes $\kappa(p,\tau)$ has been explained by means of a suitable generalization of the multifractal theory. The basic idea is that the dissipation scale η (in the eulerian framework) is a fluctuating quantity which is related to the velocity difference via the relation

$$\frac{\delta v(\eta)\eta}{\nu} \sim 1 \tag{6}$$

A similar expression is also valid in the lagrangian framework. Eq. (6) implies that $\eta = \eta(h)$, i.e. the dissipation scale depends on the local exponents h which leads to a complex and high non trivial behavior of the structure functions in the dissipation range. This argument, however, does not give us the information on whether the coherent structures are the causes or the effect of the anomalous scaling or, following [2] whether they are the "dog" or the "tail" in turbulence.

One possible way to answer this question is by using a completely different approach based on the "shell models". In the last twenty years, it has been shown that there exists a class of simplified models, named shell model, which shows multifractal intermittency (anomalous scaling) similar qualitatively and quantitatively to what it is observed in the Navier-Stokes equation. Among many different shell models, we shall consider the shell model proposed in [16] (see also [17] for a review). Shell models of turbulence, can be seen as a truncated description of the Navier-Stokes dynamics, preserving some of the structure and conservation laws of the original equations but *destroying* all spatial structures. In figure (2) we plot the local scaling exponents

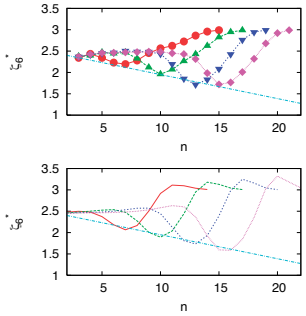

FIG. 3 – Same as in figure (2) for the sixth order scaling exponents $\kappa(6,k_n)$. The straight line has the slope -0.056

$$\kappa(4,k_n) \equiv \frac{d\ log(S_4(k_n)}{d\ log(S_2(k_n))}.$$

computed from the numerical simulations of the shell model (upper panel) and predicted by the multifractal theory using the idea of a fluctuating dissipation scale (lower panel). Different colors refer to different Reynolds numbers. The first striking result is that the numerical simulations of the model clearly show a well defined dip in the dissipative region (i.e. large value of n in the figure), similar to what it is observed in experiments and in the numerical simulations. The dip is increasing towards small scales as the Reynolds number increases and it deepens. The straight line in the figure is a qualitative fit on the behavior of the dip as a function of Re. Clearly, the increase of intermittency in the dissipative region is scaling as $log(Re)$. Notice that this scaling behaviour was not visible in the experimental and numerical data shown in [11, 12] because of the limited range of Reynolds spanned in those cases.

From the above analysis we can draw some interesting conclusions. First of all, the increase of intermittency in the dissipative range is not due to coherent vortices (there are no vortices in the shell model). Moreover, the increase of intermittency is predicted by the multifractal conjecture because of the fluctuations of the dissipative scale. Translating back these results to the real Navier-Stokes equation, we are tempted to conclude that coherent structures exists but their dynamics is nor relevant to explain intermittency in turbulent flows. They are the tail more than the dog. Actually, one can take the opposite point of view : the matching between inertial range (scale invariance) intermittency and the dissipation range produces an increase in fluctuations and, consequently, an increase of vorticity. This effect is dominant at low Reynolds number, as it is clearly observed in the shell model : i.e. at low Reynold numbers no scaling behavior is observed and intermittency is strongly dominated by the fluctuations in the dissipation range. Let us also point out that our observations is in

qualitative agreement to the known phenomenology of boundary layer turbulence. Near the wall, the local Reynolds number is relatively low and strong intermittency is observed together with a rich dynamic behavior of coherent structures (hairpin vortices). The full dynamics is dominated by strong intermittent fluctuations and it is tempting to relate our previous discussion to this specific well known turbulent flows.

References

[1] PARISI, G. and FRISCH, U. in *Turbulence and Predictability in Geophysical Fluid Dynamics*, Proceed. Intern. School. of Physics "E. Fermi", eds. GHIL, M., BENZI, R., PARISI, G. 84–87. (1985).

[2] FRISCH, U. , *Turbulence : the legacy of A.N. Kolmogorov* (Cambridge University Press, Cambridge UK, 1995).

[3] MORDANT, N. , METZ, P. , MICHEL, O. and PINTON, J.-F. , Phys. Rev. Lett. **87**, 214501 (2001).

[4] BERG, J. et al., Phys. Rev. E **74**, 016304 (2006).

[5] XU, H. et al., Phys. Rev. Lett. **96**, 024503 (2006).

[6] HOMANN, H. et al. J. Plasma Physics **73**, 821 (2007).

[7] BIFERALE, L. et al., Phys. Fluids **17**, 021701 (2005).

[8] YEUNG, P.K. , POPE, S.B. and SAWFORD, B.L. , J. Turb. **7** (58), 1 (2006).

[9] FISHER, R. et al., IBM Journ. Res. Devel. **52** Num. (1/2), (2008). See also Benzi, R., Biferale, L., Fisher, R., Kadanoff, L., Lamb, D. and Toschi, F. Phys. Rev. Lett. 100, 234503, (2008)

[10] TOSCHI, F. and BODENSCHATZ, E., Ann. Rev. Fluid Mech. (to appear in 2009).

[11] ICTR Coll. ; ARNEODO, A. et al., Phys. Rev. Lett. **100**, 254504 (2008).

[12] BIFERALE, L., BODENSCHATZ, E. , CENCINI, M. , LANOTTE, A., OUELLETTE, N., TOSCHI, F. and XU, H., Phys. Fluids **20**, 065103 (2008).

[13] M.S. Borgas, Phil. Trans. R. Soc. London A **342**, 379 (1993).

[14] G. Boffetta, F. De Lillo and S. Musacchio, Phys. Rev. E **66**, 066307 (2002).

[15] L. Chevillard et al., Phys. Rev. Lett. **91**, 214502 (2003).

[16] L'VOV, V., PODIVILOV, E.,POMYALOV, A., PROCACCIA, I. and VANDEMBROUCQ, D., Phys. Rev. E **58** 1811 (1998).

[17] BIFERALE, L., Ann. Rev. Fluid Mech. **35**, 441, (2003).

Scale dependence of coarse-grained velocity gradients in turbulence

HAITAO XU*, ALAIN PUMIR**, EBERHARD BODENSCHATZ***

Abstract. *We report here experimental results of coarse-grained velocity gradients from Lagrangian particle tracking measurements in fully developed turbulence. The coarse-grained velocity gradients are obtained from the tetrad model proposed by Chertkov et al. (Phys. Fluids, 11:2394, 1999). We investigated the scale dependence of the coarse-grained velocity gradient by varying the size of the tetrads. We observed more "flattening" in the inertial range while the coarse-grained velocity gradients approach Gaussian at large scales.*

Keywords: velocity gradient, coarse-graining, inertial range, scale dependence

1. Introduction

Turbulence dynamics at different scales is the central part of the turbulence problem itself and is related to many practical applications such as turbulent dispersion and mixing. At scales below the Kolmogorov scale, progress has been achieved by studying the transport equations for the velocity gradient [2, 3]. The results are usually presented in terms of the two non-trivial invariants of the velocity gradient tensor: $R \equiv -(1/3)\mathbf{tr}(\mathbf{m}^3)$ and $Q \equiv -(1/2)\mathbf{tr}(\mathbf{m}^2)$, where $\mathbf{m}$ is the velocity gradient tensor. It has been shown that the turbulence velocity gradient preferentially distribute along the "Vieillefosse tail": $R > 0$, $Q = -(27R^2/4)^{1/3}$. At large scales, it is generally believed that the turbulence may be approximated as a random Gaussian field [4]. Chertkov *et al.* [1] proposed a phenomenological model to describe the coarse-grained velocity gradient $\mathbf{M}$ in the inertial range. In three-dimensional turbulence, the coarse-grained velocity gradients are obtained from the fluctuation velocities at 4 points in space – the so-called "tetrad model". Numerical [1, 5, 6] and experimental investigations [7, 8] demonstrated the merit of this model. In this work, we study the change of the coarse-grained velocity gradient with the size of the tetrads, i.e., the scale dependence.

*Max Planck Institute for Dynamics and Self-Organization, Göttingen, D-37077 Germany
E-mail: haitao.xu@ds.mpg.de
**Laboratoire de Physique de l'Ecole Normale Superieure de Lyon, 46, allee d'Italie, 69007, Lyon, France
E-mail: alain.pumir@ens-lyon.fr
***Max Planck Institute for Dynamics and Self-Organization, Göttingen, D-37077 Germany
E-mail: eberhard.bodenschatz@ds.mpg.de

2. Experiments

We measured the turbulence velocity by following, in three dimensions, neutrally buoyant tracer particles (with a specific density $\rho_p/\rho_w = 1.06$ and a diameter $d_p = 25\mu$m) in a von Kármán swirling water flow between counter-rotating disks. The high-speed Phantom v7.2 cameras that we used provide sub-τ_η temporal resolution. For details, see Refs. [9, 10].

To measure the coarse-grained velocity gradients, we conditioned our statistics on nearly isotropic tetrads by selecting tetrads whose edges are of length within $\pm 10\%$ of a nominal scale r_0. We then fit velocity gradients from the differences of fluctuation velocities using the tetrad model [1]. The incompressibility constraint is enforced at the fit. We normalize the invariants using the turbulence dynamical time scale corresponding to the length scale r_0: $R = (r_0^2/\varepsilon)R$ and $Q = (r_0^2/\varepsilon)^{2/3}Q$.

3. Results

Figure 1 shows the joint probability density distribution function (PDF) $P(R,Q)$ at different scales in the inertial range. It is clear that the PDFs are skewed toward the "Vieillefosse tail", which corresponding to the flattening by the turbulence. This is consistent with previous observations.

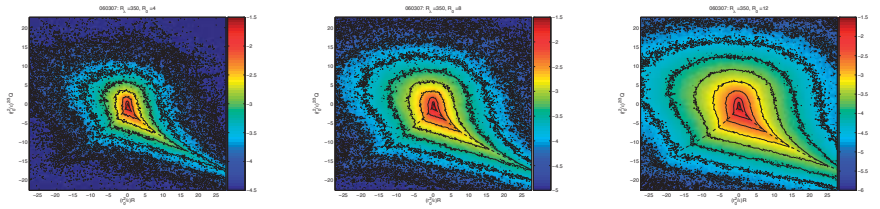

(a) (b) (c)

Figure 1: Result from $R_\lambda = 350$ experiment: the joint probability density function of the invariants of the coarse-grained velocity gradient $\mathbf{M}$: $R \equiv -(1/3)\mathbf{tr}(\mathbf{M}^3)$ and $Q \equiv -(1/2)\mathbf{tr}(\mathbf{M}^2)$ at different spatial scales. (a) $r_0 = 6$mm. (b) $r_0 = 8$mm. (c) $r_0 = 12$mm. The integral scale of the turbulence is $L \approx 70$mm.

Figure 2 shows the PDF of R conditioned on the sign of Q. It can be seen that depending on the sign of Q, the conditional PDFs skew to different directions. If the velocity gradient is Gaussian, then the conditional PDFs would be symmetrical. There is evidence of approaching Gaussian distribution as scale increases. Quantitatively, both the unconditional and conditional mean and

skewness of R approach zero as scale increase.

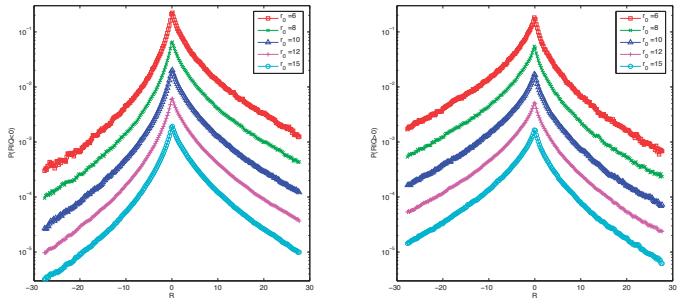

Figure 2: Conditional PDF of R. (a) $P(R|Q<0)$. (b) $P(R|Q>0)$.

Finally, we measured the eigenvalues (λ_1, λ_2, and λ_3, ordered as $\lambda_1 \geq \lambda_2 \geq \lambda_3$) of the symmetric part of the coarse-grained velocity gradients. Since $\lambda_1 + \lambda_2 + \lambda_3 = 0$, the sign and the value of the intermediate eigenvalue λ_2 are tightly related to the characteristics of turbulence. At scales larger than the integral scale, the velocities are uncorrelated and $\langle\lambda_2\rangle = 0$. In the dissipative range, it has been found empirically that $\langle\lambda_2\rangle/\langle\lambda_1\rangle \approx 0.15$ [11, 12, 13]. As shown in Figure 3, our measurements confirm the sign of λ_2 in the inertial range and show that the ratio $\langle\lambda_2\rangle/\langle\lambda_1\rangle$ increases continuously from nearly zero at large scales to values close to previous measurements in the viscous range.

4. Conclusions

We measured the coarse-grained velocity gradient in the inertial range of fully-developed turbulence using Lagrangian particle tracking. We observed more "flattening" in the inertial range while the coarse-grained velocity gradients approach Gaussian at large scales.

5. Acknowledgment

We are grateful to Boris Shraiman for many insightful discussions during this work.

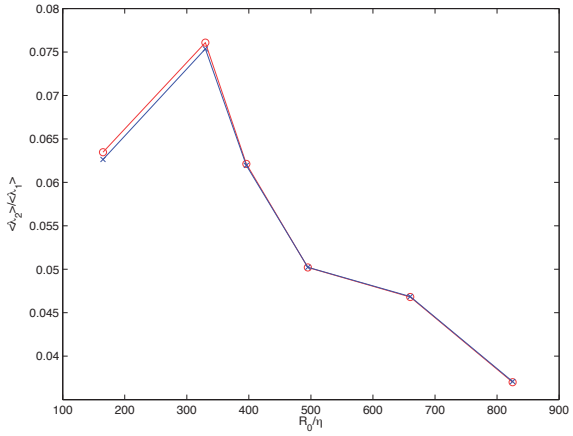

Figure 3: Result from $R_\lambda = 690$ experiment: The ratio of the eigenvalues $\langle\lambda_2\rangle/\langle\lambda_1\rangle$ of the coarse-grained velocity gradient as a function of scale. The scale separation of the inertial range is $L/\eta \approx 2300$ at this Reynolds number.

References

[1] CHERTKOV M., PUMIR A., AND SHRAIMAN B.I., *Lagrangian tetrad dynamics and the phenomenology of turbulence*, Phys. Fluids **11** (1999), 2394-2410.

[2] VIELLEFOSSE P., *Internal motion of a small element of fluid in an inviscid flow*, Physica A **125** (1984), 150-162.

[3] CANWELL B.J., *Exact solution of a restricted Euler equation for the velocity gradient tensor*, Phys. Fluids A **4** (1992), 782-793.

[4] FRISCH U., *Turbulence: The Legacy of A. N. Kolmogorov*, Cambridge University Press, England (1995).

[5] BIFERALE L., BOFFETTA G., CELANI A., DEVENISH B.J., LANOTTE A., AND TOSCHI F., *Multiparticle dispersion in fully developed turbulence*, Phys. Fluids **17** (2005) 111701.

[6] NASO A., CHERTKOV M., AND PUMIR A., *Scale dependence of the coarse-grained velocity derivative tensor: Influence of large-scale shear on small-scale turbulence*, J. Turbul. **7** (2006) 41.

[7] LÜTHI B., OTT S., BERG J., AND MANN J., *Lagrangian multi-particle statistics*, J. Turbul. **8** (2007) 45.

[8] XU H., OUELLETTE N.T., AND BODENSCHATZ E., *Evolution of geometric structures in intense turbulence*, New J. Phys. **10** (2008) 013012.

[9] BOURGOIN M., OUELLETTE N.T., XU H., BERG J., AND BODENSCHATZ E., *The role of pair dispersion in turbulent flow*, Science **311** (2006) 835-838.

[10] XU H., BOURGOIN M., OUELLETTE N.T., AND BODENSCHATZ E., *High order Lagrangian velocity statistics in turbulence*, Phys. Rev. Lett. **96** (2006) 024503.

[11] KHOLMYANSKY M., TSINOBER A., AND YORISH S., *Velocity derivatives in the atmospheric turbulent flow at* $Re_\lambda = 10^4$, Phys. Fluids **13** (2001) 311–314.

[12] LUETHI B., TSINOBER A., KINZELBACH W., *Lagrangian measurements of vorticity dynamics in turbulent flow*, J. Fluid Mech. **528** (2005) 87-118.

[13] BERG J., LUETHI B., MANN J., AND OTT S., *Backwards and forwards relative dispersion in turbulent flow: An experimental investigation*, Phys. Rev. E **74** (2006) 016304.

Reynolds number effect on the velocity increment skewness in isotropic turbulence

WOUTER J.T. BOS*, LAURENT CHEVILLARD**, JULIAN F. SCOTT*

Abstract. *The velocity increment skewness of isotropic turbulence is computed using the EDQNM model and compared to results of the multifractal formalism. At the highest Reynolds number available in wind-tunnel experiments, $R_\lambda = 2500$, both the multifractal model and EDQNM give power-law corrections to the inertial range scaling. For EDQNM, this correction is a finite Reynolds number effect, whereas for the multifractal formalism it should persist at high Reynolds number. Therefore, at $R_\lambda = 2500$, corrections to the inertial range scaling of the skewness are not an adequate measure for intermittency, since the influence of intermittency cannot be distinguished from the influence of the Reynolds number.*

Keywords: isotropic turbulence, Reynolds number, EDQNM model.

The nonlinearity in the Navier-Stokes equations gives rise to an interaction between different length-scales in a turbulent flow. These interactions are the basic mechanism behind the celebrated Kolmogorov-Richardson energy cascade. In the Lin equation for the turbulent energy spectrum $E(k)$,

$$\frac{\partial E(k)}{\partial t} = T(k) - 2\nu k^2 E(k), \tag{1}$$

(k being the wavenumber and ν the kinematic viscosity), these scale interactions are represented by the nonlinear transfer $T(k)$. In physical space, the second-order and third-order longitudinal structure functions, $D_{ll}(r)$ and $D_{lll}(r)$, are related to $E(k)$ and $T(k)$ by the following expressions,

$$D_{ll}(r) = 4\int_0^\infty E(k)\left[\frac{1}{3} - \frac{\sin kr - kr\cos kr}{(kr)^3}\right]dk, \tag{2}$$

$$D_{lll}(r) = 12r\int_0^\infty T(k)\left[\frac{3\left(\sin kr - kr\cos kr\right) - (kr)^2\sin kr}{(kr)^5}\right]dk. \tag{3}$$

The possibility of corrections to the inertial range scaling of structure functions, due to the intermittent character of the energy dissipation was advanced

*LMFA, Ecole Centrale de Lyon, CNRS, Univeristé de Lyon, Ecully, France.
E-mail: wouter.bos@ec-lyon.fr
**Laboratoire de Physique, ENS Lyon, CNRS, Université de Lyon, Lyon, France.

by Kolmogorov [1]. A phenomenological model which succeeds to give a coherent picture of the influence of intermittency is the multifractal model [2]. This model compares well to measurements and gives non-zero intermittency corrections to the inertial range scaling of the energy spectrum at high Reynolds numbers. For $D_{ll}(r)$ this correction is believed to yield the scaling

$$D_{ll}(r) \sim r^{2/3+\mu}, \tag{4}$$

with μ the intermittency correction, of the order of 0.03. For $D_{lll}(r) \sim r$, there is no correction. This gives for the (longitudinal velocity increment) skewness,

$$Sk(r) = D_{lll}(r)/D_{ll}(r)^{3/2}, \tag{5}$$

a scaling $Sk(r) \sim r^{-0.045}$. In the present communication we will compare the skewness as computed from spectral closure, with the prediction of the multifractal model and experimental measurements of windtunnel turbulence.

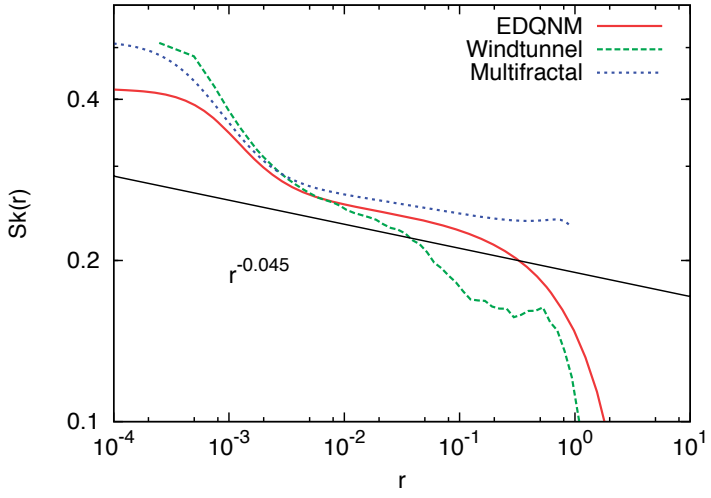

Figure 1: The velocity increment skewness at $R_\lambda \approx 2500$. Results from EDQNM computations, the multifractal formalism and experimental results.

The spectral closure used here is the EDQNM model [3]. This model, which is a simplification of the DIA-closure family developed by Kraichnan (*e.g.* [4, 5]), closes the Lin-equation by giving a closed expression for $T(k)$ as a function of the energy spectrum. It is known to be a valuable tool to study the influence of the Reynolds number on some statistical properties of

turbulent flows [6]. It is however not able to take into account intermittency in the sense that at asymptotically high Reynolds number no corrections to the inertial range scaling of the energy spectrum remain.

In figure 1, the results of EDQNM computations of freely decaying turbulence, the multifractal formalism as described in [7] and experimental measurements of windtunnel turbulence [8] are compared, all at a Taylor-scale-based Reynolds R_λ number of approximately 2500. A good qualitative agreement is observed at small scales. At large scales, the statistics of the experiment are not fully converged. Both EDQNM and the multifractal prediction follow a powerlaw with an exponent close to -0.045. At very high Reynolds number this exponent should tend to zero for the EDQNM results. Therefore, at physically relevant Reynolds numbers ($R_\lambda = 2500$ is the highest value obtained in windtunnels until now), the inertial range scaling of the skewness is not an adequate measure for intermittency, since the influence of intermittency cannot be distinguished from the influence of the Reynolds number. Other quantities, such as the flatness, would perhaps give a better measure, since their corrections due to intermittency should be larger.

References

[1] A.N. KOLMOGOROV, *A refinement of previous hypotheses concerning the local structure of turbulence ...* , J. Fluid Mech. **13** (1962), 82.

[2] U. FRISCH, *Turbulence, the legacy of A.N. Kolmogorov*, Cambridge University Press (1995).

[3] S.A. ORSZAG, *Analytical theories of turbulence*, J. Fluid Mech. **41** (1970), 363.

[4] R. KRAICHNAN, *The structure of isotropic turbulence at very high Reynolds numbers*, J. Fluid Mech. **5** (1959), 497.

[5] R. KRAICHNAN, *An almost-Markovian Galilean-invariant turbulence model*, J. Fluid Mech. **47** (1971), 513.

[6] W.J.T. BOS, H. TOUIL, AND J.-P. BERTOGLIO, *Reynolds number dependency of the scalar flux spectrum in isotropic turbulence with a uniform scalar gradient*, Phys. Fluids **17** (2005), 125108.

[7] L. CHEVILLARD, B. CASTAING, E. LÉVÊQUE, AND A. ARNEODO, *Unified multifractal description of velocity increments statistics in turbulence: Intermittency and skewness*, Phys. D **218** (2006), 77.

[8] H. KAHALERRAS, Y. MALECOT, Y. GAGNE, AND B. CASTAING, *Intermittency and Reynolds number*, Phys. Fluids **10** (1998), 910.

Clustering of inertial particles in shear flows

CARLO M. CASCIOLA*, PAOLO GUALTIERI*,
FRANCESCO PICANO*, GAETANO SARDINA*

Abstract. *Particles with finite inertia present anomalous transport properties such as small scale clustering, a feature usually addressed in homogeneous and isotropic conditions. Here the effect of the mean shear on the particle clustering is analyzed by using DNS in several configurations of shear flows: homogeneous shear, pipe flow, and free jet. Data evidence that the segregation process is essentially anisotropic, even in the range of scales where isotropization of velocity statistics already occurred. Spatial inhomogeneity adds additional features associated with the migration of particles towards specific regions of the flow*

Keywords: Inertial particles, Clustering, Preferential Accumulation.

Transport of particles is a classical problem in fluid mechanics since the pioneering contributions of Richardson and Taylor. In many cases the inertia of the particles plays a crucial role in their dynamics. An essential phenomenology induced by inertia is clustering, thoroughly analyzed for statistically homogeneous and isotropic flows[1]. In such conditions the most striking result concerns the singular behavior exhibited by the radial distribution function showing that, under proper conditions, clustering may occur at small scales, below the Kolmogorov length. Actual flows are neither isotropic nor homogeneous. Purpose of this work is to describe recent contributions addressing the effects of shear and inhomogeneity on particle dynamics. The effects of shear are evident in the instantaneous configuration of particles shown in the top panel of figure 1, taken from homogeneous turbulent shear flow [2]. The presence of clusters is apparent, as it is their orientation induced by the velocity field anisotropy. Technically clustering amounts to an increased probability to find particles at a given distance r and it is quantified by the radial distribution function (RDF), bottom-left panel of figure 1. The main parameter controlling the dynamics for small, diluted, heavy particles is the Stokes number, $St_\eta = \tau_p/\tau_\eta$, where $\tau_p = \rho_p d_p^2/(18\mu)$ is the particle relaxation time and τ_η is the Kolmogorov time. Clustering is maximum when $St_\eta \simeq 1$, see the slope of the RDF at small scales. The anisotropy of the advecting field results in a strong directionality of the probability to find particles at small separation, bottom-right panel of figure 2. The data provide evidence of the substantial anisotropy of the particle

*Dipartimento di Meccanica e Aeronautica, Sapienza University of Rome, via Eudossiana 18, 00184 Roma, Italy.
E-mail: carlomassimo.casciola@uniroma1.it

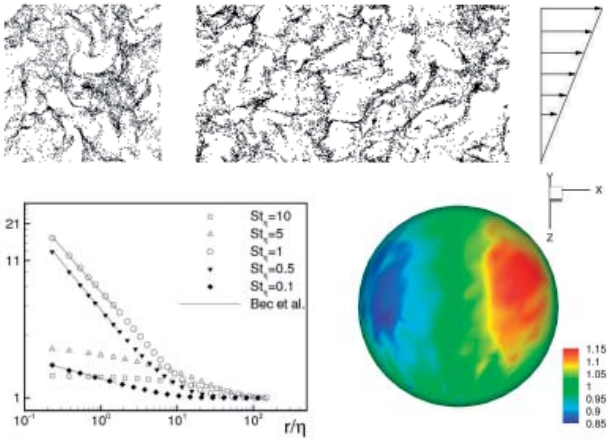

Figure 1: Top panel: instantaneous slice of particle distribution at $St_\eta = 1$ in homogeneous shear flow at $Re_\lambda = 100$. Left-bottom panel: radial distribution function for different Stokes numbers; right-bottom panel angular distribution function for $St_\eta = 1$ and $r = 4\eta$. See [2] for more details.

distribution which, under appropriate conditions, may easily reach the small scales of the flow where isotropization of velocity statistics already occurred.

Anisotropic clustering is a generic property of particle-laden turbulent shear flows, see e.g. figure 2 providing the instantaneous particle distribution in a free turbulent jet at $Re_D = 4000$. Inhomogeneity adds new features, inducing the migration of particles towards specific regions of the flow. The effect is striking in wall bounded flows [4], where particles of suitable mass $St^+ \simeq 10 \div 50$

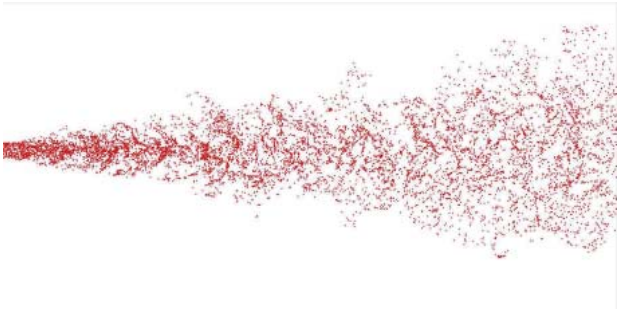

Figure 2: Snapshot of particles with $St_D = \tau_p U_0/D = 4$ in a turbulent jet at $Re_D = 4000$

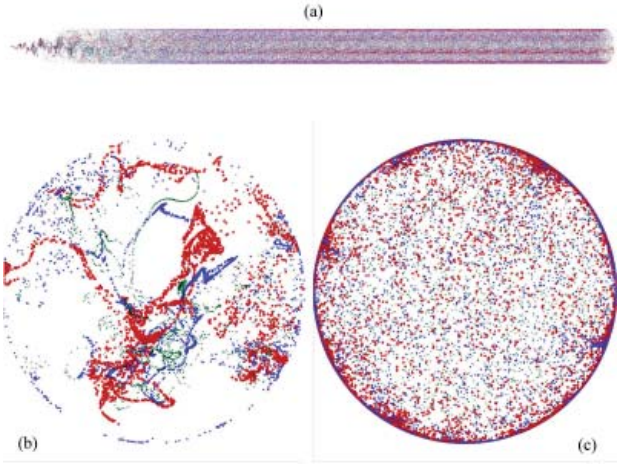

Figure 3: Snapshots of particle distributions in a spatial developing pipe flow at $Re_\tau = 200$. Colors correspond to different Stokes numbers $St^+ = 0.1$ green, $St^+ = 10$ blue, $St^+ = 100$ red. Panel (a) whole domain with length $L_z = 200R$ (not to scale). Panels (b) and (c): cross sections at $z/R = 25$ (developing region) and at $z/R = 200$ (far field), respectively. region. See [3] for more details.

drift towards the wall reaching concentration up to thousands times the value in the bulk. Accumulation at the wall, figure 3, occurs together with spatial localization of the particles in elongated patterns, which, as discussed in [3], are necessary features of the equilibrium distribution.

References

[1] BEC, J., BIFERALE, L., CENCINI, M., LANOTTE, A., MUSACCHIO, S. & TOSCHI, F. *Heavy particle concentration in turbulence at dissipative and inertial scales*. Phys. Rev. Lett. **98** (8) (2007), 084502.

[2] GUALTIERI P., PICANO F. AND CASCIOLA C.M. *Anisotropic clustering of inertial particles in homogeneous shear flow*. Journal of Fluid Mechanics, **629** (2009), 25–39.

[3] PICANO F., SARDINA G. AND CASCIOLA C.M. *Spatial development of particle-laden turbulent pipe flow*. Phys. Fluids, (2009) in press.

[4] SOLDATI A. AND MARCHIOLI C. *Physics and modelling of turbulent particle deposition and entrainment: Review of a systematic study.* International Journal of Multiphase Flow, (2009), in press.

A Stochastic Representation of the Local Structure of Turbulence

LAURENT CHEVILLARD*, RAOUL ROBERT**, VINCENT VARGAS***

Abstract. *Based on the Euler dynamics at short-time, we propose a stochastic incompressible vectorial field that mimics the main properties of fully developed turbulence in the inertial range, including intermittency, the non-vanishing skewness of longitudinal increments, the teardrop shape of the RQ-plane and the preferential alignments of vorticity with the intermediate eigenvector of the deformation. A free parameter, the intermittency parameter, needs to be specified on empirical grounds. Here, we present the main statistical properties of a numerical simulation of this process.*

Keywords: stochastic process, intermittency.

Here, based on former works [1, 2], we propose a stochastic method to build an incompressible, skewed and intermittent velocity field. This method is motivated by the early stage mechanics of the Euler equation during when vorticity is stretched by the local deformation, whereas early advection by the large scale velocity is neglected. We have shown in Ref. [3] that such a Recent Fluid Deformation (RFD) closure [1] leads to an incompressible differentiable velocity field which reproduces well known facts of empirical turbulence, namely the teardrop shape of the RQ plane and a skewed probability density function (PDF) for the longitudinal gradients. Unfortunately, it is seen numerically that this field is not skewed in the inertial range, leading to vanishing mean energy transfer through scales, and furthermore, alignment properties of vorticity deviate from empirical findings. Thus, to take into account both long-time vorticity streching and advection (or mixing) of fluid particles, that have been formely neglected, we will call for multifractal principles in order to impose the inherent long-range correlations of small scales such as dissipation or enstrophy. We end up [3] with the following explicit incompressible vectorial field

$$\widetilde{\mathbf{u}}_\varepsilon(\mathbf{x}) = -\frac{1}{4\pi}\int \varphi_L(\mathbf{x}-\mathbf{y})\frac{\mathbf{x}-\mathbf{y}}{|\mathbf{x}-\mathbf{y}|_\varepsilon^{\frac{3}{2}+\frac{2}{3}}} \wedge e^{\widetilde{\mathbf{S}}} d\mathbf{W}(\mathbf{y}) \qquad (1)$$

*Laboratoire de Physique de l'ENS Lyon, CNRS, Université de Lyon, 46 allée d'Italie, 69007 Lyon, France.

E-mail: laurent.chevillard@ens-lyon.fr

**Institut Fourier, CNRS, Université Grenoble 1, 100 rue des Mathématiques, BP 74, 38402 Saint-Martin d'Hères cedex, France.

E-mail: Raoul.Robert@ujf − grenoble.fr

***Ceremade, CNRS, Université Paris-Dauphine, F-75016 Paris, France.

E-mail: vargas@ceremade.dauphine.fr

where $\widetilde{\mathbf{S}}$ is a tensorial Gaussian log-correlated noise, given explicitly as an integral form of the very same white noise $d\mathbf{W}(\sigma)$ entering in (1):

$$\widetilde{\mathbf{S}}(\mathbf{y}) = \frac{3}{8\pi}\frac{\lambda}{\sqrt{4\pi}}\int\left[\frac{(\mathbf{y}-\sigma)\otimes[(\mathbf{y}-\sigma)\wedge d\mathbf{W}(\sigma)]}{|\mathbf{y}-\sigma|_\varepsilon^{7/2}} + \frac{[(\mathbf{y}-\sigma)\wedge d\mathbf{W}(\sigma)]\otimes(\mathbf{y}-\sigma)}{|\mathbf{y}-\sigma|_\varepsilon^{7/2}}\right]\varphi_L(\mathbf{y}-\sigma)\,,$$

where, in order to get mathematically well defined integrals, we have introduced both a large scale cutoff $\varphi_L(\mathbf{x}-\mathbf{y})$ in the definition of $\mathbf{u}$ and $\widetilde{\mathbf{S}}$, and a small scale regularization ε: $|\mathbf{x}|_\varepsilon = \theta_\varepsilon * |\mathbf{x}|$ (see Ref. [2] for further details).

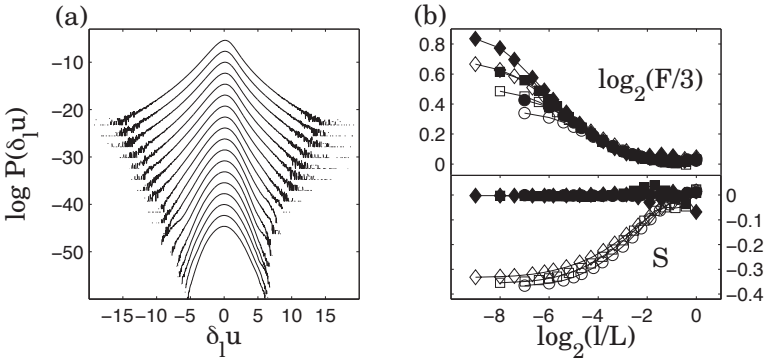

Figure 1: Numerical results of the process given in (1). (a) PDFs of longitudinal velocity increments $\delta_\ell u$ ($N = 1024$), scales ℓ are logarithmically spaced between dx and L (see text). (b) Scale dependence of the Skewness S (bottom) and Flatness F (top) of longitudinal (open symbols) and transverse (filled symbols) for the three resolutions: $N = 256$ (○), $N = 512$ (□) and $N = 1024$ (◇).

The velocity field (1) is expected to be asymptotically multifractal [2] with a quadratic structure exponent, i.e. for the longitudinal case $\langle|\delta_\ell u|^q\rangle \sim \ell^{\zeta_q}$ where $\zeta_q = \left(\frac{1}{3} + a(c\lambda)^2\right)q - (c\lambda)^2\frac{q2}{2}$. A rigorous derivation of the constants a and c is still missing; numerics show that a is of order 1 and $c \approx 1$. The intermittency coefficient λ is a free parameter and is chosen as $\lambda^2 = 0.025$ on empirical grounds [3]. The exponent $\frac{3}{2} + \frac{2}{3}$ in (1) can be slightly modified in order to impose $\zeta_3 = 1$.

We reproduce in figs. 1 and 2 the results of the simulation proposed in ref. [3]. In fig. 1 are reproduced the results related to the intermittency

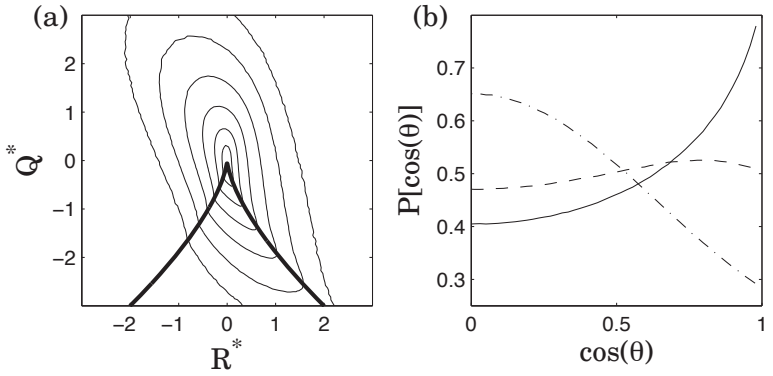

Figure 2: (a) Contour plots of the logarithm of the joint probability of the two invariants of $\mathbf{A}$ ($N = 1024$ case) non-dimensionalized by the average strain $Q^* = Q/\langle S_{ij}S_{ij}\rangle$ and $R^* = R/\langle S_{ij}S_{ij}\rangle^{3/2}$. The thick line corresponds to the zero discriminant (Vieillefosse) line. Contour lines correspond to probabilities $10^{-2.5}, 10^{-2}, 10^{-1.5}, 10^{-1}, 10^{-.5}, 1$. (b) PDF of the cosine of the angle θ between vorticity and the eigenvectors of the strain (see text) associated to three eigenvalues λ_1 (dashed-dot), λ_2 (solid) and λ_3 (dashed), for the $N = 1024$ case.

phenomenon, both the probability density functions (PDFs) of the longitudinal velocity increments $\delta_\ell u$, and the dependence on the scale of the Flatness $F = \langle(\delta_\ell u)^4\rangle/\langle(\delta_\ell u)^2\rangle^2$ and Skewness $S = \langle(\delta_\ell u)^3\rangle/\langle(\delta_\ell u)^2\rangle^{3/2}$. Given the free parameter $\lambda^2 = 0.025$, results are realistic of empirical measurements. In fig. 2, we focus more on geometrical properties of 3D turbulence, such as the joint probability of the invariants $Q = -\frac{1}{2}\mathrm{tr}(\mathbf{A}^2)$ and $R = -\frac{1}{3}\mathrm{tr}(\mathbf{A}^3)$, where $\mathbf{A} = \nabla\mathbf{u}$ is the velocity gradient tensor, and the alignment of vorticity with the eigenvector of the deformation $\mathbf{S} = \frac{1}{2}(\mathbf{A} + \mathbf{A}^\top)$ (eigenvalues ordered as $\lambda_1 \le \lambda_2 \le \lambda_3$). The proposed process (1) reproduces both the dissymetry of the RQ-plane along the Vieillefosse-line, and the preferential alignment of vorticity along the intermediate eigenvector of the deformation.

References

[1] CHEVILLARD, L., MENEVEAU, C., Phys. Rev. Lett. **97**, 174501 (2006).

[2] ROBERT, R., VARGAS, V., Comm. Math. Phys. **284**, 649 (2008).

[3] CHEVILLARD, L., ROBERT, R. and VARGAS, V., arXiv:0906.5225 (2009).

Is there an energy cascade in strong wave turbulence?

COLM CONNAUGHTON*, R. RAJESH**, OLEG ZABORONSKI***

Abstract. *Constant fluxes of conserved quantities in stationary wave turbulence exactly determine the inertial range scalings of appropriate flux-carrying correlation functions just as energy conservation determines the scaling of the third order structure function in hydrodynamic turbulence. This constraint on the flux-carrying correlation function, which we refer to as a* constant flux relation *(CFR) requires no assumption of weak nonlinearity. It thus provides a natural departure point for the study of strong wave turbulence. In this paper we state the theoretical results and illustrate the ideas using a finite dimensional toy model. We predict that the energy cascade in strong wave turbulence, provided that a local cascade is possible, would be of a different character to most familiar cascade mechanisms and must involve a non-trivial conversion between linear wave energy and nonlinear wave self-interaction energy.*

Keywords: strong wave turbulence, higher order correlation functions.

Wave turbulence [1] is modelled as a Hamiltonian equation for the complex wave amplitudes, $a_{\mathbf{k}}$, coupled to a source and sink of energy which are widely separated in $\mathbf{k}$ (wave-vector) space :

$$\partial_t a_{\mathbf{k}} = i\frac{\delta H}{\delta \bar{a}_{\mathbf{k}}} + f_{\mathbf{k}} - \gamma_{\mathbf{k}} a_{\mathbf{k}}. \tag{1}$$

H has a linear and nonlinear part, $H = T + gU$. The latter induces interactions between waves enabling transfer of energy among normal modes resulting in cascades in $\mathbf{k}$-space. The linear part of the energy describes a collection of linear oscillators: $T = \int \omega_{\mathbf{k}} a_{\mathbf{k}} \bar{a}_{\mathbf{k}} d\mathbf{k}$. For 3-wave interactions, the nonlinear part of the energy is $U = \int V_{\mathbf{k}\mathbf{k}_1\mathbf{k}_2} \left(a_{\mathbf{k}} a_{\mathbf{k}_1} \bar{a}_{\mathbf{k}_2} + \bar{a}_{\mathbf{k}} \bar{a}_{\mathbf{k}_1} a_{\mathbf{k}_1}\right) \delta(\mathbf{k} - \mathbf{k}_1 - \mathbf{k}_2)\, d\mathbf{k} d\mathbf{k}_1 d\mathbf{k}_2$. We take the dispersion relation, $\omega_{\mathbf{k}}$, and the triad interaction coefficient, $V_{\mathbf{k}\mathbf{k}_1\mathbf{k}_2}$ to be homogeneous functions of their arguments having degree α and γ respectively. Almost everything is known [1] about the stationary statistics of Eq. (1)

*Centre for Complexity Science, University of Warwick, Coventry CV4 7AL, UK.
E-mail: connaughtonc@gmail.com
**Institute of Mathematical Sciences, Taramani, Chennai-600 113, India.
E-mail: rrajesh@imsc.res.in
***Mathematics Institute, University of Warwick, Coventry CV4 7AL, UK.
E-mail: O.V.Zaboronski@warwick.ac.uk

in the limit of weak nonlinearity when the interactions between waves can be treated perturbatively. In particular, T, is conserved to leading order and cascades to small scales in an analytically tractable way. Practically nothing is known about the strong nonlinearity limit when both T and U cascade.

In the stationary state [2], conservation of energy, $T+U$, requires that

$$\int \prod_{i=1}^{2} (dk_i k_i^{d-1}) \left[T_{k;k_1,k_2} \Pi_{0;1,2} - T_{k_1;k,k_2} \Pi_{1;0,2} \right] = 0 \tag{2}$$

in the inertial range. In this equation

$$\Pi_{0;1,2} = \int \prod_{i=0}^{2} d\Omega_i \langle Re(a_{\vec{k}}\, \partial_t \bar{a}_{\vec{k}_1}\, \bar{a}_{\vec{k}_2}) \rangle \tag{3}$$

is the energy flux correlation function. Note the unusual structure of this correlation function: it involves time derivatives of amplitudes and is thus a composite quantity. Assuming a locality condition requiring convergence of a certain integral involving an unknown scaling function, one may show that this is only possible if $\Pi_{0;1,2}$ has homogeneity degree $-3d-\gamma$. This result, analogous to Kolmogorov's $4/5$-Law, holds regardless of the strength of the underlying wave turbulence. This is the only general exact result known to us for strong wave turbulence. In the weak limit, the assumption of locality can be checked a-posteriori. This is not the case in general. Locality can be non-trivial [3]. In general, we require numerical simulation to study locality of a cascade.

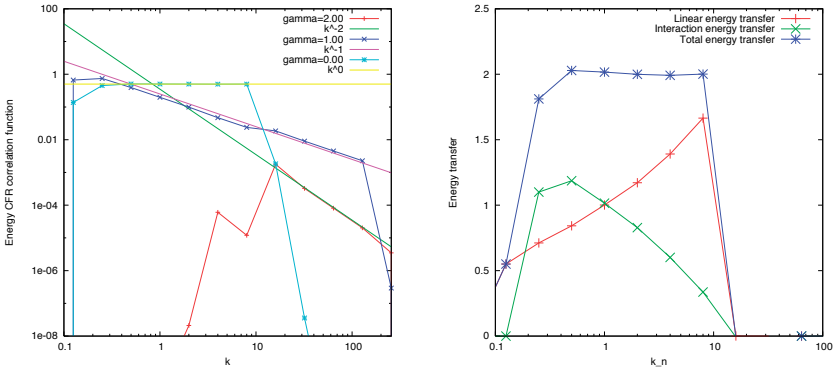

Figure 1: Left panel: Verification of CFR scaling, Eq. (6), for the toy model. Right panel: Stationary fluxes of linear, nonlinear and total energy for $\gamma = 0.0$.

To separate complications coming from the unusual structure of $\Pi_{0;1,2}$ from those coming from locality, we studied a toy model of strong 3-wave interactions. The model is a discrete chain of oscillators with wavenumbers, $k_n = 2^n$

and frequencies $\omega_n = k_n^{\alpha}$. Energy is injected by forcing oscillator 0 and removed by damping at both ends. The Hamiltonian is $H = \sum_{n=-N}^{n=N} T_n + U_n$ where

$$T_n = \omega_n a_n \bar{a}_n \qquad U_n = k_{n-1}^{\gamma} \left(\bar{a}_n a_{n-1}^2 + a_n \bar{a}_{n-1}^2 \right). \tag{4}$$

The chain reaches a statistically stationary state in which energy is injected at the centre, cascades through the chain and is removed at the ends. The flows of linear and nonlinear energies are:

$$\frac{dT_n}{dt} = Q_n^{(T)} - Q_{n-1}^{(T)} - R_n \qquad \frac{dU_n}{dt} = Q_n^{(U)} - Q_{n-1}^{(U)} + R_n \tag{5}$$

where $Q_n^{(T)} = -4g\omega_n k_n^{\gamma} \mathrm{I}m[a_{n+1}\bar{a}_n^2]$, $Q_n^{(U)} = -4g^2 (k_n k_{n-1})^{\gamma} \mathrm{I}m[\bar{a}_{n+1} a_n a_{n-1}^2]$ and $R_n = \left(1 - \frac{\omega_n}{2\omega_{n-1}}\right) Q_n^{(T)}$ Taking averages in the stationary state yields for the average transfer of total energy: $\langle Q_n^{(H)} \rangle - \langle Q_{n-1}^{(H)} \rangle = 0$ where $Q_n^{(H)} = Q_n^{(T)} + Q_n^{(U)}$ is the flux of total energy. This has the simple solution

$$\mathrm{R}e \langle \bar{a}_{n+1} a_n d_t a_n \rangle = -\frac{Q_0}{4g} k_n^{-\gamma}, \tag{6}$$

where Q_0 is the rate of dissipation of total energy. This is the analogue of the constant flux relation for our toy model. Its numerical verification for several values of γ is shown in the left panel of Fig. 1. The right panel of Fig. 1 demonstrates the constancy of the flux of total energy for the case $\gamma = 0$. The results indicate that the flux carrying correlation function can indeed exhibit scaling behaviour despite its composite nature. The cascade of total energy in the toy model is clearly of a different character to a more familiar cascade of a quadratic quantity. The cascade involves the transmutation of linear energy into nonlinear energy in order to maintain a constant flux of the sum of the two.

We have not yet studied the extent to which these lessons carry over to the original wave turbulence problem. It is clear, however, that there is some potential here for some interesting new results on strong wave turbulence.

References

[1] V.S. Zakharov, V.S. Lvov, and G. Falkovich. *Kolmogorov Spectra of Turbulence*. Springer-Verlag, Berlin, 1992.

[2] C. Connaughton, R. Rajesh, and O. Zaboronski. Constant Flux Relation for driven dissipative systems. *Phys. Rev. Lett.*, 98:080601, 2007.

[3] C. Connaughton, R. Rajesh, and O. Zaboronski. Constant Flux Relation for diffusion limited cluster–cluster aggregation. *Phys. Rev. E*, 78(041403), October 2008.

Axisymmetric description of the scale-by-scale scalar transport

LUMINITA DANAILA*

Abstract. *In anisotropic axisymmetric turbulence, the kinetic energy at a scale r, $\langle(\delta u_i)^2\rangle$ with $\delta u_i = u_i(\mathbf{x}+\mathbf{r}) - u_i(\mathbf{x})$, depends upon two scalars: r (the modulus of the spatial separation* $\mathbf{r}$*) and* μ_r *(the cosinus of the angle made by* $\mathbf{r}$ *with the axisymmetry direction). A scale-by-scale energy budget equation is derived for axisymmetric turbulence, with particular emphasis on the central region of a round jet. This equation includes inhomogeneous and anisotropic effects (decay, production, variations of the mean energy dissipation rate). All the involved quantities could be estimated from planar measurements, such as PIV.*

Keywords: scale-by-scale energy budget, local isotropy, axisymmetry.

The behaviour of a scalar (kinetic energy, scalar variance etc.) at a given scale in turbulent flow depends upon the advecting field, the molecular effects and large-scale effects (decay, mean shear, mean scalar gradient etc). The simplest exact way to describe statistical properties at any scale is to study the second-order moments, which naturally involves the third-order moments of the scalar. This was first developed by A.M. Yaglom [1] and further extended for the turbulent kinetic energy [2] under the ideal assumption of local isotropy. However, for moderate Reynolds numbers of slightly heated grid turbulence, Yaglom's equation is only valid for a restricted range of scales, notwithstanding the approximate validity of local isotropy in this flow. Clearly, it is important to identify and quantify the terms that allow the energy balance to be closed, in order to better understand all the physical phenomena brought into play in a flow/region of a flow. Several methodologies are outlined below in increasing order of difficulty:

- 1) When local isotropy holds, large-scales effects are to be taken into account, e.g. [3], [4].
- 2) In flows and mixing where local isotropy is not appropriate, different approaches should be considered. This paper only considers axisymmetrical flows [5], [6].

The starting point is the scale-by-scale energy budget equation for the total kinetic energy $(\delta q)^2 \equiv \langle \delta u_i \delta u_i \rangle$, which writes in the context of local isotropy [2],

$$-\langle \delta u_1 (\delta q)^2 \rangle + 2\nu \frac{d}{dr}\langle (\delta q)^2 \rangle = \frac{4}{3}\langle \varepsilon \rangle r, \tag{1}$$

* CORIA UMR 6614, Saint Etienne du Rouvray, France.
E-mail: danaila@coria.fr

where $\langle\varepsilon\rangle$ is the mean energy dissipation rate. The focus herein is to write the counterpart of Eq. (1) in the anisotropic/axisymmetric context. Note that the exact tensorial representation of the axisymmetric field [5] is beyond the scope of this contribution. Following the same mathematical development as presented in [3], we write the incompressible Navier–Stokes equations at the two points $\mathbf{x}$ and $\mathbf{x}^+$, which are separated by the increment $\mathbf{r} = \mathbf{x}^+ - \mathbf{x}$, and further focus on the central region of a round jet, for which: the flow is statistically stationary, pressure containing terms as well as turbulent diffusion terms are neglected. The result is

$$2\langle\delta\left(U_\alpha\frac{\partial u_i}{\partial x_\alpha}\right)\delta u_i\rangle(\mathbf{r}) + 2\langle\delta\left(u_\alpha\frac{\partial U_i}{\partial x_\alpha}\right)\delta u_i\rangle(\mathbf{r}) + \frac{\partial}{\partial r_\alpha}\langle\delta u_\alpha(\delta q)^2\rangle(\mathbf{r}) = \\ + 2\nu\frac{\partial^2}{\partial {r_\alpha}^2}\langle(\delta q)^2\rangle(\mathbf{r}) - 2\left(\langle\varepsilon\rangle + \langle\varepsilon\rangle^+\right). \quad (2)$$

In Eq. (2), each term depends on the spatial vector $\mathbf{r}$. Let us assume that the flow is axisymmetric about a direction specified by $\mathbf{n}$ (the jet axis). The statistical correlations of the flow properties will then be invariant for rotations in planes normal to $\mathbf{n}$ and symmetries with respect to planes containing $\mathbf{n}$. We note $r^2 = \mathbf{r}\cdot\mathbf{r}$ and $r\mu_r \equiv \mathbf{r}\cdot\mathbf{n}$. In this context, each term of Eq. (2) depends on two variables r, μ_r. The advection term $\frac{\partial}{\partial r_\alpha}\langle\delta u_\alpha(\delta q)^2\rangle(\mathbf{r})$ is written in a manner similar to [6]:

$$\langle\delta u_\alpha(\delta q)^2\rangle(\mathbf{r}) = M_a(r,\mu_r)r_\alpha + N_a(r,\mu_r)n_\alpha, \quad (3)$$

where only two scalars M_a and N_a appear. The scalars $M_a(r,\mu_r)$ and $N_a(r,\mu_r)$ can be determined from planar experiments (e.g., PIV) which include the axisymmetry vector $\mathbf{n}$, via the measureable $\langle\delta u_\parallel(\delta q)^2\rangle$ and $\langle\delta u_\perp(\delta q)^2\rangle$. Here, $\perp$ indicates any direction perpendicular to the axisymmetry axis $\mathbf{n}$ and $\parallel$ designates the direction of $\mathbf{n}$. This leads to the experimentally determinable scalars $M_a(r,\mu_r)$ and $N_a(r,\mu_r)$. Therefore, for the axisymmetric case, $\frac{\partial}{\partial r_\alpha}\langle\delta u_\alpha(\delta q)^2\rangle(\mathbf{r})$ becomes

$$\frac{\partial}{\partial r_\alpha}\langle\delta u_\alpha(\delta q)^2\rangle(\mathbf{r}) \equiv \left(r\frac{\partial}{\partial r} + 3\right)M_a(r,\mu_r) + \left(\mu_r\frac{\partial}{\partial r} + \frac{1-\mu_r^2}{r}\frac{\partial}{\partial\mu_r}\right)N_a(r,\mu_r). \quad (4)$$

The kinetic energy dissipation term $\langle\varepsilon\rangle^+$ reads, in the context of axisymmetry $\langle\varepsilon\rangle^+ = \langle\varepsilon\rangle + \frac{d\langle\varepsilon\rangle}{dn}(r\mu_r)$.

In order to simplify the mathematical form of the final equation, we put $N_a(r,\mu_r) = \left[2 + r\frac{\partial}{\partial r}\right]V = \frac{1}{r}\frac{\partial}{\partial r}\left[r^2V\right], N_a^* = \left(\mu_r\frac{\partial}{\partial r} + \frac{1-\mu_r^2}{r}\frac{\partial}{\partial\mu_r}\right)V$, and $G = M_a(r,\mu_r) +$

$N_a^*(r,\mu_r)$. After integration with respect to r, the final axisymmetric form of scale-by-scale energy budget equation is

$$G(r,\mu_r) = -\frac{4}{3}\langle\varepsilon\rangle - \frac{1}{2}\frac{d\langle\varepsilon\rangle}{dn}(r\mu_r) + 2\nu\frac{1}{r^3}\left[\int_0^r s^2\frac{\partial^2}{\partial s^2}\langle(\delta q)^2\rangle \mathrm{d}s\right] +$$
$$2\nu\frac{1}{r^3}\left[2(1-\mu_r^2)\frac{\partial^2}{\partial\mu_r^2}\int_0^r s^2\langle(\delta q)^2\rangle \mathrm{d}s\right] - \frac{1}{r^3}\int_0^r s^2\left(D(r,\mu_r)+P(r,\mu_r)\right)\mathrm{d}s, \quad (5)$$

where $D(r,\mu)$ and $P(r,\mu)$ are the decay and production terms respectively. Note the importance of (5) with respect to the classical equation (1): i) it obviously reduces to the isotropic '4/3' law ; ii) it contains large-scale terms (decay and production) which are very important in the context of the validation against experimental data; iii) it contains an explicit variation of the mean kinetic energy dissipation rate $\frac{d\langle\varepsilon\rangle}{dn}$. Equation (5), and its counterpart for the scalar energy, are tested against experimental data obtained by PIV and PLIF (Planar Laser Induced Florescence) for scalars, in either a single round jet or multiple opposed/sheared jets. A decomposition of each term in a more explicit dependence on r and μ_r is possible by using *e.g.* spherical harmonics [7].

Financial support of ANR under the activities 'Micromélange' ANR-05-0242-01 and 'Aniso' ANR-08-BLAN-0076 is gratefully acknowledged.

References

[1] YAGLOM A.M., *On the local structure of a temperature field in a turbulent flow*, Dokl. Akad. Nauk SSSR **69** (1949), 743.

[2] R.A. ANTONIA, M. OULD-ROUIS, F. ANSELMET AND Y. ZHU, *Analogy between predictions of Kolmogorov and Yaglom*, J. Fluid Mech. **33** (1997), 395-409.

[3] L. DANAILA, R.A. ANTONIA AND P. BURATTINI, *Progress in studying small-scale turbulence using 'exact' two point equations*, New J. Phys. **6** (2004), 128.

[4] L. DANAILA AND L. MYDLARSKI, *Effect of gradient production on scalar fluctuations in decaying grid turbulence*, Phys. Rev. E. **64** (2001), 016316.

[5] CHANDRASEKAR S., *The theory of axisymmetric turbulence*, Phil. Trans. R. Soc. Lond. A **242** (1950), 557-577.

[6] B.K. SHIVAMOGGI AND R.A. ANTONIA, *Isotropic and axisymmetric turbulence of passive scalars*, Fluid Dyn. Research **26** (2000), 95-104.

[7] S. KURIEN, K.G. AIVALIS AND K.R. SREENIVASAN, *Anisotropy of small-scale scalar turbulence*, J. Fluid Mech. **448** (2001), 279-288.

Small scales dynamics in dilute polymers solutions

ELISABETTA DE ANGELIS*, CARLO M. CASCIOLA**, RENZO PIVA**

Abstract. *An analysis of spectral budgets of homogeneous and isotropic (HI) turbulence in dilute polymers based on a set of newly proposed equations is performed. The results confirm the value of the presented tool for the study of energy transfer in viscoelastic turbulence.*

Keywords: homogeneous isotropic turbulence, dilute polymers.

In this contribution the analysis of spectral budgets of homogeneous and isotropic (HI) turbulence based on the set of newly proposed equations is performed for a dilute polymer solution in the mild stretch regime at low-Reynolds number. In this regime, the dynamics of the polymers is described by the linear and homogeneous equation for the conformation tensor, $\mathbf{R}$, [1]

$$\frac{\partial \mathbf{R}}{\partial t} + \mathbf{u}\cdot\nabla\mathbf{R} = \mathbf{K}\mathbf{R} + \mathbf{R}\mathbf{K}^{\dagger} - \frac{2}{\tau}\mathbf{R}, \tag{1}$$

accounting for advection, stretching, re-orientation and linear elastic restoring force. As follows from its physical meaning, the conformation tensor must be a symmetric positive definite second order tensor. It can be factorized in terms of $\mathbf{X}$, the matrix of the right-eigenvectors, and $\mathbf{L}$, the diagonal matrix of the eigenvalues, as $\mathbf{R} = \mathbf{X}\mathbf{L}\mathbf{X}^{\dagger}$. As such, its square root, i.e. the tensor $\mathbf{Q}$ such that $\mathbf{R} = \mathbf{Q}\mathbf{Q}^{\dagger}$ with $\mathbf{Q} = \mathbf{X}\sqrt{\mathbf{L}}$ exists and obeys the evolution equation

$$\frac{\partial \mathbf{Q}}{\partial t} + \mathbf{u}\cdot\nabla\mathbf{Q} = \mathbf{K}\mathbf{Q} - \frac{1}{\tau}\mathbf{Q}. \tag{2}$$

In this framework, the elastic energy can be expressed as a quadratic form in terms of $\mathbf{Q}$, $\mathcal{E}_{\mathrm{p}}(\mathbf{x},t) := \nu_{\mathrm{p}}/\tau\,\mathrm{tr}\left[\mathbf{Q}(\mathbf{x},t)\mathbf{Q}^{\dagger}(\mathbf{x},t)\right]$ while the production term can be written as $\Pi_{\mathrm{p}}(\mathbf{x},t) = 2\nu_{\mathrm{p}}/\tau\,\mathrm{tr}\left[\mathbf{K}(\mathbf{x},t)\mathbf{Q}(\mathbf{x},t)\mathbf{Q}^{\dagger}(\mathbf{x},t)\right]$. In other words the adoption of $\mathbf{Q}$ as descriptor for the polymers allows the energy to be expressed as the L^2-norm of the relevant field. Under homogeneity assumption, the mean elastic energy equation takes the form $d\langle\mathcal{E}_{\mathrm{p}}(t)\rangle/dt = \langle\Pi_{\mathrm{p}}\rangle(t) - 2/\tau\langle\mathcal{E}_{\mathrm{p}}\rangle(t)$. For the velocity, the mean kinetic energy density, $\langle\mathcal{E}_{\mathrm{k}}(t)\rangle = 1/2\,\langle\mathbf{u}\cdot\mathbf{u}\rangle(t)$, follows a balance equation which reads $d\langle\mathcal{E}_{\mathrm{k}}\rangle(t)/dt = \langle W\rangle(t) - \langle\varepsilon_{\mathrm{N}}\rangle(t) - \langle\Pi_{\mathrm{N}}\rangle(t)$

*DIEM, Università di Bologna, 47100 Forlì, Italy.
E-mail: e.deangelis@unibo.it
**Dipartimento di Meccanica e Aeronautica, Università di Roma La Sapienza, 00184 Roma, Italy
E-mail: carlomassimo.casciola@uniroma1.it

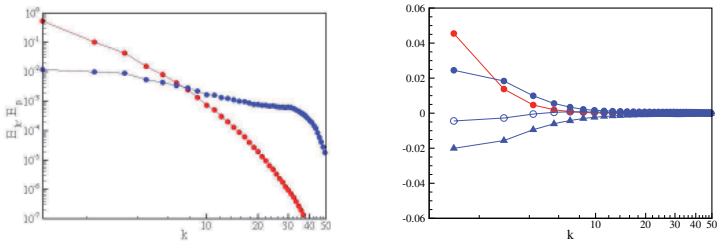

Figure 1: Left: Spectra of the kinetic (red [on line]) and polymer free energy (blue [on line]).
Right: Spectral balance 2(blue curves), filled circles represent the stretching term H_{sp}, the emply circles the convective term H_{cp} and the triangles the dissipation. Superimposed is the stretching term H_{sk} of the kinetic energy (red).

. HI turbulence was simulated via a spectral code on 96^3 points for the dealiasing procedure. The corresponding Newtonian case, i.e. with same viscosity and energy input, presented a $Re_\lambda = 80$ and the Deborah number based on the Newtonian Kolmogorov time scale was equal to 5.

Moreover the three-dimensional spectrum of elastic energy may be defined from the correlation tensor of the field $\mathbf{Q}$, $\mathbf{C}_\mathrm{p}(\mathbf{r},t) := \langle \mathbf{Q}(\mathbf{x},t)\mathbf{Q}^\dagger(\mathbf{x}+\mathbf{r},t)\rangle$, as

$$E_\mathrm{p}^{(3D)}(\mathbf{k},t) = \frac{1}{(2\pi)^3}\frac{\nu_\mathrm{p}}{\tau}\int_{\mathbf{R}^3} \mathrm{tr}\,[\mathbf{C}_\mathrm{p}(\mathbf{r},t)]\, e^{\mathbf{I}\mathbf{k}\cdot\mathbf{r}}\, d^3\mathbf{r} \tag{3}$$

where $\mathbf{k}$ is the wave-vector. Equation (3) implies the spectral decomposition

$$\langle \mathcal{E}_\mathrm{p}(t)\rangle = \int_{\mathbf{R}^3} E_\mathrm{p}^{(3D)}(\mathbf{k},t)\, d^3\mathbf{k} = \int_0^\infty E_\mathrm{p}(k,t)\, dk\,. \tag{4}$$

where the spectrum of elastic energy is defined, as usual, as an integral on the solid angle Ω of $E^{(3D)}$. The corresponding evolution equation is obtained by the product of the Fourier transform of equation (2) with the conjugate transpose of the Fourier transform of $\mathbf{Q}$ and reads

$$\frac{d}{dt}E_\mathrm{p}(k,t) = H_\mathrm{cp}(k,t) + H_\mathrm{sp}(k,t) - \frac{2}{\tau}E_\mathrm{p}(k,t)\,, \tag{5}$$

where H_cp and H_sp come from the convective term, $\mathbf{u}\cdot\nabla\mathbf{Q}$, and the stretching term, $\mathbf{K}\mathbf{Q}$, in equation (2), respectively. In equation (5), the contribution, H_cp, whose integral over k vanishes, has the meaning of a redistribution of spectral energy among different bands with no net change in the overall energy content.

On the contrary, the stretching term $H_{\rm sp}$ represents a net injection of energy into the polymeric sub-structure. For a steady state (5) yields the equation

$$\int_0^\infty H_{\rm sp}(k)\,dk = \frac{2}{\tau}\int_0^\infty E_{\rm p}(k)\,dk \geq 0\,. \tag{6}$$

For the macroscopic field the evolution equation for the spectrum

$$\frac{d}{dt}E_{\rm k}(k,t) = H_{\rm ck}(k,t) + H_{\rm sk}(k,t) - 2\nu k^2 E_{\rm k}(k,t) + F(k,t)\,, \tag{7}$$

where F is the energy from the forcing, reduces at steady state

$$-\int_0^\infty H_{\rm sk}(k)\,dk + 2\nu\int_0^\infty k^2 E_{\rm k}(k,t)\,dk = \int_0^\infty F(k)\,dk \geq 0\,. \tag{8}$$

According to Lumley time criterion, [3], the range of scales where the polymers can be stretched by the turbulence is confined below the scale $r_{\rm L} = \sqrt{\langle\varepsilon_{\rm T}\rangle\tau^3}$. In the present simulation $r_{\rm L} = 0.41$ and this value is consistent with the crossover between the spectra, see left panel of figure 1, which identifies, following De Gennes[3], the k values where polymers are most effective.

At larger Reynolds numbers, such that $k_{\rm F} << k_{\rm L} << k_\eta$, one should expect a classical inertial range, with no polymer effect in $k_{\rm F} << k << k_{\rm L}$ with the energy flux given by the input power $\langle W\rangle = \langle\varepsilon_{\rm T}\rangle$. Below, one should observe a mixed inertial-elastic range, where a leaking cascade progressively reduces the total energy flux. Equations (6) and (8) lead to the fact that

$$-\int_0^\infty H_{\rm sk}(k)\,dk \;\;=\;\; \int_0^\infty H_{\rm sp}(k)\,dk\,. \tag{9}$$

It should be stressed that, for each k, $-H_{\rm sk}(k) \neq H_{\rm sp}(k)$, as shown by the right panel of figure 1, even if for a steady state, the energy removed from the kinetic field by the polymers is positive and exactly the same amount of energy feeds the micro-structure, as shown by equation (9).

References

[1] C.M. CASCIOLA, E. DE ANGELIS, *Energy transfer in turbulent polymer solutions*, Journal of Fluid Mechanics, **581**, 419 (2007).

[2] E. DE ANGELIS, C.M. CASCIOLA, R. BENZI, R. PIVA, *Homogeneous isotropic turbulence in dilute polymer solutions* Journal of Fluid Mechanics, **531**, 1 (2005).

[3] K.R. SREENIVASAN, C.M. WHITE, *The onset of drag reduction by dilute polymer additives and the maximum drag reduction asymptote*, Journal of Fluid Mechanics, **409**, 149 (2000).

Coherent enstrophy production and turbulent dissipation in two-dimensional turbulence, with and without walls, in the vanishing viscosity limit

MARIE FARGE*, ROMAIN NGUYEN VAN YEN*, KAI SCHNEIDER**

Abstract. *The viscosity dependence of two-dimensional turbulence is studied by means of direct numerical simulation. We consider either periodic or no-slip boundary conditions. We compare the Navier-Stokes solutions to those of the regularized Euler equations. The regularization is perfomred at each time step by applying the wavelet-based CVS filter which splits turbulent fluctuations into coherent and incoherent contributions. We show that for $Re > 10^5$ the dissipation of coherent enstrophy tends to become independent of Re, while dissipation of incoherent enstrophy grows logarithmically with Re. In the wall bounded case we observe an additional production of enstrophy at the wall. As a result coherent enstrophy diverges when Reynolds tends to infinity, however its time derivative seems to remain bounded.*

Keywords: two-dimensional turbulence, vanishing viscosity limit, no-slip walls.

In the fully-developed turbulent regime one observes that dissipation becomes independent on the molecular viscosity of the fluid for three-dimensional incompressible flows when Reynolds number is larger than 10^5. This has been confirmed by numerical experiments [1]. Here, we will study if incompressible two-dimensional turbulent flows may exhibit a similar behaviour in the vanishing viscosity limit.

For this, we apply the coherent vorticity simulation (CVS) filter, introduced in [2], to incompressible decaying two-dimensional turbulence, in periodic and wall-bounded domains, for Reynolds numbers varying from 10^3 to 10^7. CVS expands the vorticity field into an orthogonal wavelet basis and splits the flow into two orthogonal contributions: a coherent and an incoherent flow. The coherent vorticity field and the induced coherent velocity field are reconstructed from the largest wavelet coefficients, which correspond to the coherent vortices

*LMD-CNRS, Ecole Normale Supérieure, 24 rue Lhomond, 75231 Paris cedex 5, France.
E-mail: farge@lmd.ens.fr
*LMD-CNRS, Ecole Normale Supérieure, 24 rue Lhomond, 75231 Paris cedex 5, France.
E-mail: rnguyen@lmd.ens.fr
** M2P2-CNRS & CMI Université de Provence, 39 rue Joliot–Curie, 13453 Marseille cedex 13, France.
E-mail: kschneid@cmi.univ − mrs.fr

and are the only components advanced in time. In previous work [3], we have shown that applying the CVS filter at each time step to the inviscid Burgers equation models dissipation.

We examine the viscosity dependence of the solutions of the two-dimensional Navier-Stokes equations and we compare them to those of the two-dimensional Euler equations regularized by the CVS filter at each time step. The solutions of both equations are computed with a parallelized fully-dealiased pseudo-spectral code (written in C++), using a fourth-order Runge-Kutta time scheme and up to 8192^2 grid points, on the IBM BlueGene/P of IDRIS-CNRS with up to 1024 processors. For the wall-bounded case we consider a circular domain and use a volume penalization method to impose no-slip boundary conditions, as in [4].

In the periodic case (Fig. 1, left), we observe that the enstrophy dissipation vanishes like $(\ln Re)^{-1}$ in the inviscid limit, which confirms previous results [5]. In contrast, dissipation of coherent enstrophy does not vanish in the same limit and tends to become independent of Re.

For the wall-bounded case (Fig. 1, right), we observe an additional production of enstrophy at the wall. As a result, coherent enstrophy diverges when $Re \to \infty$, but its time derivative seems to remain bounded independently of Re. This may indicate that a balance has been established between coherent enstrophy production at the wall and coherent enstrophy dissipation.

In conclusion, the above results for two-dimensional turbulence, investigated for Reynolds numbers up to 10^7, suggest that the dissipation of coherent enstrophy becomes constant when $Re > 10^5$. We propose to define this as the onset of the fully-developed turbulent regime where viscous dissipation, due to the fluid's molecular viscosity, becomes negligible in front of the turbulent dissipation due to the flow nonlinear dynamics of Euler equations.

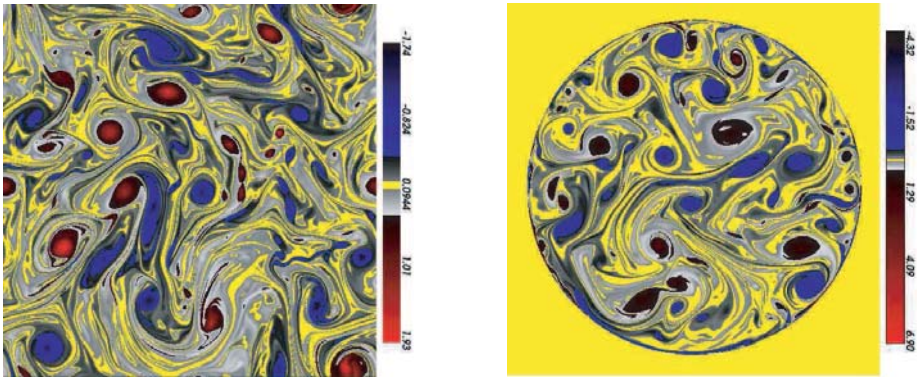

Figure 1: Vorticity field at $Re = 10^4$, $t \simeq 60$ turnover times. Left: periodic domain. Right: circular domain.

Acknowledgements: We thankfully acknowledge financial from the Association CEA-Euratom contract N^0 V.3258.001.

References

[1] KANEDA Y., ISHIHARA T., YOKOKAWA M., ITAKURA K. AND UNO A., *Energy dissipation rate and energy spectrum in high resolution direct numerical simulations of turbulence in a periodic box*, Phys. Fluids, **15** (2003), L21-L24.

[2] FARGE M., SCHNEIDER K. AND KEVLAHAN N., *Non–Gaussianity and Coherent Vortex Simulation for two-dimensional turbulence using an adaptive orthonormal wavelet basis*, Phys. Fluids, **11** (1999), 2187-2201.

[3] NGUYEN VAN YEN R., FARGE M., KOLOMENSKIY D., SCHNEIDER K. AND KINGSBURY N., *Wavelets meet Burgulence: CVS filtered Burgers equation*, Physica D, **237** (2008), 2151-2157.

[4] NGUYEN VAN YEN R., FARGE M. AND SCHNEIDER K., *Wavelet regularization of a Fourier-Galerkin method for solving the 2D incompressible Euler equations*, ESAIM: Proc., (2009), submitted.

[5] SCHNEIDER K. AND FARGE M., *Decaying two-dimensional turbulence in a circular container*, Phys. Rev. Lett., **95** (2005), 244502.

[6] TRAN C.V. AND DRITSCHEL D.G., *Vanishing enstrophy dissipation in two-dimensional Navier-Stokes turbulence in the inviscid limit*, J. Fluid Mech., **559** (2006), 107-116.

Kinetic Equations for Turbulent Vorticity Statistics

RUDOLF FRIEDRICH*, MICHAEL VOSSKUHLE*, OLIVER KAMPS*

Abstract. *We investigate kinetic equations for the description of vorticity statistics in two dimensional turbulence. The assessment of conditional expectations of the turbulent velocity field either by means of direct numerical simulations or by modeling allows one to formulate stochastic processes describing the Lagrangian dynamics of point particles.*
Keywords: kinetic equation, turbulent vorticity.

Recent experimental progress in particle tracking in turbulent fields has renewed the interest in the N-point statistics of turbulent velocity and vorticity fields. Central quantities are the Eulerian probability distributions (pdf's) for the vorticity field $\omega(\mathbf{x},t)$,

$$f(\{\omega_i,\mathbf{x}_i\},t) = f(\omega_1,\mathbf{x}_1;..;\omega_N,\mathbf{x}_N;t) = \Pi_{i=1}^N < \delta(\omega_i - \omega(\mathbf{x}_i,t) > \quad , \quad (1)$$

or the corresponding Lagrangian pdf's. The brackets denote a suitably defined statistical average.

The probability distributions (1) obey an infinite set of evolution equations relating distributions of N points to the one of $(N+1)$ points [1]. Novikov [2] has pointed out that the introduction of conditional averages formally lead to closed kinetic equations. In [3] the case of the single point vorticity pdf has been studied. In the present contribution we pursue this approach for the statistics of two dimensional turbulence, which, as Kraichnan has pointed out in his seminal work [4], can exhibit an inverse energy cascade. Our procedure will allow us to make contact with the *tetrad models* [5], [6], which have revealed geometric characteristics of turbulence beyond pure scaling properties.

We consider a two dimensional fluid motion, which is exposed to white noise stirring with spatial correlation $< F(\mathbf{x},t)F(\mathbf{x}',t') >= 2Q(\mathbf{x}-\mathbf{x}')\delta(t-t')$:

$$\left[\frac{\partial}{\partial t} + \mathbf{u}(\mathbf{x},t)\cdot\nabla_x\right]\omega(\mathbf{x},t) = \nu\Delta_x\omega(\mathbf{x},t) - \gamma\omega(\mathbf{x},t) + F(\mathbf{x},t) \quad (2)$$

*Institute of Theoretical Physics, Westfälische Wilhelms- Universität, Wilhelm-Klemm-Str. 9, G-48149 Münster.
E-mail: fiddir@uni-muenster.de
*E-mail: michel.v@uni-muenster.de
*E-mail: okamp@uni-muenster.de

The statistical properties of the turbulence is described by the hierarchy of evolution equations for the vorticity probability distributions:

$$(\frac{\partial}{\partial t}+\sum_i \nabla_{\mathbf{x}_i}\cdot\mathbf{U}(\mathbf{x}_i;\{\omega_l,\mathbf{x}_l\})f(\{\omega_l,\mathbf{x}_l\};t)=\nu\sum_i\Delta_{x_i}f(\{\omega_l,\mathbf{x}_l\};t)+$$
$$\left[\gamma\sum_j\frac{\partial\omega_j}{\partial\omega_j}+\sum_{jk}\frac{\partial^2}{\partial\omega_j\partial\omega_k}\left(Q(\mathbf{x}_j-\mathbf{x}_k)-\delta_{jk}\varepsilon(\mathbf{x}_l|\{\omega_l,\mathbf{x}_l\})\right)\right]f(\{\omega_l,\mathbf{x}_l\};t) \quad (3)$$

We have introduced the conditional velocities

$$\mathbf{U}(\mathbf{x}|\omega_1,\mathbf{x}_1;..;\omega_N,\mathbf{x}_N)=\int d\omega'\omega'\mathbf{u}(\mathbf{x}-\mathbf{x}')p(\omega',\mathbf{x}'|\omega_1,\mathbf{x}_1;...;\omega_N,\mathbf{x}_N) \quad (4)$$

as well as the conditional dissipation anomaly field $\varepsilon(\mathbf{x}|\omega_1,\mathbf{x}_1;...;\omega_N,\mathbf{x}_N)$, where $p(\omega',\mathbf{x}'|\omega_1,\mathbf{x}_1;...;\omega_N,\mathbf{x}_N)$ denotes the conditional pdf.

Assuming that the conditional expectation values are given as functions of ω_i, $\mathbf{x}_i$ the kinetic equation (3) can be interpreted as a Fokker-Planck equation for $f(\{\omega_i,\mathbf{x}_i\}),t)$ with the set of Langevin equations

$$\begin{aligned}\dot{\mathbf{x}}_i &= \mathbf{U}(\mathbf{x}_i|\{\omega_j,\mathbf{x}_j\})+\eta_i(t)\\ \dot{\omega}_i &= -\gamma\omega_i+H(\mathbf{x}_i,t)\end{aligned} \quad (5)$$

The fluctuating forces $H(\mathbf{x}_i,t)$ and $\eta_i(t)$ are Gaussian white noise forces, whose statistical characteristics follow from eq. (3).

The conditional velocity fields can be taken from numerical solutions of the vorticity equation. Figure (1) exhibits an example obtained from a 1024×1024 simulation of forced two dimensional turbulence as described in [7]. The topology of the obtained fields reminds one of the velocity field generated by point vortices, which suggests to investigate *stochastic point vortex models*.

On the other side it is instructive to model the conditional velocity fields. The simplest approach is to take the conditional probability distribution on the basis of a Gaussian approximation. In this case the conditional velocity field can be evaluated explicitly to yield

$$\mathbf{U}(\mathbf{x}|\{\omega_j,\mathbf{x}_j\})=\sum_{i,j}\mathbf{e}_z\times\nabla_x\chi(\mathbf{x}-\mathbf{x}_i)C^{-1}(\mathbf{x}_i-\mathbf{x}_j)\omega_j \quad (6)$$

where $C(\mathbf{x}_i-\mathbf{x}_j)=<\omega(\mathbf{x}_i,t)\omega(\mathbf{x}_j,t)>$ is the vorticity correlation tensor and the stream function is determined according to $\Delta_x\chi(\mathbf{x}-\mathbf{x}_i)=-C(\mathbf{x}-\mathbf{x}_i)$. The conditional velocity field is a superposition of *dressed* point vortices, i.e. vortices whose radial velocity profiles are modified.

We have investigated the Langevin equation (5) using the Gaussian approximation (6) for three points in a way similar to the treatments of [5] and [6].

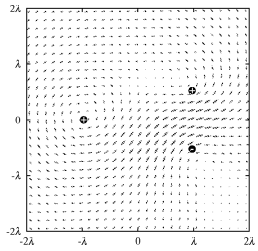

Figure 1: Conditional velocity field $\mathbf{U}(\mathbf{x}|\omega_1,\mathbf{x}_1;\omega_2,\mathbf{x}_2;\omega_3,\mathbf{x}_3)$ from DNS

We obtain similar phenomena concerning the evolution of triangular configurations. Scaling behaviour of the size is under current investigation. It may be that in order to obtain a correct behaviour of the size one has to include terms proportional to $\omega_i\omega_j$ in (6). The presence of such terms are responsible for the breaking of time symmetry and detailed balance, and the emergence of the inverse cacade. This can explicitly be shown considering the case of two points.

References

[1] MONIN A.S. AND YAGLOM A.M., *Statistical Fluid Mechanics*, Dover Publications, Mineola (2007).

[2] NOVIKOV E. A., *A new approach to the problem of turbulence, based on the conditionally averaged Navier-Stokes Equation*, Fluid Dynamics Research **12** (1993), 107.

[3] WILCZEK,M. AND FRIEDRICH, R. *Dynamical origins for non-Gaussian vorticity distributions in turbulent flows*, Phys. Rev. **E 80** (2009), 016316.

[4] KRAICHNAN R., *Inertial ranges in two-dimensional turbulence*, Phys. Fluids **10** (1967), 1417.

[5] CASTIGLIONE P. AND A. PUMIR A., *Evolution of triangles in a two-dimensional turbulent flow*, Phys. Rev. **E 64** (2001), 056303.

[6] A. PUMIR A., B.I. SHRAIMAN B.I. AND M. CHERTKOV M., *Geometry of Lagrangian Dispersion in Turbulence,*, Phys. Rev. Lett. **85** (2000), 5324.

[7] KAMPS,O. AND FRIEDRICH, R., *Lagrangian statistics in forced two dimensional turbulence*, Phys. Rev. **E 78** (2008), 036321.

The simplest interaction

MASSIMO GERMANO*

Abstract. *In the paper that we propose to the attention of the Euromech Colloquium we will study the simplest decomposition of a turbulent field and the related simplest interaction of turbulent scales. The large scale filtering operator is simply given by the two-point average in space and the associated fluctuation is given by the two-point difference. In the paper we will present the general properties of this simple decomposition and the related properties of the associated interaction between the sum and the difference of a turbulent field.*

Keywords: Turbulence structure, Scale interaction.

The interest for the universal properties of turbulence dates probably to the first studies on it, but the great step on is undoubtedly due to the Kolmogorov assumptions, see Frisch [1] for a recent presentation. The idea that the small scales of a turbulent flow are asymptotically provided with some geometric and dynamic universality has been very fruitful and plenty of useful results. During the years however some doubts on these assumptions have arisen and a more detailed exploration based on the exact Navier-Stokes equations, conducted in particular by Hill [2], have paved the way to a reexamination of many assumption concerning the isotropy, the homogeneity and the universality of the small turbulent scales, see Sreenivasan and Dhruva [3] and Frisch, Bec and Aurell [4]. One point in particular is the object of an extended study, the assumed statistical independence of the large and the small turbulent scales that recent papers have vigorously put on discussion. A simple exact relation equivalent to the Kolmogorov $4/5$ law pointed out by Hosokawa [5] and experimentally verified by Kholmyansky and Tsinober [6] put a lot of doubts on the assumed independence of large and small scales under the assumption of isotropic turbulent flows. The same happens for another exact relation derived by the present author [7] that generalize the Kolmogorov $4/5$ law to the case of homogeneous fields.

Consistently with Kolmogorov all these studies define as a small scale the difference of a turbulent quantity between two points. The simplest large scale associated to the two-point difference seems the two-point sum for a lot of reasons. First it is well known that given two random variables their sum and difference are statistically orthogonal, and in particular if they are jointly normal

*Dipartimento di Ingegneria Aeronautica e Spaziale, Politecnico di Torimo, Italy.
E-mail: massimo.germano@polito.it

they are independent. Secondly these particular linear combinations represent the simplest decomposition of a turbulent field. We remark that every approach to turbulence is based on a decomposition of the original turbulent field in two or more contributions. Due to the nonlinearity of the physical phenomena the different modes interact among them and exchange energy. The associated nonlinearity of the equations produces coupling terms between the different levels, and the study of such interactions is fundamental both to theory and to the practical computation of turbulent flows. The Reynolds decomposition, the spectral and the wavelets decompositions, the proper orthogonal decomposition, the large eddy decompositions based on hierarchies of filters are different formulations of such strategy. Multilevel and multiscale methods are more and more applied to the study of turbulence and the interest for simple decompositions, particularly in the physical space, is actually very high in order to extend the study of turbulent flows to nonhomogeneous situations.

Strangely enough the simple decomposition produced by the two-point sum in space and the associated difference has not received till now a similar interest. We remark that the simplest large eddy simulation of a turbulent field is that produced by the two-point average, see Germano [8], where it is shown that the subgrid quantities are intimately related to the two-point difference. This simple average is a useful tool to understand some peculiar aspects of the large eddy simulation and the duality between the two-point average and the two-point difference is important as regards the elementary interaction between large and small scales. We remark again that since the fundamental paper of Kolmogorov the statistical properties of the two-point difference have been explored in great detail both in the case of a velocity field and in the case of a passive scalar, but strangely enough the study of the statistical properties of the simplest large eddy scale, the two-point sum, has not received a similar attention. It is clear that in order to better understand the dependence and the interaction between large and small scales we need more information on the two-point sum, in particular as regards its relations with the two-point difference, and in this paper we will consider them together, the elementary dual faces of the turbulence representation. Main results are an equivalent form of the generalized inertial Kolmogorov law, and an equivalent form of the Yaglom [9] inertial law for passive scalars.

References

[1] FRISCH U., *Turbulence. The Legacy of A. N. Kolmogorov*, Cambridge University Press, (1995)

[2] HILL R. J., *Opportunities for use of exact statistical equations*, J. of Turbulence **7**, (2006), 43

[3] SREENIVASAN K. R. AND DHRUVA B., *Is there scaling in high Reynolds-number turbulence?*, Prog. Theor. Phys. Supp. **130**, (1998) 103

[4] FRISCH U., BEC J. AND AURELL E., *Locally homogeneous turbulence: Is it an inconsistent framework ?*, Phys. Fluids **17**, (2005), 081706

[5] HOSOKAWA I., *A paradox concerning the refined similarity hypothesis of Kolmorogov for isotropic turbulence*, Prog. Theor. Phys. **118**, (2007) 169

[6] KHOLMYANSKY M. AND A. TSINOBER A., *Kolmogorov* $4/5$ *law, nonlocality, and sweeping decorrelation hypothesis"*, Phys. Fluids **20**, (2008), 041704/4

[7] GERMANO M., *The elementary energy transfer between the two-point velocity mean and difference*, Phys. Fluids **19**, (2007), 085105/5.

[8] GERMANO M., *The two point average and the related subgrid model*, In: Turbulence and Shear Flow Phenomena TSFP-5. Conference Proceedings **1**,(2007), 309

[9] YAGLOM A. M., *On the local structure of the temperature field in a turbulent flow*, Dokl. Akad. Nauk SSSR **69**, (1949), 743

Scalar flux and scalar variance transfer in isotropic turbulence

TOSHIYUKI GOTOH*, TAKESHI WATANABE*

Abstract. *Statistics of a passive scalar flux and scalar variance transfer in homogeneous isotropic turbulence under the mean constant scalar gradient are studied by using very high resolution DNS. It is found that the spectrum of the scalar flux obeys Lumley's scaling $E_{u\theta} \propto k^{-7/3}$ in the inertial range and Nusselt number increases as $Nu \propto R_\lambda^2$ for $Sc = 1$. One point PDF of the scalar flux is negatively skewed and exponential. In order to analyze intermittency of transfer flux of the scalar variance to small scales, local scaling exponent $\zeta_p^{L\theta}(r)$ of the combined velocity-scalar structure functions $\left\langle (\delta u_r^L (\delta\theta_r)^2)^{p/3} \right\rangle \propto r^{\zeta_p^{L\theta}}$ is computed and compared to those of the velocity and scalar.*

Keywords: scalar turbulence, scalar flux, Nusselt Number, scaling exponents

We study statistics of a passive scalar flux $q = u_3\theta$ and inter-scale transfer flux of the variance of scalar increment $r^{-1}\delta u^L(\delta\theta)^2$ under a uniform mean scalar gradient $\Gamma = \langle \nabla_3 T \rangle$ for $Sc = 1$ by using the very high resolution DNS with grid points up to 2048^3 [1, 2]. The Taylor microscale Reynolds number R_λ is $174, 263, 468$, and 586.

Three dimensional spectrum of the scalar flux is shown in Fig. 1 and the compensated spectrum $\Gamma^{-1}\overline{\varepsilon}^{-1/3}k^{7/3}E_{u\theta}(k)$ is in the inset figure for $R_\lambda = 586$ [2]. The present DNS data supports the Lumley scaling, $E_{u\theta}(k) \propto k^{-7/3}$ [3].

A nondimensional measure of the scalar flux is the Nusselt number defined by $Nu = -\langle \theta u_3 \rangle \,/\, \kappa\Gamma$, where κ is the molecular diffusivity. Figure 2 shows that DNS data obey $Nu \propto R_\lambda^2$ irrespective of Schmidt (Prandtl) number [4], while experimental data follow $Nu \propto R_\lambda^{1.09}$ in which the power is obtained by the least square fit (note that $Pe_\lambda = u'\lambda/\kappa = R_\lambda Sc$) [5]. If we neglect the diffusion effects, then the scalar fluctuation θ is given by time integral of the Lagrangian velocity $u_3(\mathbf{x}, t|s)$ along fluid trajectory and we can compute the mean scalar flux as

$$\langle \theta(\mathbf{x},t) u_3(\mathbf{x},t) \rangle = -\Gamma \int_{-\infty}^{t} \langle u_3(\mathbf{x},t|s) u_3(\mathbf{x},t|t) \rangle \, \mathrm{d}s = -\Gamma u'^2 T_L = -C_q \Gamma u' L$$

*Nagoya Institute of Technology, Nagoya, 466-8555, Japan. JST CREST.
E-mail: gotoh.toshiyuki@nitech.ac.jp, E-mail: watanabe@nitech.ac.jp

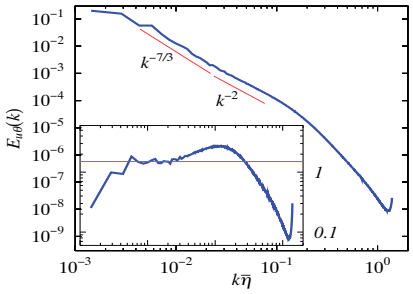

Figure 1: Three dimensional spectrum of the scalar flux. Inset figure shows the compensated three dimensional spectrum $\Gamma^{-1}\bar{\varepsilon}^{-1/3}k^{7/3}E_{u\theta}(k)$ for $R_\lambda = 586$ at $Sc = 1$.

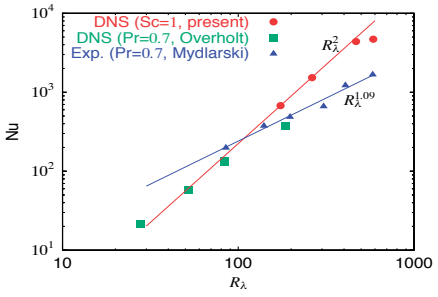

Figure 2: Variation of the Nusselt number with Reynolds number.

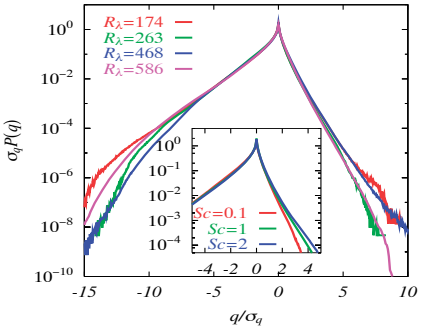

Figure 3: PDFs of scalar flux for $R_\lambda = 174, 263, 468, 586$ at $Sc = 1$. Inset figure shows scalar flux PDF for $Sc = 0.1, 1, 2$ at $R_\lambda = 170$.

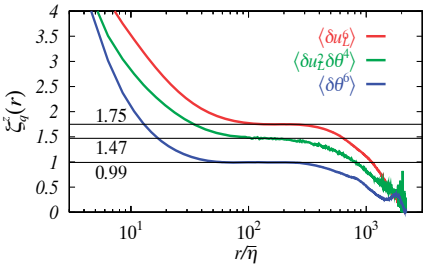

Figure 4: Local scaling exponents $\zeta_6^L, \zeta_6^{L\theta}$, and ζ_6^θ for $R_\lambda = 586, Sc = 1$. Plateau value of each curve is $\zeta_6^L = 1.75 \pm 0.05$, $\zeta_6^{L\theta} = 1.47 \pm 0.02, \zeta_6^\theta = 0.99 \pm 0.05$.

where C_q is a nondimensional positive constant of order one, and thus we obtain $Nu = -\langle \theta u_3 \rangle \,/\, \kappa\Gamma = C_q R_L Sc \propto R_\lambda^2$.

Figure 3 shows normalized probability density functions of the scalar flux fluctuations for $R_\lambda = 174, 263, 468, 586$, and inset figure shows PDFs for $Sc = 0.1, 1, 2$ at $R_\lambda = 170$. The curves collapse well onto a single curve, suggesting that the scalar flux PDF is insensitive to R_λ and very weakly dependent on Sc. It can be found from a simple argument on the dimensional ground that PDF of q is of the form of $P(q)dq \propto |q|^{-1/2}\exp(-c_\pm q/\sigma_q)$, where σ_q is the standard deviation of q and $c_\pm$ are nondimensional positive constants of the order of unity. Asymmetry of the scalar flux PDF is due to $c_- < c_+$, and $c_- = 0.77, c_+ = 1.85$ for the present DNSs.

The scalar variance is transferred to small scales by the action of fluid motion and the scalar transfer in the inertial convective range is well described

by the 4/3 law $S_3^{L\theta} = \left\langle [\delta u_r^L (\delta\theta_r)^2]^{p/3} \right\rangle \rangle|_{p=3} = -(4/3)\overline{\chi} r$, where $\overline{\chi}$ is the average rate of the scalar dissipation. Then the average rate of transfer of the scalar variance across scale r is estimated as $\partial S_3^{L\theta}/\partial r = -(4/3)\overline{\chi}$, and from this observation we may regard $S_3^{L\theta}/r$ as a surrogate transfer flux of the variance of the scalar increment (a passive scalar analogue in real space to the kinetic energy transfer flux in the wavenumber space). It is important and interesting to examine intermittency of the transfer flux of the scalar increment variance and to compare with that of the transfer flux of the kinetic energy $S_3^L/r = r^{-1}\left\langle [(\delta u_r^L)^3]^{p/3} \right\rangle \rangle (= -(4/5)\overline{\varepsilon})$. For this purpose we have computed the local scaling exponents of the combined velocity-scalar structure functions and plotted in Fig. 4 as well as those of the structure functions of the velocity and scalar alone; $S_6^L \propto r^{\zeta_6^L}, S_6^{L\theta} \propto r^{\zeta_6^{L\theta}}, S_6^{\theta} \propto r^{\zeta_6^{\theta}}$ for $R_\lambda = 586$ and $Sc = 1$. It is seen that each curve has a single plateau in the range about $100 < r/\eta < 300$, and $\zeta_6^{\theta} < \zeta_6^{L\theta} < \zeta_6^L$, which means that the transfer flux of the passive scalar is more intermittent than that of the kinetic energy but less intermittent than the passive scalar. The value $\zeta_6^{L\theta} = 1.47 \pm 0.02$ obtained by the present DNS is slightly lower than the experimental value 1.52 [5]. We will present several results on the scaling exponents.

T.G. and T.W's work were supported by Grant-in-Aid for Scientific Research No.21360082 and No.20760112, respectively, from the Ministry of Education, Culture, Sports, Science and Technology of Japan. The authors thank the Theory and Computer Simulation Center of the National Institute for Fusion Science (NIFS08KTAL014) for their computational support. T.W. thanks Tatematsu foundation for financial support.

References

[1] WATANABE T. AND GOTOH T. *Intermittency in passive scalar turbulence under the uniform mean scalar gradient* Phys. Fluids **18**, (2006), 058105.

[2] WATANABE T. AND GOTOH T. *Scalar flux spectrum in passive scalar convected by homogeneous turbulence under a uniform mean scalar gradient* Phys. Fluids, **19**, (2007), 121701.

[3] LUMLEY J. L. *The Spectrum of Nearly Inertial Turbulence in a Stably Stratified Fluid* J. Atmos. Sci., **21**, (1964), 99-102.

[4] OVERHOLT M. R. AND POPE S. *Direct numerical simulation of a passive scalar with imposed mean gradient in isotropic turbulence* Phys. Fluids, **8**, (1996). 3128–3148.

[5] MYDLARSKI L. *Mixed velocity-passive scalar statistics in high-Reynolds-number turbulence* J. Fluid Mech. **475**, (2003), 173-203.

Pair Dispersion in a Shell Model Field

MOGENS H. JENSEN*, BO S. MADSEN*, SAGAR CHAKRABORTY**

Abstract. *Pair dispersion is studied in a turbulent flow, generated by Fourier transforming the dynamics of the GOY shell model into real space. At very high Reynolds numbers we investigate the cross-over scale between the Batchelor and Richardson regimes. In particular we study how the cross over time scales with the initial separations of a particle pair.*

Keywords: Turbulent relative dispersion, Richardson-Obukhov law, Batchelor's scaling law, cross-over time.

We study pair dispersion in a turbulent flow, applying the GOY shell model [1] and Fourier transforming the complex shell-velocities back into real space [2]. This procedure results in strongly turbulent velocity field (Reynolds numbers up to $\sim 10^{14}$) where the dispersion of pair of particles can be easily studied by advecting the passive particles in the velocity field. In particular, we can investigate how the dispersion depends on the initial separations.
From the work of Richardson[3] (and subsequently Obukhov[4]), we have the well-known Richardson-Obukhov law (valid in the inertial range): $\langle r(t)^2 \rangle = g\varepsilon t^3$. Here, $r(t)$ is the separation of the pair at time t, ε is the energy dissipation rate per unit mass, and g is termed as the Richardson constant. Batchelor [5] extended the study to both short-time and intermediate-time, and obtained

$$\left\langle |\mathbf{r}(t)^2 - \mathbf{r}_0^2| \right\rangle = \begin{cases} \frac{11}{3} C_2 \varepsilon^{2/3} r_0^{2/3} t^2 & t \ll t_0 \\ g\varepsilon t^3 & t \gg t_0 \end{cases}, \tag{1}$$

where C_2 is the Kolmogorov constant for the longitudinal second-order velocity structure function and

$$t_0 \equiv \left(\frac{r_0^2}{\varepsilon} \right)^{1/3}, \tag{2}$$

the classical correlation time of an eddy of size r_0, is the time for which a particle-pair "remembers" its initial separation. t_0 is also called Batchelor time.

*Niels Bohr Institute, Blegdamsvej 17, DK-2100 Copenhagen. Denmark.
E-mail: mhjensen@nbi.dk
*Niels Bohr Institute, Blegdamsvej 17, DK-2100 Copenhagen. Denmark.
E-mail: bomadsen@fys.ku.dk
**Niels Bohr International Academy, Blegdamsvej 17, DK-2100 Copenhagen. Denmark.
E-mail: sagar@nbi.dk

We have numerically investigated this "cross-over time" between the two scalings, $\sim t^2$ and $\sim t^3$, and investigated how it is related to r_0. In what follows, we shall mention the first relation in equation (1) as Batchelor's scaling law; the second one is obviously the Richardson-Obukhov law.
Interestingly, with our simulations, both scalings are clearly visible as shown by a representative figure in the left panel of figure (1). Please note that we have plotted $\left\langle |\mathbf{r}(t) - \mathbf{r}_0|^2 \right\rangle$ and not $\left\langle |\mathbf{r}(t)^2 - \mathbf{r}_0^2| \right\rangle$ on the y-axis. This is just to make contact with the experimental results[6] which demonstrate that the correlation between the initial separation and the relative velocity of the pair may not be neglected when the flow is not perfectly homogeneous. However, the GOY model— by construction— is a shell model of a perfectly homogeneous and isotropic turbulence. So, within the paradigm of shell models, probably it doesn't make much of a difference if one chooses to work with $\left\langle |\mathbf{r}(t)^2 - \mathbf{r}_0^2| \right\rangle$.

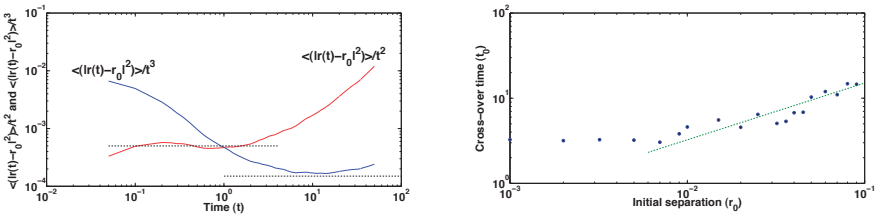

Figure 1: *Left figure*: the initial separation r_0 is 10^{-4} and the data are averaged over 10000 different simulations. One can distinctly note the presence of both the Richardson-Obukhov law and the Batchelor's scaling law. The cross-over time t_0 is somewhere in the third decade on the x-axis. The deviation of the blue curve from Richardson-Obukhov scaling at higher times is due to the fact that the pair-separations are no longer in the inertial regime. *Right figure:* the cross-over times t_0 plotted the initial pair-separations r_0. The dashed line has the theoretical slope predicted by Batchelor.

With no knowledge of the exact functional dependence of $\left\langle |\mathbf{r}(t) - \mathbf{r}_0|^2 \right\rangle$ on various parameters of the flow, it is quite a tough task to exactly locate t_0. However, we can use the following rather crude but effective method to see whether equation (2) is validated by our simulations. To investigate where the crossover happens, we found the slope of the blue curve in figure (1) at various points on it. Obviously, when the slope comes close to zero, we are in Richardson-Obukhov scaling regime. As the crossover happens before the slope is zero, we decide on the following algorithm: determine the time corresponding to the point where the slope is -0.5 and decide to call it t_0; repeat the procedure for the curves with various different r_0. We have used the post-processed data generated this way to get right panel of figure (1) where we plot the cross-

over times t_0 versus the initial pair-separations r_0. One can note the excellent agreement of the data with the theoretical prediction (the dashed line). It is a remarkable achievement for a model as simple as GOY shell-model of turbulence.
Similar result is obtained if one repeats the aforementioned algorithm for the red curve in figure (1) focusing on the Batchelor's scaling regime.
Another way to find the relation between the r_0 and t_0 comes from the fact that Richardson-Obukhov scaling is $\langle r^2 \rangle = g\varepsilon t^3$ while Batchelor considered $\langle |\mathbf{r}(t)^2 - \mathbf{r}_0^2| \rangle$. So, if we plot $\langle r^2 \rangle$ and $\langle |\mathbf{r}(t)^2 - \mathbf{r}_0^2| \rangle$ versus time, they will become indistinguishable when Richardson-Obukhov scaling sets in and this will happen around t_0 for the corresponding r_0. Thus, one can conveniently devise an algorithm to find t_0 in this case. Though we do not supply a figure here, we just mention that from this indirect method too equation (2) stands validated.
In the closing, we mention that this is probably for the first time that a shell-model of turbulence has shown the simultaneous existence of both the Richardson-Obukhov and the Batchelor regimes in turbulent pair dispersion. Whereas devising a better method of finding t_0 would be worth investigating, the temporal extent over which these laws are valid can easily be increased if one uses a larger number of shells.

References

[1] BOHR T., JENSEN M. H., PALADIN G. AND VULPIANI A., *Dynamical Systems Approach to Turbulence*, Cambridge University Press, Cambridge (1998).

[2] JENSEN M. H., *Multiscaling and structure functions in turbulence: an alternative approach*, Phys. Rev. Lett., **83** (1999), 76.

[3] RICHARDSON L. F., *Atmospheric diffusion shown on a distance-neighbour graph*, Proc. R. Soc. London A, **110** (1926), 709.

[4] OBUKHOV A. M., *On the distribution of energy in the spectrum of turbulent flow*, Izv. Akad. Nauk SSSR, Ser. Geogr. Geofiz., **5** (1941), 453.

[5] BATCHELOR G. K., *The application of the similarity theory of turbulence to atmospheric diffusion*, Q. J. R. Meteo. Soc., **76** (1950), 76.

[6] OUELLETTE N., XU H., BOURGOIN M. AND BODENSCHATZ E., *An experimental study of turbulent relative dispersion models*, New Journal of Physics, **8** (2006), 109.

Constraints on energy distribution in the rotating Boussinesq system

SUSAN KURIEN*

Abstract. *Numerical and phenomenological studies of the small scale distribution of energy in three regimes in the parameter space of Rossby and Froude numbers are presented for high Reynolds number rotating and stably stratified flows in the Boussinesq approximation. We exploit regimes in which near-linearization of the potential vorticity constrains the distribution of horizontal kinetic energy and potential energy in fourier space. Data from high-resolution simulations of the Boussinesq equations spanning a wide range of Rossby and Froude numbers are used to check our predictions. We show that the distribution of horizontal kinetic energy and potential energy in wavenumber space depends on both the ratio $\frac{Ro}{Fr}$ as well as on the aspect ratio $\frac{k_z}{k_h}$ of the wavevector $\boldsymbol{k}$. These results do not require projections or filtering of the Boussinesq solutions, and thus may be useful in applications to experimental and empirical data.*

Keywords: Boussinesq, rotation, stratification, turbulence.

The potential vorticity fluctuation q for the rotating Boussinesq equations is given in its non-dimensional form in physical and spectral space by:

$$\begin{aligned} q &= \boldsymbol{\omega}\cdot\nabla\theta + Ro^{-1}\frac{\partial\theta}{\partial z} - Fr^{-1}\omega_3 \\ \tilde{q} &= \tilde{\boldsymbol{\omega}}\cdot\tilde{\nabla}\tilde{\theta} - iRo^{-1}k_z\tilde{\theta} + iFr^{-1}k_h\tilde{u}_h \end{aligned} \tag{1}$$

where Ro (Rossby) and Fr (Froude) numbers are the non-dimensional rotation rate and bouyancy frequencies respectively, $\boldsymbol{\omega}$ is the local vorticity, θ is the scalar (temperature) dimensioned as the velocity. In what follows we will assume that viscosity $\nu \to 0$ and scalar diffusion coefficient $\kappa \to 0$ such that Prandtl number $Pr = \nu/\kappa = 1$, and the force $\mathcal{F}$ is confined to the lowest modes. Thus we assume a conventional 'inertial-range' of turbulent scales wherein the transfer of conserved quantities dominates over both their dissipation and forcing [1]. Following Kraichnan for 2d turbulence [2] and Charney for quasi-geostrophy turbulence [3] we seek to find constraining relationships

*Theoretical Division, Los Alamos National Laboratory, Mail Stop B284, Los Alamos, NM 87545, USA. E-mail: skurien@lanl.gov

between energy and potential enstrophy for the rotating Boussinesq system and thus find universal scaling properties of energy spectra.

Assuming that velocity, vorticity and scalar remain reasonably bounded, the potential vorticity linearizes in the dynamical variables, while Q becomes a quadratic simply related to energy (in fourier space) in the following limits. The final result in each limit is a derivation of the scaling exponents for the high wavenumber for horizontal kinetic and potential energy spectra, as given below. The details of these calculations involve simple dimensional and phenomenological arguments which are given in [4].

For $Ro = Fr = \varepsilon \to 0$ and small aspect ratio modes $\dfrac{k_h}{k_z} \gg 1$

$$E_h(k_h,k_z) \sim \varepsilon_Q^{2/5} k_h^{-3}. \tag{2}$$

where the horizontal kinetic energy $E_h(k_h,k_z) = \frac{1}{2}|\tilde{u}_h(k_h,k_z)|^2$ and ε_Q is the potential enstrophy dissipation rate.

For $Ro = Fr = \varepsilon \to 0$ and large aspect ratio modes $\dfrac{k_z}{k_h} \gg 1$

$$P(k_h,k_z) \sim \varepsilon_Q^{2/5} k_z^{-3} \tag{3}$$

where the potential energy spectral density is $P(k_h,k_z) = \frac{1}{2}|\tilde{\theta}(k_h,k_z)|^2$
For $Fr \ll Ro$, $Ro \sim O(1)$,

$$E_h(k_h) \sim \varepsilon_Q^{2/5} k_h^{-3} \tag{4}$$

independent of k_z.
And finally for $Ro \ll Fr$, $Fr \sim O(1)$,

$$P(k_z) \sim \varepsilon_Q^{2/5} k_z^{-3} \tag{5}$$

independent of k_h.

We check each of the predictions (2)-(5) using simulations of the Boussinesq equations in unit aspect ratio, 640^3 gridpoints, stochastic forcing of the velocity and scalar in the low modes (peaked at $k_f = 4$), hyperviscosity power 8 for the dissipation scheme. Figure 1 shows the results. For $Ro = Fr$ and both small, the dependence of the scaling regime of $P(k_h,k_z)$ and $E_h(k_h,k_z)$ on the aspect ratio of the wavevector is clearly displayed while the scaling itself is even steeper than the k^{-3} predicted. In the lower half of the figure, the dependence of the scaling on the aspect ratio nearly vanishes with near collapse of the curves for $E_h(k_h,k_z)$ as a function of k_h for various fixed k_z and significant (though not as pronounced) collapse for $P(k_h,k_z)$ as a function of k_z for various fixed k_h.

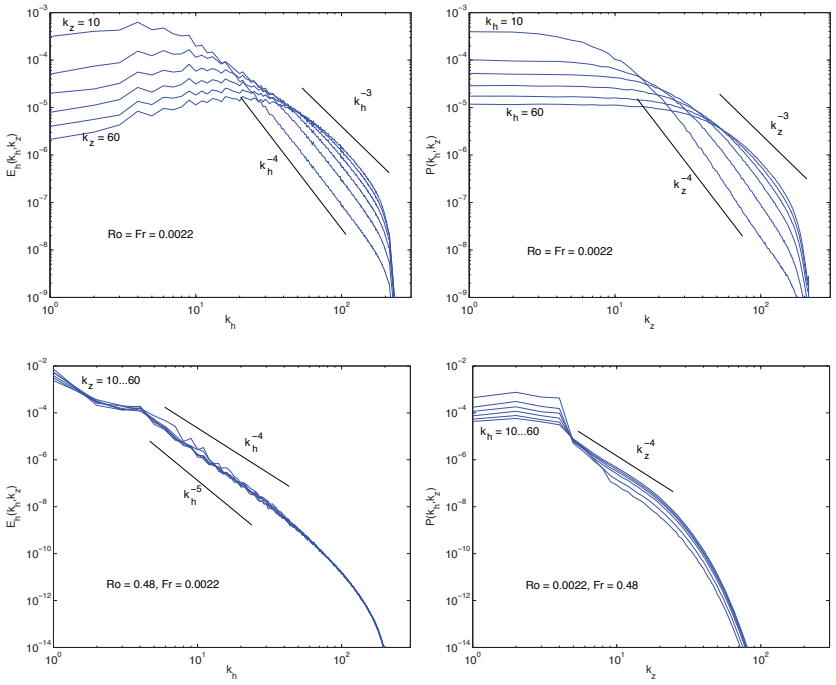

Figure 1: Top left: $Ro = Fr = \varepsilon \to 0$, the steep scaling of $E_h(k_h,k_z)$ in k_h for small aspect ratio modes. Top right: $Ro = Fr = \varepsilon \to 0$, the steep scaling of $P(k_h,k_z)$ in k_z for large aspect ratio modes. Bottom left: $Fr \ll Ro \sim O(1)$, $E_h(k_h,k_z)$ becomes independent of k_z. Bottom left: $Ro \ll Fr \sim O(1)$, $P(k_h,k_z)$ scaling in k_z becomes (nearly) independent of k_h.

References

[1] KOLMOGOROV A.N. *Dissipation of energy in a locally isotropic turbulence*, Doklady Akad. Nauk SSSR, **32** (1941), 141-145.

[2] KRAICHNAN R., *Inertial ranges in two-dimensional turbulence*, Phy. Fluids **10** (1967), 1417-1423.

[3] CHARNEY, J.G., *Geostrophic turbulence*, J. Atmos. Sci. **28** (1971), 1087-1095.

[4] KURIEN,S., WINGATE, B., AND TAYLOR, M.A., *Anisotropic constraints on energy distribution in rotating and stratified turbulence*, Europhys. Lett. **84** (2008), 24003.

Dispersion of heavy particles in turbulent flows

ALESSANDRA S. LANOTTE*, JEREMIE BEC**,
LUCA BIFERALE***, ANDREA SCAGLIARINI***, FEDERICO TOSCHI****

Abstract. *Relative dispersion of heavy point particles is studied by means of direct numerical simulations of homogeneous and isotropic turbulence at the Taylor-scale Reynolds number $Re_\lambda = 400$. Numerical data show that inertia can significantly influence particles dynamics and dispersion: i) affecting small-scale velocity increment statistics; ii) inducing strong deviations from the Richardson behaviour, typical of tracers. In a nutshell, turbulent dispersion of heavy pairs is found to be governed by two temporal regimes. The first is characterised by an increased diffusivity with respect to tracers, due to the presence, at large Stokes numbers, of small-scale caustics in the particle velocity statistics: it lasts until particle velocities have relaxed towards the underlying flow velocities. Next, a second regime starts where heavy particles separate as tracers particles would do, but their diffusivity is depleted in amplitude.*

Keywords: Turbulent diffusion, Particle-laden flows.

The statistical properties of small-scale Eulerian velocity increments is responsible for the way, initially close pairs of tracers separate in turbulent flows. As a result, depending on the values of time and space scales, we can observe different regimes for relative dispersion, see e.g. [1]. The application of similarity theory for the stationary velocity statistics is at the base of the turbulent Lagrangian relative dispersion for inertial particle pairs also, i.e. of small, finite-size particles with a density contrast with respect to the advecting flow. Heavy particles of different radius a and density ρ_p can be described in terms of their Stokes number St, defined as $St = \tau_s/\tau_\eta$, where τ_η is the flow Kolmogorov timescale. The particle response time is $\tau_s = a^2(\rho_f + 2\rho_p)/(9\nu\rho_f)$, a being the particle radius much smaller than the Kolmogorv scale η, and ρ_f and ν are the fluid density and kinematic viscosity, respectively.
A phenomenon which gathered much of the attention is *preferential concentration*, i.e. the tendency of heavy particles with moderate inertia to concentrate in specific (hyperbolic) regions of the flow. More recently, it has been shown that

*ISAC-CNR, 00133 Rome, and INFN, Sez. Lecce, 73100 Lecce, Italy
E-mail: a.lanotte@isac.cnr.it
**Univ. De Nice Sophia-Antipolis, CNRS OCA, 06304 Nice, France
**Dept. Physics, Univ. of Tor Vergata, 00133 Rome, Italy
****Dept. Physics, and of Mathematics and Computer Science, Univ. of Technology, 5600 MB Eindhoven, The Netherlands, and IAC-CNR, Rome, Italy

when inertia is high enough, the particle pair velocity difference may exhibit non trivial behaviour with scale, a phenomenon connected to the formation of *caustics*, see e.g. [2]. This implies that, for moderate inertia, spatially close particles can have very large velocity difference, and in the limit of $St \gg 1$, when the Stokes time is larger than any turbulent flow time scale, nearby particles can move with uncorrelated velocities.
Here, we discuss the role of inertia in relative dispersion by considering pairs of heavy particles, starting from initially close positions. In our set up, appropriate for dilute suspensions of small (point) particles, the equation ruling their dynamics is: $\ddot{\mathbf{X}}(t) = -1/\tau_s \left[\dot{\mathbf{X}}(t) - \mathbf{u}(\mathbf{X},t)\right]$, where the particle position and velocity are $\mathbf{X}$ and $\mathbf{V} = \dot{\mathbf{X}}$, respectively. Also, $\mathbf{u}(\mathbf{X}(t),t)$ is the Eulerian fluid velocity evaluated at the particle position. In Fig. 1, it is plotted the growth with time of the mean square pair separation $\langle R^2(t)|R(t_0) = R_0\rangle$, where $\mathbf{R}(t) = \mathbf{X_1}(t) - \mathbf{X_2}(t)$ and R_0 is the pair initial distance. It is clear from the

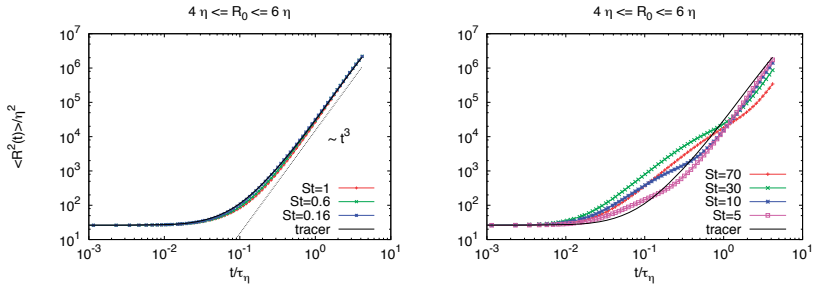

Figure 1: Mean square separation versus time, for heavy particles at changing St and for the initial distance $R_0 \in [4:6]\eta$. Left: data for $St = 0.16, 0.6, 1$, compared with tracers ($St = 0$). Right: data for pairs with strong inertia, $St = 5, 10, 30, 70$, and tracers. Average is performed over 10^4 pairs per Stokes number. Particles move in a homogeneous and isotropic flow, which solves Navier-Stokes eqs. in a cubic, periodic box with 2048 collocation points per spatial direction. Reynolds number is $Re_\lambda = 400$. Details can be found in [3].

right panel that pairs with small to moderate Stokes numbers, up to $St \simeq 1$ - where preferential concentration is maximal-, are not really affected by inertia, at least for such low order moments of the separation. We remark that the long time behaviour agrees with the Richardson law $\langle R^2(t)\rangle \sim t^3$. On the contrary, particles with larger St, strongly deviate from the tracers behaviour. At intermediate time lags, they separate much faster than tracers would do; next, after a time lag that varies with inertia, they separate in time as tracers, but with a depleted prefactor, which is again function of the inertia. This can be understood as follows: for pairs of small inertia, the relative velocity difference at initial time, $\delta_{R_0} V = V_1(t_0) - V_2(t_0)$, is of the order of the fluid ve-

locity difference at that scale. This is immediately clear if we consider the pair diffusivity $d/dt\langle R^2(t)\rangle = 2\langle \mathbf{R}\cdot\delta_R\mathbf{V}\rangle$, (see also [4]). For $St \leq 1$, $\delta_R\mathbf{V} \simeq \delta_R\mathbf{u}$, and thus according to the similarity theory $d/dt\langle R^2(t)\rangle \propto \langle R^2(t)\rangle^{2/3}$ (see right panel of Fig. 2). Differently, for pairs with moderate-large St, initially the relative velocity difference $\delta_{R_0}V$ is much higher than that of tracers. It takes a time of the order of the particle Stokes time τ_s for such velocity to decay on that of tracers pairs (see [3]): before such time, heavy particles separate according to an almost ballistic motion which results in a diffusivity scaling as $d/dt\langle R^2(t)\rangle \propto \langle R^2(t)\rangle^{1/2}$. After such transient, pair velocity difference has syncronised with the fluid one, except for an amplitude prefactor which decreases as inertia increases. This implies that heavy pairs diffusivity recovers that of tracers, but with a smaller amplitude.

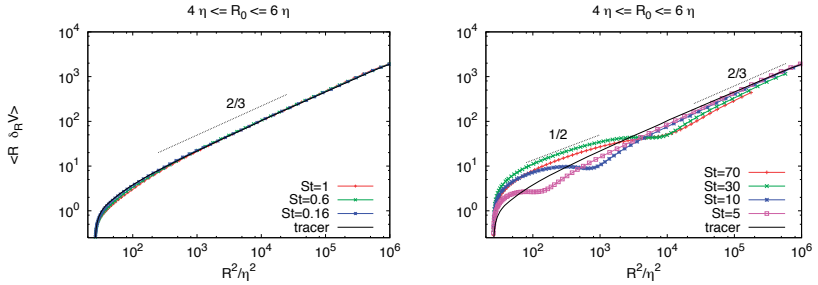

Figure 2: Pair diffusivity versus the square relative separation, at varying inertia. Average is performed over the same data of Fig.1. Dashed lines give the diffusivity scaling $\sim \langle R^2\rangle^{1/2}$ for the quasi-ballistic motion, and $\sim \langle R^2\rangle^{2/3}$ of tracer diffusion.

References

[1] SAWFORD B., *Turbulent relative dispersion*, Ann. Rev. Fluid Mech., **33** (2001), 289 – 317.

[2] BEC J., BIFERALE L., CENCINI M., LANOTTE A.S., TOSCHI F. *Intermittency in the velocity distribution of heavy particles in turbulence*, submitted to J. Fluid Mech. (2009).

[3] BEC J., BIFERALE L., LANOTTE A.S., SCAGLIARINI A., TOSCHI F. *Turbulent Pair Dispersion of Inertial Particles*, submitted to J. Fluid Mech. (2009); *arXiv:0905.1192*.

[4] EL MAIHY A., NICOLLEAU, F. *Investigation of the dispersion of heavy-particle pairs and Richardson's law using kinematic simulation*, Phys. Rev. E, **71** (2005), 046307.

Structural aspects of acceleration in turbulent flow

BEAT LÜTHI*, MARKUS HOLZNER*, ALEX LIBERZON**, ARKADY TSINOBER***
SØREN OTT****, JACOB BERG****, JAKOB MANN****

Abstract. *Three-dimensional particle tracking velocimetry (3D-PTV) was applied to measure acceleration and spatial velocity gradients in quasi-homogeneous and isotropic turbulent flow. The focus is on the spatial distribution of extreme values of acceleration with respect to the fields of vorticity and rate-of-strain. We show that strong acceleration is not only an "attribute" of strong vorticity, but that it occurs with equal probability in the regions of strong strain.* Keywords*:* particle tracking,
Keywords: particle tracking, acceleration, enstrophy, rate-of-strain.

Introduction Accelerations in turbulent flows are intimately related to the field of spatial velocity gradients. Results of acoustic tracking [1] had shown that strong vorticity filaments, which are surrounded by strong strain, are responsible for intense acceleration. Numerical studies [2, 3] demonstrated that high acceleration events appear in intense vorticity regions and that they are mainly associated with "vortex trapping". Other authors, e.g. [4] suggest that high acceleration events occur at stagnation points, rather than strong vortices. High resolution numerical simulations of [5] proposed that fluid particles are drawn into zones of high vorticity with a larger acceleration compared with zones of high strain rate, although the contrast becomes weaker at high Reynolds number. At higher Reynolds numbers, vorticity time scales become very short, therefore vortex orientation can not be maintained for a substantial period of time. In this work both, acceleration and the velocity gradient tensor are accessed instantaneously in a quasi-homogeneous and quasi-isotropic flow. We demonstrate that high acceleration occurs due to vortex trapping and due to straining motion in the so-called "jet colliding" situations, first described by [6].

Experimental method Lagrangian trajectories of fluid elements in water are obtained by tracking neutrally buoyant particles in space and time in the setup described elsewhere [7]. Parameters of the turbulent flow as obtained from PTV measurements are given in the following table:

* Institute of Environmental Engineering, Swiss Federal Institute of Technology, ETH Hönggerberg, CH 8093 Zurich, Switzerland

** Turbulence Structure Laboratory, School of Mechanical Engineering, Tel Aviv University, Ramat Aviv 69978, Israel.

*** Corresponding author, e-mail: alexlib@eng.tau.ac.il

**** Risø National Laboratory, DK-4000 Roskilde, Denmark.

Re_λ	σ_u	σ_a	$\mathcal{L}$	ε	η	τ_η
84	15mm/s	31mm/s^2	48mm	20mm^2/s^3	0.5mm	0.2s

Results We use conditional sampling analysis to probe the distributions of enstrophy and strain in respect to the acceleration. The results are presented for the whole dataset and separately for our conditional subsets of the data ($\langle\omega^2\rangle \approx \langle 2s^2\rangle \approx 20$ s^{-2}): (1) *low gradients*, i.e. $\omega^2 < \langle\omega^2\rangle$, $s^2 < \langle s^2\rangle$, (2) *high vorticity*, $\omega^2 > \langle\omega^2\rangle$, $\omega^2 > 2s^2$ (i.e. below the separatix in 1b), (3) *high strain* , $2s^2 > \langle 2s^2\rangle$, $2s^2 > \omega^2$ (i.e. above the separatix).

Firstly, figure 1a presents the probability density functions (PDFs) of the acceleration magnitude $|\mathbf{a}|$. We observe that acceleration tends towards higher values for both, high enstrophy, and high strain. In figure 1b acceleration magnitude is shown as the joint PDF conditioned on both, enstrophy and strain, i.e., $(\mathbf{a}_{r.m.s.};\omega^2,s^2)/\mathbf{a}_{r.m.s.}$. The horizontal and vertical lines in figure 1b mark the average strain and enstrophy. The lower left region contains two thirds of all events that fall into the "low gradient" region and the high strain and high enstrophy region contain each 1/6 of all events. It appears that two distinct populations of intense acceleration co-exist. One for *high enstrophy and lower strain*, where conditional mean values are up to 5 $\mathbf{a}_{r.m.s.}$. This population contains the events that are referred to as "vortex trapping" events. The second population with high acceleration is governed by *high strain and lower enstrophy* where conditional means reach values up to 4 $\mathbf{a}_{r.m.s.}$. This region can presumably be associated with "jet colliding" events.

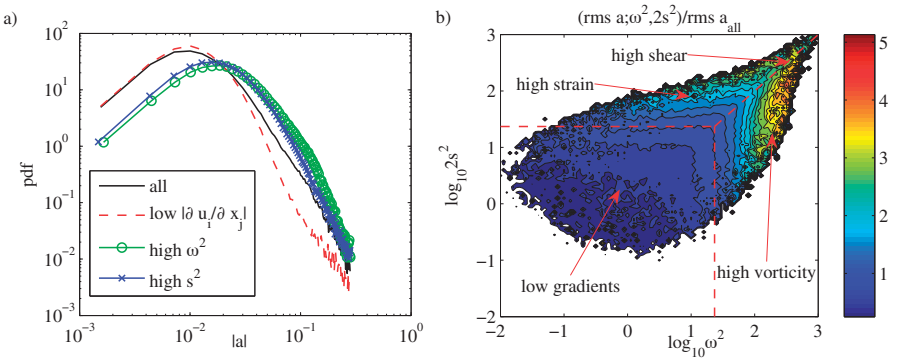

Figure 1: (a) PDFs for **a** conditioned on low velocity gradients, high enstrophy - low strain and high strain - low enstrophy. (b) $\mathbf{a}_{r.m.s.}$ conditioned on joint PDF of enstrophy and strain. The vertical, horizontal and diagonal dashed lines are at $\omega^2 = \langle\omega^2\rangle$, $s^2 = \langle 2s^2\rangle$, and $\omega^2 = s^2$, respectively.

Summary and conclusion Acceleration in a quasi-isotropic turbulent flow has been studied via particle tracking velocimetry with particular attention to the

relation of intense acceleration events with the velocity gradient fields (strain, shear and vorticity), obtained simultaneously. On a plane spanned by vorticity and strain the joint probability density function forms an arrow tip like pattern. On this plane, we identify three regions: low gradients, anti-correlated moderately strong strain and vorticity regions. In the ω^2, s^2 arrow tip, we find that the most intense acceleration events are comprised by two distinct populations of either high vorticity or high strain.

The presented work adds to the understanding of how the magnitude of total acceleration depend upon the field of velocity gradients in a complicated way and how their interplay affects important issues such as the energy flux over scales.

Acknowledgements The authors would like to thank the following funding sources: A. Liberzon visits to ETH have been supported by the ERCOFTAC visiting scientist program.

References

[1] N. Mordant, E. Levveque, and J.-F. Pinton. Experimental and numerical study of the Lagrangian dynamics of high Reynolds turbulence. *New J. of Physics*, 6:1–44, 2004.

[2] L. Biferale, G. Boffetta, A. Celani, A. Lanotte, and F. Toschi. Particle trapping in three-dimensional fully developed turbulence. *Phys. Fluids*, 17(2):021701, 1–4, 2005.

[3] L. Biferale and F. Toschi. Joint statistics of acceleration and vorticity in fully developed turbulence. *J. of Turbulence*, 40(6):1–8, 2005.

[4] S. Goto, D.R. Osborne, J.C. Vassilicos, and J.D. Haigh. Acceleration statistics as measures of statistical persistence of streamlines in isotropic turbulence. *Phys. Rev. E*, 71(1):1–4, 2005.

[5] P.K. Yeung, S.B. Pope, E.A. Kurth, and A.G. Lamorgese. Lagrangian conditional statistics, acceleration and local relative motion in numerically simulated isotropic turbulence. *J. Fluid Mech.*, 582:399–422, 2007.

[6] R. Betchov. An inequality concerning the production of vorticity in isotropic turbulence. *J. Fluid Mech.*, 1:497–503, 1956.

[7] J. Berg, B. Lüthi, J. Mann, and S. Ott. An experimental investigation: backwards and forwards relative dispersion in turbulent flow. *Phys. Rev. E*, 74(1):016304, 2006.

Expanding the Q-R space to three dimensions

BEAT LÜTHI*, MARKUS HOLZNER*, ARKADY TSINOBER**

Abstract. *The two dimensional space spanned by the velocity gradient invariants Q and R is expanded to three dimensions (3D) by the decomposition of R into its strain production $-1/3 s_{ij}s_{jk}s_{ki}$ and enstrophy production $1/4\omega_i\omega_j s_{ij}$ terms. The $\{Q;R\}$ space is a planar projection of the new 3D representation. In the $\{Q;-sss;\omega\omega s\}$ space the Lagrangian evolution of the velocity gradient tensor A_{ij} is studied via conditional mean trajectories (CMT) as introduced by [4]. From an analysis of a numerical data set for isotropic turbulence of $Re_\lambda \sim 237$, taken from the JHU Turbulence database, we observe a pronounced cyclic evolution that is almost perpendicular to the $Q-R$ plane. The relatively weak cyclic evolution in the $Q-R$ space is thus only a projection of a much stronger cycle in the $\{Q;-sss;\omega\omega s\}$ space.*

Keywords: velocity gradient, dynamics, invariants.

Q is the second invariant, $Q = 1/4(\omega^2 - 2s^2)$, of the velocity gradient tensor A_{ij} and R is its third invariant, $R = -1/3 s_{ij}s_{jk}s_{ki} - 1/4\omega_i\omega_j s_{ij}$. In joint PDF plots of Q versus R a qualitatively identical 'tear drop' shape for different kinds of turbulent flows was found by a number of investigators. [1] argue that the shape is a universal characteristic of the small-scale motions of turbulence. This statement is corroborated by a compilation of $Q-R$ plots of different flows, [6], and velocity gradient measurements at $Re_\lambda = 6600$, see [2]. The most characteristic feature is that in strain dominated regions the strain production term, $-s_{ij}s_{jk}s_{ki}$, is dominant over $\omega_i\omega_j s_{ij}$, resulting in the so-called Vieillefosse tail, see [7].

Here we expand the $\{Q;R\}$ space to three dimensions (3d) by the decomposition of R into its strain production $-1/3 s_{ij}s_{jk}s_{ki}$ and enstrophy production $1/4\omega_i\omega_j s_{ij}$ terms. For our analysis we have used the JHU Turbulence database that is developed as an open resource by the Johns Hopkins University, see [5, 3]. The data is from a direct numerical simulation of forced isotropic turbulence on a 1024^3 periodic grid with a Taylor Reynolds number is $Re_\lambda = 237$. Similar to $\{Q;R\}$ space, see [4], we define the conditional mean rates of change

* ETH Zürich, Switzerland.
E-mail : luethi@ifu.baug.ethz.ch holzner@ifu.baug.ethz.ch
** Tel Aviv University, Israel.
E-mail : tsinober@eng.tau.ac.il

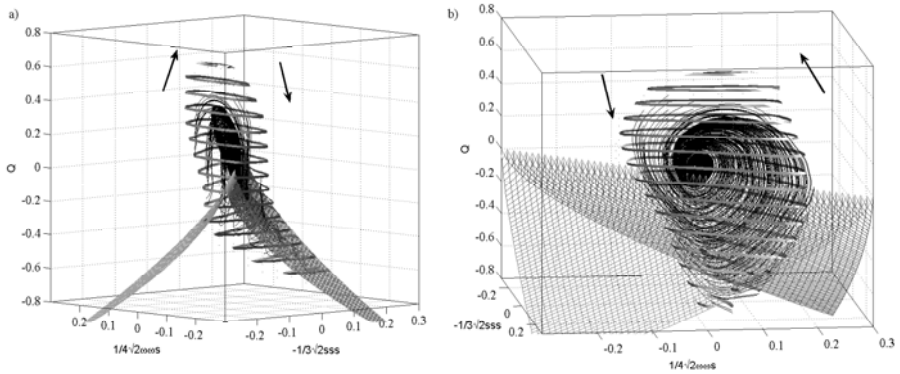

FIGURE 1 – CMT's of the evolution of A_{ij} in the $\{Q;-sss;\omega\omega s\}$ space are shown for two different views inside $V_{95\%}$ represented by ribbons, with the arrows indicating the direction of the CMT's. The surface with the discriminant $D = 27/4 \cdot R^2 + Q^3 = 0$ is shown as a wire mesh. The view point of a) is chosen such that the envelope of the ribbons resemble the 'tear-drop' shape and the clockwise cyclic evolution, known from the 2D $Q-R$ representation. The 3D view (b) reveals the cyclic evolution more clearly.

for the $\{Q;-sss;\omega\omega s\}$ space as

$$\begin{aligned}
\overline{\mathbf{v}}_Q &= \langle \frac{DQ}{Dt} \cdot \tau_\eta^3 \mid Q, -1/3\sqrt{2}sss, 1/4\sqrt{2}\omega\omega s \rangle \\
\overline{\mathbf{v}}_{sss} &= \langle \frac{D(-1/3\sqrt{2}s_{ij}s_{jk}s_{ki})}{Dt} \cdot \tau_\eta^4 \mid Q, -1/3\sqrt{2}sss, 1/4\sqrt{2}\omega\omega s \rangle \\
\overline{\mathbf{v}}_{\omega\omega s} &= \langle \frac{D(1/4\sqrt{2}\omega_i\omega_j s_{ij})}{Dt} \cdot \tau_\eta^4 \mid Q, -1/3\sqrt{2}sss, 1/4\sqrt{2}\omega\omega s \rangle. \qquad (1)
\end{aligned}$$

To illustrate that the $Q-R$ plane is a projection of the $\{Q;-sss;\omega\omega s\}$ space we show in figure 1a the evolution of conditional mean trajectories (CMT's) starting from the center of each bin within $V_{95\%}$ from a view point approximately perpendicular to the $Q-R$ plane, i.e., $\{Q \cdot \mathbf{e}_1; [-1/3\sqrt{2}sss \cdot \mathbf{e}_2 - 1/4\sqrt{2}\omega\omega s \cdot \mathbf{e}_3]\}$. The surface of $D = 0$, with the discriminant $D = 27/4 \cdot R^2 + Q^3$, is rendered as a wire-mesh. From this view point the well known clockwise evolution is evident in the enstrophy dominated regions where $Q > 0$, while around the Vieillefosse tail the evolution is less clear. However, if the view-point is moved such that it is facing almost the $Q - \omega\omega s$ plane (fig. 1b), our main result becomes much clearer : There is a pronounced anti-clockwise

cyclic evolution, with a rotation axis that is almost perpendicular to the $Q-R$ plane. This non trivial cyclic evolution is one of the manifestations of the time irreversibility of turbulent flows, as reflected by other manifestations, such as positive net enstrophy and strain production and the $4/5$ Kolmogorov law.

References

[1] Chacín, J. M. and Cantwell, B. J. (2000). Dynamics of a low Reynolds number turbulent boundary layer. *J. Fluid Mech.*, 404 :87–115.

[2] Gulitski, G., Kholmyansky, M., Kinzelbach, W., Lüthi, B., Tsinober, A., and Yorish, S. (2007). Velocity and temperature derivatives in high Reynolds number turbulent flows in the atmospheric surface layer. Part I. Facilities, methods and some general results. *J. Fluid Mech.*, 589 :57–81.

[3] Li, Y., Perlman, E., Wan, M., Yang, Y., Burns, R., Meneveau, C., Burns, R., Chen, S., Szalay, A., and Eyink, G. (2008). A public turbulence database cluster and applications to study lagrangian evolution of velocity increments in turbulence. *J. of Turbulence*, 9.

[4] Martín, J., Dopazo, C., and Valiño, L. (1998). Dynamics of velocity gradient invariants in turbulence : Restricted Euler and linear diffusion models. *Physics of Fluids*, 10(8) :2012–2025.

[5] Perlman, E., Burns, R., Li, Y., and Meneveau, C. (2007). Data Exploration of Turbulence Simulations using a Database Cluster. *Supercomputing SC07, ACM, IEEE*.

[6] Tsinober, A. (2001). *An Informal Introduction to Turbulence*. Kluwer Academic Publishers.

[7] Vieillefosse, P. (1982). Local interaction between vorticity and shear in a perfect incompressible fluid. *Le journal de Physique*, 43(6) :837–842.

Turbulent mixing of cloud with the environment: small scales of two-phase evaporating flow seen by particle imaging velocimetry

SZYMON P. MALINOWSKI*, PIOTR KORCZYK**, TOMASZ A. KOWALEWSKI**

Abstract. *Cloud-clear air mixing is investigated in the laboratory experiment by means of Particle Imaging Velocimetry (PIV). It occurs that turbulent velocities depend on thermodynamic contrasts between the cloud and its environment. Evaporative cooling at the edges of cloud/clear filaments and/or uneven mass loading result in buoyancy fluctuations which affect the smallest scales of turbulence. These effects are illustrated by means of second order structure functions of velocity field.*

Keywords: turbulent mixing, anisotropy, clouds.

Experimental evidence of the small-scale turbulence in clouds is very limited. By small-scale we understand here turbulence close to dissipation range, i.e. for the range of scales from 10cm down to a fraction of 1 mm. Since it is hard to observe it in natural conditions [1], [2], laboratory simulations mimicking some aspects of cloud-clear air turbulent mixing is prformed. The setup of these experiments closely follows earlier studies by [3],[4],[5].

In brief, cloud-clear air mixing is investigated by observation of motion of cloud droplets in a glass walled chamber. A box placed on the top contains saturated air with suspended water droplets of diameters in range from 7 to 25 μm, similar to those in real clouds. After opening the hole between the chambers air from the box descends, forming a negatively buoyant, turbulent plume undergoing mixing with the unsaturated air in the main chamber. The plume is illuminated with a narrow sheet of laser light in a vertical cross-section through the central part of the chamber. Light scattered on cloud droplets is imaged with a high-resolution CCD camera. PIV technique is used to study the flow (Fig.1).

Similar mixing process was studied in a series of idealized numerical simulations of cloud-clear air mixing [6], [7], [5], [8]. Key findings from numerical simulations and experiments can be summarized in the follwing way. Large scale velocity fluctuation lead to filamentation of the cloud. At the cloud-clear interface droplets evaporate. Evaporative cooling and uneven mass loading

*Institute of Geophysics, University of Warsaw, Warsaw, Poland.
E-mail: malina@fuw.edu.pl
**Institute of Fundamental Technological Research, Polish Academy of Sciences, Warsaw, Poland.

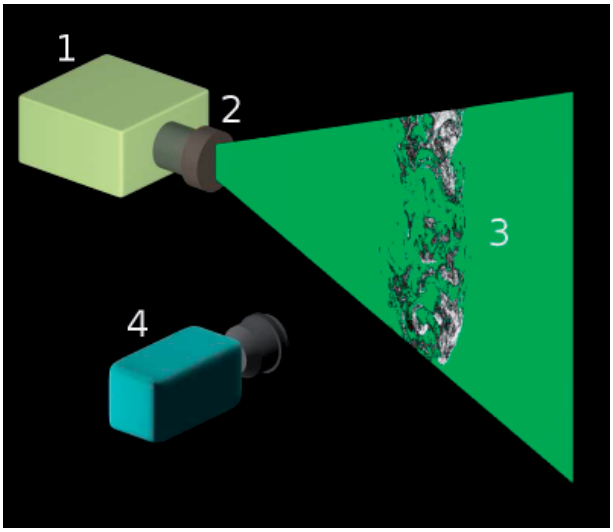

Figure 1: A sketch of the experimental setup. 1 - laser, 2- beam-shaping optical system, 3 - light sheet at the vertical cross-section through the cloudy plume undergoing mixing with the environment in the chamber, 4 - camera.

effect in small scale buoyancy fluctuations. These fluctuations result in production of additional, small scale turbulence. Since priduction of turbulence in small scale is anisotropic, small-scale velocity fluctuations are anisotropic with preferred vertical direction. Deatils of mixing process depend on thermodynamical properties of cloud and environment, mass fraction of the cloudy air in the mixing event, cloud droplet size spectrum and turbulent kinetic energy flux cascading down from large scales.

In the present study new laboratory results, focusing on the effect of evaporative cooling on the properties of small-scale turbulence are presented. A range of thermodynamic conditions and possible effects of mixing on buoyancy are illustrated by mixing diagram (Fig.2) showing dependence of a buoyancy temperature T_b ([9], eq. 4.3.6) on mixing proportion:

$$T_b = T\left[1+\left(\frac{R_v}{R_d}-1\right)q-x\right]. \tag{1}$$

Here T is the air temperature, R_v and R_d are gas constants for water vapor and dry air, q and x are the water vapor and cloud water contents. It can be seen, that conditions cover a range of buoyancy effects, allowing for more detailed investigation of the influence of evaporative cooling on small-scale turbulence.

An example result is presented in Fig.3. It shows second order structure functions of velocity drived from PIV of cloud droplets at various relative humidities in the environment. It can be seen that decrease of the environmental

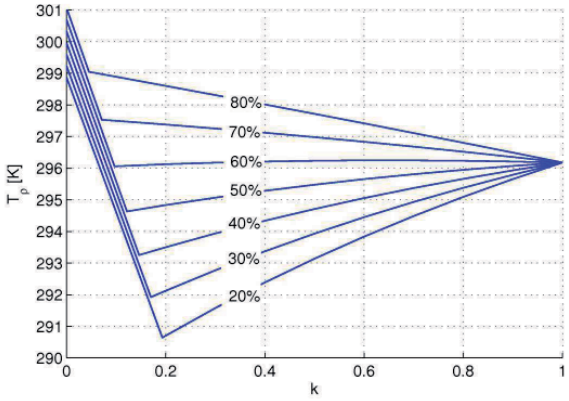

Figure 2: Mixing diagram illustraties a range of buoyancy fluctuations inside the cloud chamber at various specific humidities of the environmental air at given temperature and liquid water content of cloud. Horizontal axis depicts mixing proportion k. k=0 indicates environment, k=1 indicates cloud, intermediate values correspond to proportion of both spieces in the mixing event. Vertical axis - buoyavcy temperature of the homogeneized mixture. High buouancy temperature corresponds to low deisity of air (cloud). Successive "v shape" lines show dependence of densiity temperature of mixture on the relative humidity of the environment. At low humidities potential for evaporative cooling is high, as indicate absolute minima of the density temperature. At relative humidities higher than 0.6 the maximum density temperature of the mixture is lower than that of the cloud.

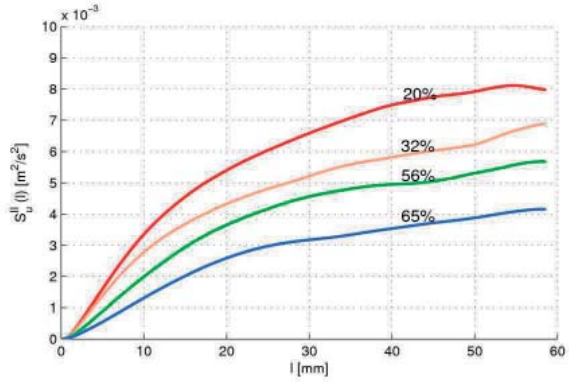

Figure 3: Second order longitudinal structure functions of horizontal velocity component for various relative humidities of the environmental air.

hymidity results in increase of squared velocity differences. It can be interpreted in a following way: at given temperature and constant conditions in cloud (Fig.2) a possible buoyancy production due to evaporative cooling depends on the relative humidity of the environment. Buoyancy effects produce turbulent kinetyc energy in small scales, which is reflected by the increase of squared velocity differences.

More detailed analyses will be presented at the ETC512 meeting.

References

[1] SIEBERT, H., LEHMANN, K. AND WENDISCH, M., *Observations of small-scale turbulence and energy dissipation rates in the cloudy boundary layer*, J. Atmos. Sci. **63** (2006), 1451.

[2] SIEBERT, H., SHAW, R.A. AND WARHAFT, Z. , *Statistics of Small-Scale Velocity Fluctuations and Internal Intermittency in Marine Stratocumulus Clouds*, J. Atmos. Sci. (2009), in press.

[3] MALINOWSKI, S.P., ZAWADZKI, I. AND BANAT, P. , *Laboratory Observations Of Cloud-Clear Air Mixing at Small Scales*, J. Atmos. Ocean. Technol. **15**, (1998), 1060.

[4] KORCZYK, P.M., MALINOWSKI, S.P. AND KOWALEWSKI, T.A., *Mixing of cloud and clear air in centimeter scales observed in laboratory by means of particle image velocimetry*, Atmos. Res. **82**, (2006), 17.

[5] MALINOWSKI, S.P., ANDREJCZUK,M., GRABOWSKI, W.W., KORCZYK, P.M., KOWALEWSKI, T.A. AND SMOLARKIEWICZ, P.K., *Laboratory and modeling studies of cloud-clear air interfacial mixing: anisotropy of small-scale turbulence due to evaporative cooling*, New J. of Phys. **10**, (2008), 075020.

[6] ANDREJCZUK, M., GRABOWSKI, W.W., MALINOWSKI, S.P. AND SMOLARKIEWICZ, P.K., *Numerical Simulation of Cloud-Clear Air Interfacial Mixing*, J. Atmos. Sci., **61**, (2004), 1726.

[7] ANDREJCZUK, M., GRABOWSKI, W.W., MALINOWSKI, S.P. AND SMOLARKIEWICZ, P.K., *Numerical Simulation of Cloud-Clear Air Interfacial Mixing: effects on cloud microphysics*, J. Atmos. Sci., **63**, (2006), 3204.

[8] ANDREJCZUK, M., GRABOWSKI, W.W., MALINOWSKI, S.P. AND SMOLARKIEWICZ, P.K., *Numerical Simulation of Cloud-Clear Air Interfacial Mixing: Homogeneous versus Inhomogeneous Mixing*, J. Atmos. Sci. **66** (2009), 2493.

[9] EMANUEL, K.A. *Atmospheric Convection*, Oxford University Press, 580 p.

Public database-enabled analysis of Lagrangian statistics in isotropic turbulence

CHARLES MENEVEAU, HUIDAN YU*

Abstract. *The web-services based public turbulence database enables user-friendly access to 27-Terabytes of data from a* 1024^4 *space-time history of isotropic turbulence (http://turbulence.pha.jhu.edu). It is used in this work to carry out Lagrangian analysis. The focus of the analysis is on time correlations of dynamically important tensor elements. Tensor-based time correlation functions show that rotation has much longer time memory than strain and the difference is larger than what had been previously observed from magnitude-based time correlations. Conditional averaging shows that vortical coherent structures (worms) are not the major reason for the difference between rotation and strain-rate tensor element memory time. A similar analysis for the pressure Hessian tensor exhibits significantly different correlations between the trace and deviatoric parts of the pressure Hessian.*

Keywords: web-based public turbulence database, isotropic turbulence, DNS, lagrangian time correlations.

The advent of increasingly powerful supercomputers has presented both opportunities and challenges for high-fidelity direct numerical simulations (DNS) of turbulence in recently years. It makes it possible to glean fundamental physical insight into fine-grained turbulence, whereas the generated massive datasets create serious new hard challenges and hamper practical numerical experiments due to the shortage of easy access to the vast amounts of data generated, especially for high resolution simulations [1], or more complex problems such as passive scalar turbulent mixing ([2]) and magnetohydrodynamic turbulence. Owing to the storage limitations within typical computational clusters, numerical experiments must be mostly performed simultaneously along with the simulation. Any modifications or new designs of numerical experiments means repeatedly running the DNS duplicating the computation expense. Even though a few large datasets from high-resolution simulations are stored, they are practically inaccessible to most who lack the cyber resources to handle the massive DNS data. The web-services based public turbulence database [3] applies "database technology" to computational fluid dynamics (CFD) and turbulence research. This database enables users to access 27-Terabyte DNS

*Department of Mechanical Engineering, Institute for Data Intensive Engineering and Science, Johns Hopkins University, Baltimore, MD 21218, USA. E-mails: meneveau@jhu.edu, hyu36@jhu.edu.

data and extract information such as velocity, pressure, and their derivatives simultaneously for accurate analysis of isotropic turbulence in a user-friendly fashion. Details about the isotropic turbulence DNS data and the usage of the web-based database are found at http://turbulence.pha.jhu.edu.

The Lagrangian evolution of the velocity gradient tensor has received considerable attention since the works of Vieillefosse [4] and Cantwell [5] on the dynamics of $A_{ij} = \partial u_i/\partial x_j$ that is obtained by taking gradient of the Navier-Stokes (NS) equation. Neglecting viscous effects and assuming the pressure Hessian ($H_{ij} \equiv \partial^2 p/\partial x_i \partial x_j$) isotropic lead to a closed formulation known as the Restricted-Euler (RE) equations. With analytically treatable solutions for the full tensor-level, the RE system provides a fruitful starting point for small structure modeling although there exist deficiencies of the RE dynamics which predicts non-physical finite-time singularities [5] and displays various differences with true NS dynamics. Efforts are continuing on finding and modeling regularization properties of the neglected viscous and anisotropic pressure Hessian terms, e.g.[6]. Despite recent progress, the inability to account for anisotropic pressure Hessian and viscous effects accurately continues to limit the usefulness of the RE dynamic models, especially for relatively high Reynolds (Re) number flows.

Using the public web-based turbulence database mentioned above, we are able to track [7] a large number of fluid particles randomly selected in the computation domain. Plot (a) in Fig. 1 shows the representative 100 particle trajectories in 3D following the time-evolution through an entire turn-over time-scale of the flow. It visualizes a glimpse of the complex turbulent motion. We focus on Lagrangian statistics of dynamically important tensor-based time correlation functions such as A_{ij} and H_{ij}. First, it is found that rotation has a significantly longer time correlation than strain rate, more profound than what has been observed from dynamically less transparent, magnitude-based, time correlations, i.e. vorticity vs. dissipation rate. Meanwhile, the full velocity gradient displays correlations between that of strain rate and rotation rate. To answer the question whether this trend is mainly due to vortical coherent structures (worms), we perform conditional time correlations excluding particles initially within strain or rotation dominated zones, see (b) and (c) in Fig. 1. It turns out that even with the exclusion of worms, the rotation rate remains significantly more correlated over time than the strain.

Second, the so-called finite-time Cauchy-Green tensor is a key ingredient in a new model of the pressure and velocity Hessians required to close Lagrangian velocity gradient evolution equation [6]. This model has been proven quite accurate for moderate Reynolds numbers. However at high Re, significant discrepancies between model and DNS shows the need for more in-depth analysis of the various terms needed in the modeling. Therefore, it is also of interest to study the auto-correlation structure of the pressure Hessian. Our analysis for the pressure Hessian tensor correlation function shows significantly different correlations between the trace and deviatoric parts of the pressure Hessian. The results obtained have implications for modeling, since they suggest that stochastic forcing terms may need to better represent some of the distinctions observed between deviatoric and isotropic parts of the pressure Hessian.

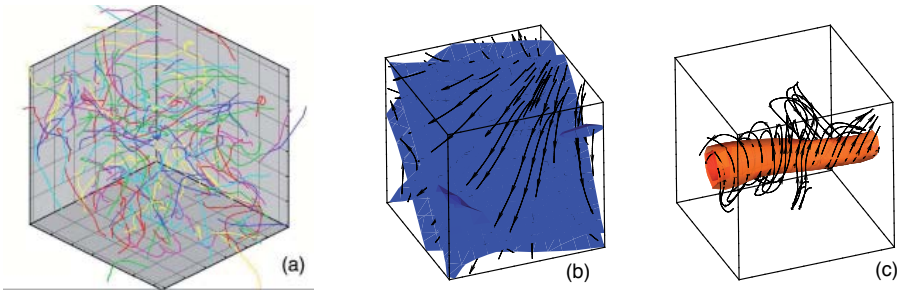

Figure 1: (a): Sample trajectories of 100 randomly selected particles in $2\pi^3$ domain. (b) and (c): Iso-countours of ω and streamlines in two representative boxes – (b) shows strain-dominated region and (c) a high rotation region which has been excluded from conditional analysis.

References

[1] ISHIHARA, T., GOTOH, T., AND KANEDA, Y., *Study of High-Reynolds number isotropic turbulence by direct numerical simulation*, Annu. Rev. Fluid Mech. **41**(2009), 165-180.

[2] YEUNG, P. K., *Lagrangian investigations of turbulence*, Annu. Rev. Fluid Mech. **34** (2002), 115-142.

[3] LI, Y., PERLMAN, E., WAN, M., YANG, Y., MENEVEAU, C., BURNS, R., CHEN, S., SZALAY, A. AND EYINK, G., *A public turbulence database cluster and applications to study Lagrangian evolution of velocity increments in turbulence*, J. Turbulence **9** (2008), 1-29.

[4] VIEILLEFOSSE, P., *Local interaction between vorticity and shear in a perfect incompressible fluid*, J. Phys. (France) **43** (1982), 837-842 .

[5] CANTWELL, B. J., *Exact solution of a restricted Euler equation*, Phys. Fluids A, bf 4(1992), 782-793.

[6] CHEVILLARD, L. AND MENEVEAU, C., *Lagrangian dynamics and statistical geometric structure of turbulence*, Phys. Rev. Lett. **97**(2006), 174501.

[7] YEUNG, P. K. AND POPE, S. B., *An Algorithm for tracking fluid particles in numerical Simulations of homogeneous turbulence*, J. Comp. Phys. **79**(1988), 373-416.

Mixing lengths scaling in a gravity flow

PHILIPPE ODIER*, JUN CHEN**,
ROBERT ECKE***, MICHAEL RIVERA***

Abstract. *We present an experimental study of the mixing processes in a gravity current. The turbulent transport of momentum and buoyancy can be described in a very direct and compact form by a Prandtl mixing length model [1]: the turbulent vertical fluxes of momentum and buoyancy are found to scale quadratically with the vertical mean gradients of velocity and density. The scaling coefficient is the square of the mixing lenth, approximately constant over the mixing zone of the stratified shear layer. We show in this paper how, in different flow configurations, this length can be related to the shear length of the flow* $\sqrt{\varepsilon/\partial_z u^3}$.

Keywords: mixing, turbulence, gravity current.

Mixing in stratified shear flows is an important process in many geophysical situations. Of particular current interest is the mixing and entrainment of oceanic overflows, which contributes to the transport of heat and salinity in the global ocean via the thermohaline "conveyor belt" [2]. The mixing processes occur at scales too small to be captured by the numerical simulations of this circulation, requiring a sub-grid parametrization. In situ measurements [3], as well as experimental studies, are necessary to provide an accurate description. In order to obtain a valid parametrization from a laboratory experiment, there is also a need for a model that extrapolates the parametrization to oceanic conditions.

We developed an experiment with a stratified flow on an inclined plane that is destabilized by shear. The experiment, described in detail elsewhere [4], consists of a turbulent, uniform-density flow injected via a pump into a tank filled with unstirred higher density fluid. The turbulence level of the injection current is enhanced by an active grid device located just before the injection nozzle. The flow, upon exiting the nozzle, is bounded from above by a transparent plate inclined at an angle of 10^o with respect to horizontal. The velocity

*Laboratoire de Physique, École Normale Supérieure de Lyon, 46, allée d'Italie 69364 Lyon Cedex 07, FRANCE. E-mail: podier@ens-lyon.fr

**School of Mechanical Engineering, Purdue University Room 129, Chaffee Hall 500 Allison Road, West Lafayette, IN 47907, USA.

***Condensed Matter & Thermal Physics Group and Center for Nonlinear Studies, Los Alamos National Laboratory, Los Alamos, New Mexico 87545, USA.

$\mathbf{u}$ has components $\{u,v,w\}$. We use the notation $\overline{\mathbf{u}}$ for a time- and ensemble-averaged quantity and $\mathbf{u}' = \mathbf{u} - \overline{\mathbf{u}}$ for its fluctuating part. The exit fluid, a solution of ethanol and water, is less dense than the fluid in the tank, water and salt (NaCl). The concentrations of ethanol and salt are adjusted so that the fluids are index matched to avoid optical distortions. Velocity and density are measured simultaneously in the $x-z$ plane (x is the mean flow direction and z the downward distance perpendicular to the plate) using particle image velocimetry (PIV) and planar laser-induced fluorescence (PLIF), respectively.

In an earlier publication [1], we reported the observation that the vertical time averaged fluxes of momentum $\overline{u'w'}$ and of density $\overline{\rho'w'}$ didn't relate to the corresponding vertical gradients via a constant eddy diffusivity assumption. The observed scaling was indeed the following : $\overline{u'w'} = L_m^2 S^2$ and $\overline{\rho'w'} = -L_\rho^2 |S| \partial_z \overline{\rho}$ where S is the vertical mean shear $\partial_z \overline{u}$. L_m and L_ρ correspond to typical scales where the turbulent mixing takes place. This observation can be understood in the framework of Prandtl mixing length theory [5].

A stratified flow results from the competition between the stabilizing effect of the stratification and the destabilizing effect of the shear. This competition is mesured by the bulk Richarson number : $Ri = g\Delta\rho/\rho U^2$. Another feature of the flow is the intensity of turbulence, which can be measured by the Taylor Reynolds number $Re_\lambda = u'^2/\sqrt{15\varepsilon\nu}$ where ε is the turbulence dissipation rate and ν the kinematic viscosity. In order to better characterize the dependence of the measured mixing lengths with these ingredients of our flow, we measured them in various flow configurations. The results are displayed in the following table. Starting from configuration 1, called "standard", (used for the data presented in [1]), we then varied stratification and/or intensity of turbulence in 5 different configurations. The fourth column shows the initial velocity of the current. Since in all cases momentum and density mixing lengths are equal (except the non stratified case where L_ρ is undefined), we give in the last column the value of L_m.

#	configuration	$\Delta\rho/\rho$	Ri	$U_0[cm/s]$	R_λ	L_m [cm]
1	standard	0.26%	0.3	8	100	0.45
2	more turbulent	same	0.2	10	140	0.6
3	no active grid	same	0.35	same	42	0.35
4	unstratified	0	0	same	115	2.1
5	double density	0.52%	0.45	same	93	0.3
6	double dens. half veloc.	0.52%	1.4	4	72	0.2

Compared to case 1, cases 2 and 3 show that the value of the mixing length increases with turbulence intensity. In the same way, as expected, cases 4 and 5 show that the stratification prevents mixing. In the last case, both the stratification is stronger and the shear weaker, resulting in very short mixing length.

As discussed in [1], for the conditions of our study, where shear dominates stratification (small Ri), the typical eddy size can be estimated based on shear

and turbulence $L_s = \sqrt{\varepsilon/S^3}$. In figure 1, we show indeed that in all cases studied, the mixing length scales as the shear length : $L_m = 1.3L_s$. This result points towards possible extrapolation to estimate the mixing length in oceanic situations, once the shear length is known. Finally, it is interesting to note that this proportionality indicates that an equivalent relationship for our system is that the eddy viscosity ν_T and eddy diffusivity γ_T are given by $\nu_T \approx \gamma_T \approx 1.3\varepsilon/S^2$.

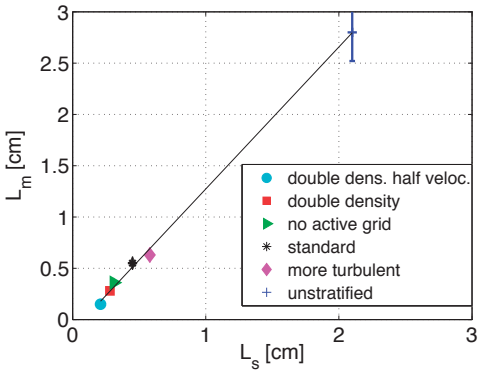

Figure 1: Measured mixing length vs computed shear length, for the different flow configurations indicated.

References

[1] ODIER P., CHEN J., RIVERA M. K., AND ECKE R. E., *Fluid mixing in stratified gravity currents: The prandtl mixing length*, Physical Review Letters **102**, 13 (2009), 134504.

[2] WILLEBRAND J., BARNIER B., ET AL., *Circulation characteristics in three eddy-permitting models of the North Atlantic*, Prog. Oceanogr. **48** (2001), 123–161.

[3] GIRTON J. AND SANFORD T., *Descent and modification of the overflow plume in the Denmark Strait*, Journal of Physical Oceanography **33** (2003), 1351–1364.

[4] CHEN J., ODIER P., RIVERA M., AND ECKE R., *Laboratory measurement of entrainment and mixing in oceanic overflows*, In Proceedings of 2007 Joint ASME/JSME Fluids Engineering Summer Conference, San Diego, CA, USA (ASME, New-York, 2007).

[5] PRANDTL L., Z. angew. Math. u. Mech. **5** (1925), 136.

Direct energy cascade in the nonlinear Schrödinger equation

DAVIDE PROMENT*, SERGEY NAZARENKO**, MIGUEL ONORATO*

Abstract. *We present a numerical study of the 3D defocusing nonlinear Schrödinger equation (NLS) which describes waves in a nonlinear medium. By forcing the system at low wave numbers and including a dissipation term at low and high wave numbers, we achieve a turbulent steady state. Depending on the form of the dissipation at high scales (friction or hypo-viscosity), we observe two power law spectra. The first is consistent with the weak wave turbulence (WWT) prediction and the second, much steeper, leads to a critical balance (CB) conjecture.*

Keywords: weak wave turbulence, critical balance.

After the seminal papers by A. Kolmogorov in 1941, it is well established that, apart from small corrections due to intermittency, the energy spectrum, $E(k)$, of the velocity fluctuations for the high Reynolds number hydrodynamic turbulence shows a power law of the form $E(k) = C\,P^{2/3}\,k^{-5/3}$, where C is the dimensionless Kolmogorov constant and P is the flux of energy in wave number space. Many decades after the work by Kolmogorov, it has been discovered that systems of weakly nonlinear, dispersive, random waves also behave qualitatively in a similar way as hydrodynamical turbulence; the nonlinear interaction of waves can produce other waves characterized by different wavelengths and so on, generating a *cascade* process (just like the one observed in classical fluids) that ultimates in power law wave spectra. In this framework, a systematic approach based on averaging the dynamical equations leads to a Boltzmann like equation (known as *wave kinetic equation*) that describes the evolution of the spectral density function for the turbulent field. The turbulence that can be described by such an equation is known as weak wave turbulence (WWT).

In this context, a nonlinear dispersive model describing the interaction of waves that has been studied by many researchers is the nonlinear Schrödinger equation (NLS):

$$i\frac{\partial\psi}{\partial t} + \nabla^2\psi + \sigma|\psi|^2\psi = \mathcal{F} + \mathcal{D}\,, \tag{1}$$

where ψ is the wave function; σ can assume the value ± 1 depending on the physics of the problem. For $\sigma = -1$ the equation takes the name of *defocusing*

*Dipartimento di Fisica Generale, Università di Torino, Via Pietro Giuria 1, 10125 Torino, Italy.
**Mathematics Institute, The University of Warwick, Coventry, CV4-7AL, UK.

nonlinear Schrödinger equation or *Gross-Pitaevskii* equation (GPE) for repulsive potentials. $\mathcal{F}$ and $\mathcal{D}$ represent forcing and dissipation functions. Equation (1) describes for example the propagations of optical pulses in a nonlinear medium or weakly nonlinear interacting bosons in the limit of low temperature.

Assuming that the nonlinear interactions are small and that the field is quasi-gaussian and homogeneous, WWT can be applied to NLS and a *four-wave* wave kinetic equation can be derived:

$$\begin{aligned}\frac{\partial n_1}{\partial t} &= 4\pi \int n_1 n_2 n_3 n_4 \left(\frac{1}{n_1}+\frac{1}{n_2}-\frac{1}{n_3}-\frac{1}{n_4}\right) \\ &\quad \times \delta(\mathbf{k}_1+\mathbf{k}_2-\mathbf{k}_3-\mathbf{k}_4)\delta(\omega_1+\omega_2-\omega_3-\omega_4)d\mathbf{k}_{234}\end{aligned} \tag{2}$$

where the *wave-action* n_i is related to the wave filed as $\langle\hat{\psi}(\mathbf{k}_i,t)\hat{\psi}^*(\mathbf{k}_j,t)\rangle = n_i\delta(\mathbf{k}_i-\mathbf{k}_j)$ and $\omega(\mathbf{k}) = |\mathbf{k}|^2$ is the angular frequency of the wave numbers. Equation (3) conserves the total wave-action $N = \int n(\mathbf{k})d\mathbf{k}$ and the total energy $E = \int \omega(\mathbf{k})n(\mathbf{k})d\mathbf{k}$ and so, besides theromodynamic solutions, it has two non-equilibrium stationary isotropic solutions of the form of $n(k) \sim k^{-\alpha}$. They correspond to a region in the spectrum characterized by a constant flux of energy or wave-action: the first has a *direct cascade* with $\alpha = 3$ and the second follows an *inverse cascade* with $\alpha = 7/3$ For all details see [1].

In our simulation the domain of computation is a cube with uniform mesh of 256^3 points and periodic boundary conditions; we integrate equation (1) by a standard split step method. In order to observe constant fluxes, energy and wave-action are injected directly in Fourier space at low wave numbers by a forcing term of the form of $\hat{\mathcal{F}} = -if_0 e^{i\varphi(k)}$ with φ randomly distributed in k-space and time; to absorb energy at high wave numbers a dissipative hyperviscous term of the form of $\mathcal{D} = i\nu_h(\nabla^2)^n\psi$ is included. Note that, due to the inverse cascade process, wave-action accumulates at large scales, i.e. a condensate $c_0 = |\tilde{\psi}(\mathbf{k}=0,t)|$ keeps growing in the simulation. In order to avoid such growth which will generate a transition to a three-wave interactions [1], a dissipation must also be included at wave numbers lower that the ones corresponding to forcing. Different options are available.

We consider firstly a *friction* type of dissipation which takes the form $\hat{\mathcal{D}} = i\mu\theta(k^*-k)\hat{\psi}$ in Fourier space: θ is the Heaviside step function, k^* corresponds to lowest wavenumber forced and μ is a friction coefficient. We present our stationary state solution in figure 1. The resulting spectral slope is consistent with the prediction of the WWT theory. The growth of the condensate is stopped by friction, as shown in the inset.

Another common way of damping the low wave numbers consists, in analogy to what is done at high wave numbers, in including an *hypo-viscosity* term in the equation of the form of $\mathcal{D} = i\nu_l(\nabla^{-2})^m\psi$ and suppressing the condensate in Fourier space. In figure 2 we show the stationary states achieved with this new damping term for different forcing coefficient f_0. The observed spectrum

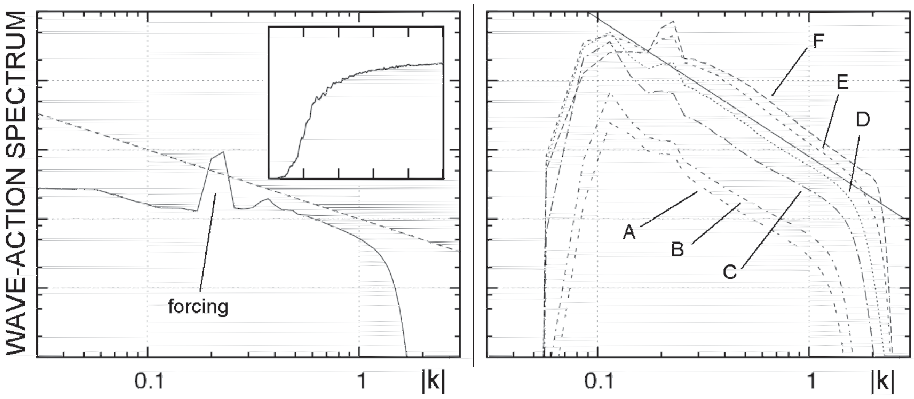

Figure 1: Integrated wave-action spectrum at steady stage of simulation in the presence of the friction term. The k^{-1} WWT prediction is also included. Inset: the condensate $c_0 = |\hat{\psi}(0,t)|$ as a function of time.

Figure 2: Integrated wave-action spectrum at steady stage of simulation with hypo-viscosity for different order of forcing coefficient from $f_0 = 0.05$ **(A)** to $f_0 = 3.0$ **(F)**. The k^{-2} slope of CB conjecture is also plotted.

is clearly much steeper than the WWT prediction and it is reasonably fitted by a power law k^{-2}. It seems that the direct energy cascade is strongly influenced by the accumulation of wave-action at wave numbers below the forcing causing an *infrared bottleneck effect*. Such a behavior leads to a critical balance (CB), i.e. the scale-by-scale balance of the linear and the nonlinear terms in equation (1). The CB is the result of the fact that the inverse waveaction cascade is arrested when the nonlinearity reaches the same level as the linear term (see [2] for details). If we evaluate CB slope in the case of three-dimensional NSL we find, for the integrated spectrum, a k^{-2} prediction.

Concluding we have found two universal regimes: one following the WWT prediction and the other arising from a CB conjecture. More details of our work can be found in [2].

References

[1] DYACHENKO S., NEWELL A.C. , PUSHKAREV A. AND ZAKHAROV V.E., *Optical turbulence: weak turbulence, condensates and collapsing filaments in the nonlinear Schrödinger equation*, Physica D **57**, 96 (1992).

[2] PROMENT D., NAZARENKO S., ONORATO M., *Energy cascades and spectra in turbulent Bose-Einstein condensates*, arXiv:0905.3263.

On the small-scale coherent structures of wall-bounded turbulence

SERGIO PIROZZOLI*

Abstract. *The small-scale vortical structures in wall-bounded turbulence are extracted by means of conditional sampling from a compressible turbulent boundary layer DNS database. The vortical patterns associated with vortex cores aligned with the streamwise and spanwise directions are separately considered. Their conditionally averaged flow fields consist, respectively, of a hairpin vortex, and of a quasi-longitudinal vortex tube.*

Keywords: boundary layers, coherent structures.

Coherent eddy structures are believed to play a major role in the dynamics of turbulent flows. In wall-bounded flows, a body of experimental [1] and numerical [4] works supports the view that boundary layers are populated by tubular hairpin vortices inclined at a positive angle with respect to the wall, either alone or arranged in packets [5]. Vortex-based models relying on 'forests' of hairpin-shaped vortex tubes [2] yield accurate predictions of many of the scaling behavior and statistics of turbulent boundary layers, supporting the notion that hairpin vortices play an important role in wall turbulence dynamics.

The present analysis relies on the supersonic boundary layer database of Ref. [3], and it is based on the swirling strength criterion [5] to educe vortex cores. We consider the conditional average fields associated with cross-stream (CS) and streamwise (SW) vortex cores by taking averages of the DNS fields under the conditions $\lambda_{ci} \geq 0.9\,\omega'$, $\omega_n/\omega \geq 0.9$, where λ_{ci} is the swirling strength, ω' is the local r.m.s. vorticity, and ω_n is the vorticity component in the spanwise and streamwise direction, respectively. The distributions of the average signed tube strength ($\omega_{t,n} = 2\lambda_{ci}\,\mathrm{sign}\,\omega_n$) and of the out-of-plane spanwise vorticity, conditioned to the occurrence of a CS and a SW vortex core (placed at $y^+ = 37$) are reported in figure 1, in the streamwise/wall-normal plane. In the CS case, the projected flow pattern consists of a shear layer fed by the wall vorticity, and having small slope with respect to the wall. The shear layer is observed to roll-up, forming a vortex tube near the origin of the conditioning event, in a fashion that recalls the Kelvin-Helmholtz mechanism of vorticity collapse. Secondary, clockwise-rotating vortex cores are also observed upstream and above, and downstream and below, with respect to the primary one. The average fields obtained by conditioning on the occurrence of a SW vortex show the roll-up of an oppositely signed vorticity sheet around the primary

*Dipartimento di Meccanica e Aeronautica, Università di Roma 'La Sapienza', Via Eudossiana 18, 00184 Roma. E-mail: sergio.pirozzoli@uniroma1.it

core, indicating the occurrence of a mechanism of near-wall vorticity stripping. In this case, only a small counter-rotating, companion vortex core is observed.

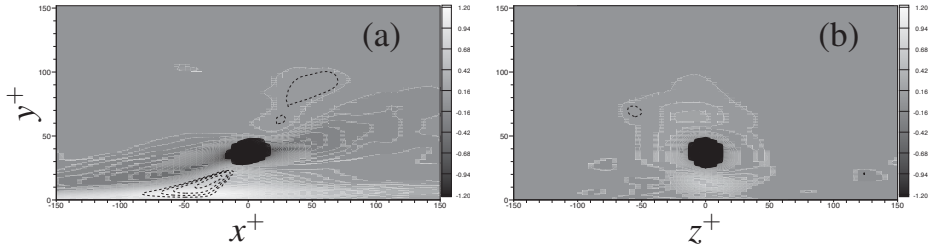

Figure 1: Expected fields of out-of-plane vorticity (flood) and signed swirling strength (lines), conditioned to vortex cores centered at $\overline{y}^+ = 37$. (a) CS vortices; (b) SW vortices. Solid lines: clock-wise vorticity; dashed lines: counter-clockwise vorticity.

To provide a three-dimensional perception for the geometry of the conditional educed structures, in figure 2 we report iso-surfaces of the swirling strength. Note that in the figure a relatively large threshold ($\lambda_{ci} = 0.50\,\omega'$) is used to isolate only the most dynamically significant features, and therefore most secondary motions seen in the two-dimensional representations are not recovered. For CS vortex cores, a pattern very similar to a canonical hairpin vortex is observed, extending for about 100^+ in the streamwise direction, and 50^+ in the spanwise direction. The conditional vortex structure exhibits extended quasi-longitudinal vortex tongues pointing in the downstream direction, that are very similar to those found in instantaneous realizations [5]. Quantitative examination of the figure indicates that the tubular part of the hairpin has a shallow inclination of $\approx 15^\circ$ in its donwstream part, whereas the head is inclined at $\approx 45^\circ$ with respect to the flow direction. The conditional average structure for SW vortex core (see figure 2(b)) consists of a quasi-longitudinal vortex having a length of approximately 200^+, and an inclination of $\approx 15^\circ$ with respect to the horizontal. The primary vortex is observed to restrict near the origin, where it is surrounded by an annular shear layer (recall figure 1(b)).

The analysis of the conditional fields associated with the occurrence of cross-stream (CS) and streamwise (SW) vortices shows that the vortex modes commonly observed in instantaneous realizations of wall turbulence, namely hairpin vortices and quasi-streamwise vortices, have statistical significance. In the CS vortex case, is seems that clock-wise cores are frequently associated with counter-rotating ones, suggesting that closed-loop structures (i.e. vortex rings) may play a relevant role in the formation and evolution of the hairpins. In particular, there is some evidence that an upstream counter-clockwise core stimulates the ejection (with subsequent roll-up) of a near-wall shear layer, and in turn the latter promotes the generation of near-wall, counter-clockwise vor-

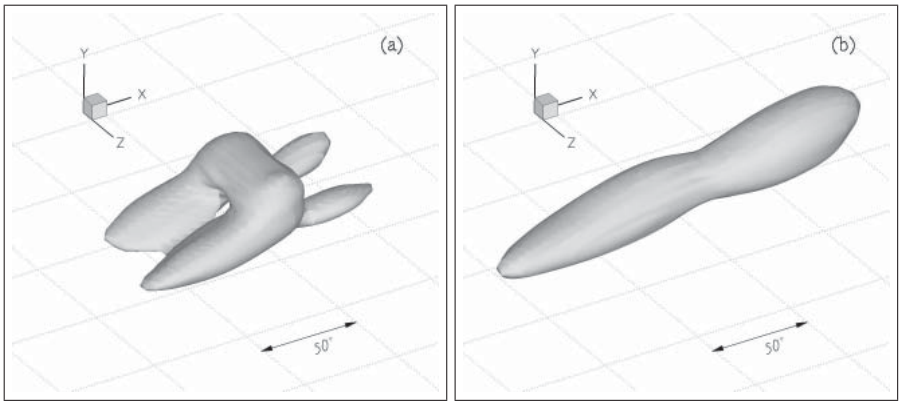

Figure 2: Iso-surfaces of swirling strength $\lambda_{ci}/\omega'(\bar{y}) = 0.50$, associated with vortex cores centered at $\bar{y}^+ = 37$: (a) CS vortices; (b) SW vortices.

ticity to satisfy the no-slip condition. In the SW vortex case, quasi-streamwise vortices are found, very often in isolation, which are observed to promote stripping of the near-wall vorticity. Further study is required to assess the dynamical relevance of the coherent vortex modes here reported.

References

[1] HEAD, M. AND BANDYOPADHYAY, P., *New aspects of turbulent boundary-layer structure*, J. Fluid Mech. **107** (1981), 297-338.

[2] PERRY, A.E. AND CHONG, M.S., *On the mechanism of wall turbulence*, J. Fluid Mech. **119** (1981), 173-217.

[3] PIROZZOLI, S. AND BERNARDINI, M. AND GRASSO, F., *Characterization of coherent vortical structures in a supersonic turbulent boundary layer*, J. Fluid Mech. **613** (2008), 205-231.

[4] WU, X. AND MOIN, P., *Direct numerical simulation of turbulence in a nominally zero-pressure-gradient flat-plate boundary layer*, J. Fluid Mech. **630** (2009), 5-41.

[5] ZHOU, J. AND ADRIAN, R. J. AND BALACHANDAR, S. AND KENDALL, T.M., *Mechanisms for generating coherent packets of hairpin vortices in channel flow*, J. Fluid Mech. **387** (1999), 353-396.

Collision rate of heavy particles in synthetic turbulents flows

LAURIS DUCASSE*, ALAIN PUMIR**

Abstract. *The collision rate of small inertial particles in turbulent flows simulated using a simplified model known as kinematic simulations [1] is studied. When inertia increases, the relative velocity of colliding particles can be substantially higher than expected from the local shear, a phenomenon reffered as the sling effect [2]. A Lagrangian method originally proposed in [3] has been used and compared to real numerical measurements of the collision rate, allowing us to estimate the sling contribution in the collision process.*

Keywords: inertial particles, collision rate, sling effect.

Understanding and predicting the collision rate of small inertial particles in turbulent flows is crucial in many natural and industrial processes. For instance, it can be a of importance to understand the growth of droplets in clouds during the phase of growth by coalescence. The collision rate K per unit of volume of equal size particles of diameter a and mean density n_0 can be written [4] :

$$K = \pi n_0^2 a^2 \langle |w_r| \rangle g(a) \tag{1}$$

where w_r is the radial relative velocity between particles and $g(a)$ the radial distribution function at contact. Numerical simulations have shown that this collision rate is larger for inertial particles than in the case of simple tracers. This observation can be explained by two effects : (i) the concentration around particles is locally larger than the mean density ($g(a) > 1$), due to "preferential concentration" [5], and (ii) the relative velocity between two colliding particles can be significantly larger than expected based on the typical rate of strain tensor, as described by the Saffman-Turner formula [6].

Aside from the Reynolds number, two dimensionless parameters characterize the problem : the Stokes number $\mathrm{St} = \tau/\tau_K$ and the Froude number $\mathrm{Fr} = u_K/g\tau$ which measure the inertia of the particles and the influence of the gravity respectively. Here, τ is the response (Stokes) time of the particles, τ_K and u_K the time and velocity at the Kolmogorov scale and g the acceleration of gravity. The equation of motion of a particle in this context can be written [5] :

$$\mathrm{d}\mathbf{v}/\mathrm{d}t = (\mathbf{u} - \mathbf{v})/\tau + \mathbf{g} \tag{2}$$

*Institut Non Linéaire de Nice, Valbonne, France. E-mail: lauris.ducasse@inln.cnrs.fr
**Ecole Normale Supérieure de Lyon, Lyon, France. E-mail: pumir@ens-lyon.fr

Differentiating Eq.(2), one can obtain the equation of evolution of the gradient velocity tensor in the Lagrangian frame [2]:

$$\mathrm{d}\sigma/\mathrm{d}t = (\mathbf{h} - \sigma)/\tau - \sigma^2 \tag{3}$$

where $\sigma_{ij} = \partial_j v_i$ and $h_{ij} = \partial_j u_i$. The quadratic nonlinear term in (3) leads to the possibility of a divergence in finite time for σ. This divergence can be interpreted physically by signalling that particles acquire a velocity, which strongly differs from the fluid velocity. Particles experiencing such a sling shot [2] are prone to collide with other particles having very different histories and velocities, hence lead to an enhancement of the term $\langle |w_r| \rangle$ in eq.(1), and thus of the collision rate K. This effect can also be understood by the formation of fold caustics in the velocity field of the particles [7].

Here, we decompose the collision rate into two components. The first one comes from collisions occurring in regions where the velocity field of the particles $\mathbf{v}$ is continuous. The relative velocity of the colliding particles can thus be estimated by $w_r = a \times \hat{\mathbf{r}}.\sigma.\hat{\mathbf{r}}$. The other case concerns collisions occurring within the caustics. In this situation, the relative velocity cannot be approximated by σ. These two types of collisions will be referred respectively as "continuous" and "sling".

We estimate separately these two contributions using the Lagrangian method proposed in [3]. At any time, the continuous contribution of a given trajectory is computed by estimating the instantaneous flux of incoming particles on a target particle, In order to obtain the continous contribution to the collision rate K_c, it is enough to follow a large number of lagrangian trajectories [3].

The estimation of the sling component is more phenomenological. We expect it to be proportional to the frequency at which the particles cross the caustics. This quantity is directly accessible in our simulation measuring the average rate at which σ diverge in time. For this reason we call it the "blowup frequency" noted f_{bu}. Thus, the sling contribution K_s will be given by,

$$K_s = \frac{n_0}{2} \times \mathcal{N}_s \times f_{bu} \tag{4}$$

where $\mathcal{N}_s$ corresponds to the average number of collisions occurring in the wake of a sling event. This latter is proportional to the typical relative velocity of the particles experiencing a sling collision w_r^s. This quantity is difficult to estimate accurately. However, a crude reasoning based on dimensional arguments suggests, $w_r^s \propto \mathrm{St}^{-1/2}$.

Our results obtained by this Lagrangian method have been compared with real numerical measurements of the collision rate. The results, normalized by the case of tracers K_{ST} [6], are shown on Fig. 1 for two different intensities of the gravity measured by the dimensionless parameter $\varepsilon_0 = \mathrm{Fr} \times \mathrm{St}$.

We observe that the sling contribution is essentially zero for $\mathrm{St} \lesssim 0.3$. This results from the fact that f_{bu} behaves asymptotically as $\exp(-A/\mathrm{St})$ for small

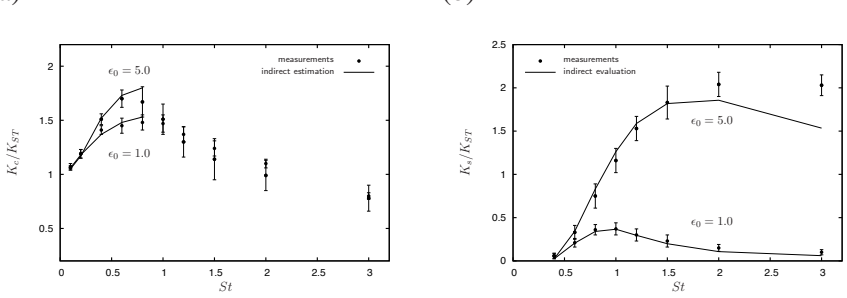

Figure 1: Comparison between direct measurements and the indirect Lagrangian evaluation of the different contributions to the collision rate normalized by the ST case for two different intensity of the gravity. (a) Continuous contribution. (b) Sling contribution.

St. We notice that the sling contribution is strongly affected by the gravity. indeed, when gravity increases, particles fall more rapidly and their interaction time with the turbulent structures decreases. For this reason, the probability for them to be accelerated enough and thus experience a sling event is reduced. We observe that for St $\lesssim 1$, K_c is higher than in the case of tracers.

References

[1] FUNG, J.C.H. ET AL., *Kinematic simulation of homogeneous turbulence by unsteady random Fourier modes*, J. Fluid Mech. **236**, 281 (1992).

[2] FALKOVICH, G. , FOUXON, A. AND STEPANOV, M.G., *Acceleration of rain initiation by cloud turbulence*, Nature **419**, 151 (2002).

[3] FALKOVICH, G. AND PUMIR, A., *Sling Effect in Collisions of Water Droplets in Turbulent Clouds*, J. Atmos. Sci. **64**, 4497 (2007).

[4] WANG, LP., WEXLER, A.S. AND ZHOU, Y., *Statistical mechanical descriptions of turbulent coagulation*, Phys. Fluids. **10**, 266-276 (1998a).

[5] SHAW, R., *Particle-Turbulence Interactions in Atmospheric Clouds*, Ann. Rev. Fluid Mech. **35**, 183-227 (2003).

[6] SAFFMAN, P.G. AND TURNER, J.S., *On the collision of drops in turbulent clouds*, J. Fluid Mech. **1**, 16-30 (1956).

[7] WILKINSON, M. AND MEHLIG, B., *Caustics in turbulent aerosols*, Europhysics Letters, **71**, 186-192 (2005).

Spectral Energy Transfer in Strongly Stratified Flows

JAMES J. RILEY*, VISHAL VASAN**

Abstract. *The dynamics of many regions of the oceans and of the atmosphere, for example in the open ocean at horizontal scales from a few meters up to hundreds of meters or more, are typified by strong, stable density stratification but weak if any effects of the earth's rotation. It is clear from numerical simulations and from the analysis of atmospheric and oceanic data that the motions at these scales are characterized by strong, forward (downscale) spectral energy transfer in the horizontal, leading to smaller-scale turbulence. Laboratory studies of strongly stratified flows also indicate a strong upscale spectral energy transfer. In the strongly stratified flow regimes of these experiments, however, the Reynolds numbers are often low enough that the strong forward spectral energy transfer is not observed. This raises the question of whether the upscale transfer observed in the laboratory would occur in the high Reynolds number environments of the oceans and atmospheres, and, more generally, the question of the overall spectral energy transfer in such flows.*

We have performed direct numerical simulations of strongly stratified flows at high enough Reynolds numbers that strong, forward energy transfer in the horizontal is observed, but in a large enough computational domain to allow for significant upscale transfer as well. We find that, contrary to the nonstratified case, significant upscale spectral energy transfer does occur, even in the presence of the strong downscale transfer. To explain the results, heuristic arguments are given regarding the inhibition by the stable stratification of the vertical velocity and of the stretching of larger-scale, vertical vorticity.

Keywords: spectral energy transfer, strongly stratified flow.

*University of Washington, Seattle.
E-mail: rileyj@u.washington.edu
**University of Washington, Seattle.
E-mail: vvasan@amath.washington.edu

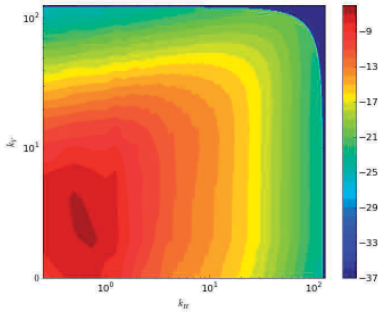

Figure 1: Horizontal kinetic energy spectrum in the k_h-k_v plane at $t = 34$, $Re = 6400$, $F = 4$.

1. Results

The simulations are performed on 1024x1024x128-point computational grids of domain size 8π x 8π x π in the two horizontal directions and the vertical direction, respectively. Approximately fully-dealiased, Fourier spectral methods were used to approximate spatial derivatives, with 4^{th}-order Runga-Kutta time stepping. The simulated flows are unforced, with Taylor-Green-type of initial conditions with uncorrelated, low-level noise added. Simulations were run at two initial Reynolds numbers, 800 and 6400, and, for the stratified case, the initial Froude number of 0.64.

As observed by Riley and de Bruyn Kops [1], as the Taylor-Green-type flow develops in time under the influence of strong stratification, vigorous vertical shearing of the horizontal velocities occurs, which leads to locally low Richardson numbers and to intermittent, small-scale instabilities and turbulent-like motions. This in turn leads to a strong, downscale cascade of energy which results, in particular, in the development of a 'stratified turbulence' inertial range.

An overall picture of spectral energy transfer can be obtained by first examining the spectral energy in the two-dimensional, horizontal-vertical, k_h-k_v plane, as shown in Figure 1, which gives the logarithm of the spectrum of the horizontal kinetic energy at the time $t = 34$, after the flow has evolved considerably. The peak in the spectrum is now at a horizontal wave number of about 0.5, whereas initially it was at the Taylor-Green scale of about 1.4. In addition, there is considerable energy in vertical wave numbers up to about 10, whereas the initial energy was localized at wave number 0.5; this is indicative of the strong vertical shearing of the horizontal velocity which occurs in strongly stratified flows.

The corresponding energy transfer spectrum is shown in Figure 2, which gives this quantity at $t = 34$. The transfer of energy out of the original horizon-

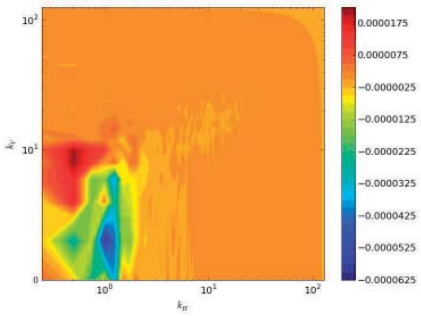

Figure 2: Horizontal kinetic energy transfer spectrum in the k_h-k_v plane for $t = 34$, $Re = 6400$, $F = 4$.

tal Taylor-Green scale ($k_h \sim 1.4$), now over a range of vertical scales, is clearly visible. Interestingly, there is also a transfer out of horizontal wave numbers lower than the Taylor-Green scale at vertical wave numbers near about 2; motion at these scales have been energized by the upscale transfer process. The transfer out of these scales is now energizing vertical wave numbers near 10, as now the strong vertical shearing of the larger scale horizontal motions occurs. In summary, significant energy is transferred to higher vertical wave numbers, as well as higher overall wave numbers. But at the same time significant energy is being transferred to lower wave numbers as well, especially for lower wave numbers with $k_v \sim 10$.

2. Conclusions

Our preliminary conclusions are that indeed there is significant upscale transfer of energy, consistent with laboratory experiments, in strongly stratified flows at high enough Reynolds numbers for instabilities and smaller-scale turbulence to exist. In our presentation at the EUROMECH Colloquium 512, we will present some theoretical arguments which justify this upscale transfer of energy, discuss some further spectral energy transfer analysis of our simulations, and present the results of some ongoing simulations on larger computational domains.

References

[1] J.J. Riley and S.M. de Bruyn Kops, Phys. Fluids, **156**(7), 2047 (2003).

Scale-by-scale energy budgets in turbulent convection

FRANÇOIS RINCON*

Abstract. *Understanding the phenomenology, statistical properties and scaling laws of turbulence forced by various natural processes such as shear or thermal convection is facilitated by analysing scale-by-scale energy budgets in experimental or numerical realizations of such flows. This contribution addresses the issue of numerical Rayleigh-Bénard convection at moderate Rayleigh number* 10^6 *and Prandtl number one. The results tend to rule out the possiblity of Bolgiano-Obouhkov scalings at moderate Ra and reveal striking similarities with studies of scale-by-scale budgets in homogeneous shear flows and turbulent channel flows.*

Keywords: turbulence, convection, scaling laws.

1. Motivation

In nature, the forcing of three-dimensional turbulence often finds its source in a large-scale gradient (of velocity, temperature etc.) and is therefore likely *anisotropic* and *broadband* in wavenumber space. Besides, natural turbulent flows are commonly observed in *inhomogeneous* environments (like the earth atmosphere or the solar surface). Hence, an important question is whether the classical Kolmogorov (K41) description of turbulence (relying on large-scale forcing, homogeneity and isotropy) provides an acceptable guidance to understand the statistical properties of such flows (overlooking intermittency effects) or if a specific theory should be formulated for each type of flow (e. g. thermal convection or shear turbulence).

A promising avenue of research to explore this issue is to construct extended versions of the Kolmogorov and Yaglom equations [1, 2] retaining forcing, anisotropic and inhomogeneous contributions. Deviations from the basic K41 assumptions can then be quantified in experiments or numerical simulations by comparing at each scale the amplitude of these extra terms with that of the classical 4/3 and diffusive terms. In the following, I highlight two important aspects of the turbulent Rayleigh-Bénard problem using this method. How does buoyancy enter the scale-by-scale budget and should Bolgiano-Obukhov (B059) scalings [4, 5] be expected ? Does turbulent thermal convection bear any statistical resemblance with other turbulent flows ?

*Laboratoire d'Astrophysique de Toulouse-Tarbes, Université de Toulouse, CNRS, 14 avenue Edouard Belin, F-31400 Toulouse, France.
E-mail: rincon@ast.obs-mip.fr

2. Theory and results

A generalization of the hydrodynamic Kolmogorov and Yaglom equations can be found in [3]. Here, I restrict the focus to the isotropic projection of the Kolmogorov equation in numerical simulations of mildly turbulent Rayleigh-Bénard convection at $Ra = 10^6$ and $Pr = 1$ (the isotropic part of the statistics is shown to dominate at all scales in [3] ; note however that inferring scaling exponents from reduced statistics computed from correlations along a single direction yields inaccurate values in this regime). Following notations used in similar derivations [6, 7], the equation reads

$$S_3 = -\frac{4}{3}\left\langle \varepsilon \right\rangle r + 2\nu \frac{\partial S_2}{\partial r} + B + NH \tag{1}$$

where $S_3(r) = 1/(4\pi r^2)\oint_{\partial B_r}\left\langle \delta u_j^2 \delta u_i \right\rangle n_i \,\mathrm{d}S_r$, $S_2(r) = 1/(4\pi r^2)\oint_{\partial B_r}\left\langle \delta u_j^2 \right\rangle \mathrm{d}S_r$, $\left\langle \varepsilon \right\rangle$ is the mean dissipation rate and B and NH stand for the isotropic components of the buoyancy correlator (involving $\left\langle \delta\theta \delta u_z \right\rangle$) and inhomogeneous terms. The various terms in this equation are shown in Fig. $1(a,b)$.

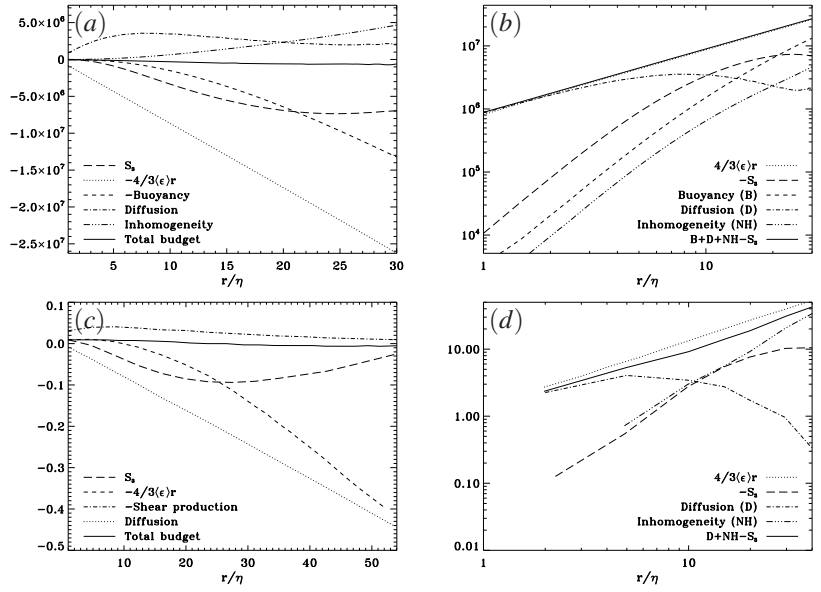

Figure 1: Scale-by-scale budgets for the Kolmogorov equation. (a) Rayleigh-Bénard convection at $Ra = 10^6$, $Pr = 1$, $Re_\lambda \sim 30$. (b) Same as (a) on a log scale. (c) Homogeneous shear turbulence at $Re_\lambda \sim 45$ (reproduced from [6], Fig. $1(a)$). (d) Channel turbulence at $Re_\lambda \sim 35$ (reproduced from [7], Fig. 4).

3. Analysis and discussion

The previous results tend to rule out the existence of BO59 for moderate Ra and $Pr = 1$. Indeed, the cross-over scale (the so-called Bolgiano scale L_B) between the 4/3 term and the buoyancy term turns out to be larger than the integral scale $L_{\rm int}$ of the system. However, at scales smaller than $L_{\rm int}$, a standard dominant balance $S_3 \sim r$ leading to a K41 spectrum is not observed either. As shown in Fig. $1(a)$, this is partly because the thermal forcing remains important at "inertial" scales and partly because the inhomogeneous contributions take over at large scales. The diffusive term also contributes in this mildly turbulent regime but it is smaller at large scales than other contributions. Hence, the *absence of inertial-range* in this regime is explained in terms of *violation of the assumptions of large-scale forcing and homogeneity in the K41 theory*.

The second point is that *the turbulent convection budget bears a lot of resemblance with the budgets of other types of moderately turbulent flows*. First, there is a striking similarity between Fig. $1(a)$ and the budget obtained from simulations of homogeneous shear flow turbulence [6], shown in Fig. $1(c)$. In both cases, the cross-over between the production term and the 4/3 term takes places at scales comparable to the integral scale, ruling out the possibility of forcing-dependent power laws. Another interesting point is that the budget of channel flow turbulence [7], shown in Fig. $1(d)$, follows the same trends as Fig. $1(b)$. Most notably, the inhomogeneous terms produce similar effects.

To conclude on a general note, scale-by-scale budgets give valuable clues on the reasons for the realization of (or lack of) scaling laws in turbulent flows.

Apologetic note: a significant amount of references on this subject could not be included due to space limitations. A much more detailed list is given in [3].

References

[1] KOLMOGOROV, A.N., *Dissipation of energy in the locally isotropic turbulence*, Doklady Akad. Nauk SSSR, **32** (1941), 16.

[2] MONIN, A.S. AND YAGLOM, A.M., *Statistical Fluid Mechanics*, MIT Press (1975).

[3] RINCON, F., *Anisotropy, inhomogeneity and inertial-range scalings in turbulent convection*, J. Fluid. Mech., **563** (2006), 43-69.

[4] BOLGIANO, R., *Structure of turbulence in stratified media.*, J. Geophys. Res., **64** (1959), 2226.

[5] OBUKHOV, A. M., Dokl. Akad. Nauk. SSR, **125** (1959), 1246.

[6] CASCIOLA, C. M., GUALTIERI, P., BENZI, R. AND PIVA, R., *Scale-by-scale budget and similarity laws for shear turbulence*, J. Fluid Mech., **476** (2003), 105-114.

[7] DANAILA, L., ANSELMET, F., ZHOU, T. AND ANTONIA, R. A., *Turbulent energy scale budget equations in a fully developed channel flow*, J. Fluid Mech., **430** (2001), 87-109.

Small-scale statistics in wall bounded shear flows

PETER E. HAMLINGTON*, DMITRY KRASNOV**,
THOMAS BOECK***, JÖRG SCHUMACHER****

Abstract. *The statistical properties of velocity gradients in a wall-bounded turbulent channel flow are discussed on the basis of three-dimensional direct numerical simulations. Our analysis is concentrated on the trends of the statistical properties of the local enstrophy and the energy dissipation rate with increasing distance from the wall.*

Keywords: Velocity gradients, Turbulent channel flow.

Turbulence is associated with large fluctuations of velocity gradients which appear preferentially at the smallest scales of the flow. The amplitudes of the fluctuations exceed the mean values by orders of magnitude when the Reynolds number of the flow is sufficiently large. This behaviour is known as small-scale intermittency. It has been discussed recently that a deeper understanding of fluid turbulence as a whole requires a detailed resolution of the intermittent dynamics at the small-scale end of the inertial range. This will include scales that are smaller than the (mean) Kolmogorov dissipation length $\eta_K = \nu^{3/4}/\langle\varepsilon\rangle^{1/4}$ with the kinematic viscosity ν and the mean energy dissipation rate $\langle\varepsilon\rangle$. Although significant progress in measurement techniques has been made, the finest structures remain still spatially unresolved or the flows are limited to very low Reynolds numbers. Direct numerical simulations can reach today sufficiently high Reynolds numbers while resolving the gradients at the small-scale end of the inertial range cascade properly.

The small-scale structure and statistics of turbulence has been mostly studied for the case of homogeneous, isotropic and statistically stationary turbulence. A wall-bounded shear flow consists of a boundary layer which is dominated by coherent streamwise structures and a central bulk region in which they are basically absent. The statistics in the wall-normal direction is inhomogeneous and requires a height-dependent analysis on account of the varying strength of the mean shear [1]. As a consequence, there is significantly less work on the properties of small-scale turbulence for wall-bounded flows than

*Aerospace Engineering, The University of Michigan, Ann Arbor, MI 48109-2140, USA.
E-mail: peterha@umich.edu
**Mechanical Engineering, TU Ilmenau, P.O.Box 100565, D-98684 Ilmenau, Germany.
E-mail: dmitry.krasnov@tu − ilmenau.de
***Mechanical Engineering, TU Ilmenau, P.O.Box 100565, D-98684 Ilmenau, Germany.
E-mail: thomas.boeck@tu − ilmenau.de
****Mechanical Engineering, TU Ilmenau, P.O.Box 100565, D-98684 Ilmenau, Germany.
E-mail: joerg.schumacher@tu − ilmenau.de

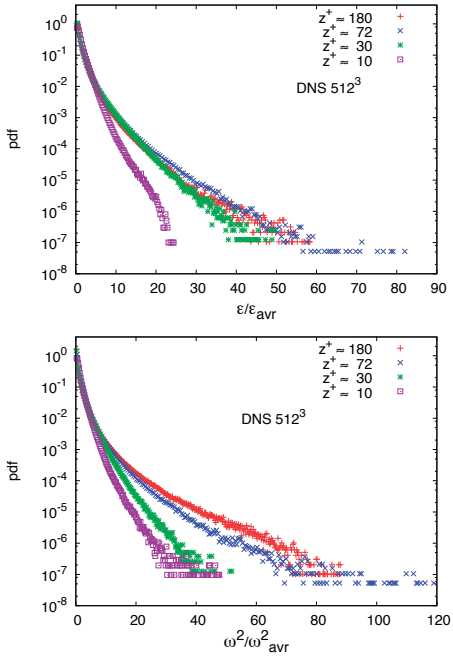

Figure 1: Probability density functions of the energy dissipation rate ε (top) and local enstrophy ω^2 (bottom) for a highly resolved turbulent channel flow at $Re_\tau = 180$. Data are obtained in planes at four different distances z^+ from the wall which are indicated in the legends. We denote $\varepsilon_{avr} = \langle\varepsilon\rangle_{A,t}$ and $\omega^2_{avr} = \langle\omega^2\rangle_{A,t}$ where $\langle\cdot\rangle_{A,t}$ is an average over planes at z^+ and a sequence of statistically independent turbulence samples. The distance $z^+ = 72$ corresponds with the logarithmic region of the channel flow.

for homogeneous isotropic turbulence. This suggests to our view a systematic study of the height-dependence of the statistics of the velocity gradient fields in turbulent shear flows.

In the present work, we want to make a step in this direction and conduct an analysis of the small-scale statistics of the velocity gradient in a wall-bounded shear flow. We perform three-dimensional direct numerical simulations of a turbulent channel flow. The applied pseudospectral method is based on Fourier series in the horizontal directions x and y and a Chebyshev polynomial expansion in the vertical z–direction [2]. Our study will be focussed to two fields, the local enstrophy field and the energy dissipation rate field.

We detect a sensitive dependence of the largest amplitudes of both fields,

which correspond with the tails of the probability density functions (PDF), on the spectral resolution. It is shown that a full statistical analysis of both fields requires a spectral resolution which is larger than the standard one. This was one objective of our study, namely to make this case in a turbulent wall-bounded shear flow. It clearly limits the range of accessible Reynolds numbers. Based on this result, we investigated the height-dependence of the statistics of the velocity gradient fields. The single-quantity PDFs as well as the joint distribution of the energy dissipation rate, $\varepsilon(\mathbf{x},t)$, and the local enstrophy, $\omega^2(\mathbf{x},t)$, vary significantly with increasing distance from the wall. In Figure 1, we show the probability density functions of ε and ω^2 for four different planes. The largest fluctuations of the velocity gradients are found in the logarithmic layer ($z^+ = 72$). This is in agreement with recent laboratory experiments which observe a bursting of hairpin vortex packets into the logarithmic region [3]. Finally, we report first studies of the distribution of locally fluctuating dissipation scales in a channel flow. Recent measurements in a turbulent pipe flow at the nearly isotropic pipe centerline and within the anisotropic logarithmic layer showed excellent agreement with distributions that were previously calculated from numerical simulations of homogeneous isotropic box turbulence and with those predicted by theory [4].

Our work is supported by the Emmy-Noether-Program (DK and TB) and the Heisenberg-Program (JS and PEH with travel support) of the Deutsche Forschungsgemeinschaft (DFG). The supercomputing ressources were provided by the Jülich Supercomputing Centre (Germany) under grant HIL01.

References

[1] WALLACE, J. M., *Twenty years of experimental and direct numerical simulation access to the velocity gradient tensor: What have we learned about turbulence?*, Phys. Fluids, **21** (2009), 021301.

[2] KRASNOV, D., ROSSI, M., ZIKANOV, O. AND BOECK, T., *Optimal growth and transition to turbulence in channel flow with spanwise magnetic field*, J. Fluid Mech., **596** (2008), 73-101.

[3] ADRIAN, R. J. *Hairpin vortex organization in wall turbulence*, Phys. Fluids, **19** (2007), 041301.

[4] BAILEY, S. C., HULTMARK, M., SCHUMACHER, J., YAKHOT, V. AND SMITS, A. J., *Measurement of local dissipation scales in turbulent pipe flow*, Phys. Rev. Lett., **103** (2009), 014502.

Segregation of inertial particles in turbulence via the Full Lagrangian Approach

RUTGERUS H.A. IJZERMANS*, MICHAEL W. REEKS*, ELENA MENEGUZ*,
MAURIZIO PICCIOTTO**, ALFREDO SOLDATI**

Abstract. *Preferential concentration of inertial particles in turbulence is studied numerically by evaluating the Lagrangian compressibility of the particle velocity field using the "full Lagrangian method". This is compared with the "mesoscopic Eulerian particle velocity field" both in a direct numerical simulation of turbulence and in a synthetic flow field.*

Keywords: particle, segregation.

Transport and agglomeration of particles/droplets in turbulent flows have been intensively studied in recent years given their importance in many environmental and engineering applications such as formation and growth of MP10 particulate, warm rain initiation, transport of chemically created aerosols, fouling of heat transfer equipment and chemical process facilities (Campolo et al., 2008).

In this work we quantificate the particle segregation by exploiting the full Lagrangian method, proposed by Osiptsov (1984), and later used by Healy and Young (2005), and the "mesoscopic Eulerian formalism" (MEF), a method essentially based on box counting and proposed by (F´evrier et al., 2005) and (Simonin et al., 2006). We also benchmark the two methods in simple two-dimensional synthetic turbulent flow field and in a direct numerical simulation (DNS) of turbulence. The FLM evaluates the size of an infinitesimally small volume of particles and tracks its changes in the course of time along each particle trajectory. The rate of deformation of this volume is related to the compressibility of the particle velocity field which is an indicator of particle concentration (Picciotto et al., 2005, IJzermans et al. 2009).

Neglecting Brownian motion, the equations of motion of identical, rigid and spherical particles are (Maxey and Riley, 1983):

$$\frac{\mathrm{d}\mathbf{x}_p}{\mathrm{d}t} = \mathbf{v}, \qquad \frac{\mathrm{d}\mathbf{v}}{\mathrm{d}t} = \frac{1}{\mathrm{St}}\big(\mathbf{u} - \mathbf{v}\big), \tag{1}$$

*School of Mechanical and Systems Engineering, Newcastle University, Claremont Road, Newcastle-upon-Tyne NE1 7RU, United Kingdom.

**Dipartimento di Energetica e Macchine, University of Udine, Via delle Scienze 208, 33100 Udine, Italy
E-mail: soldati@uniud.it

where $\mathbf{x}_p$ and $\mathbf{v}$ are the position and the velocity of the particle respectively and $\mathbf{u} = \mathbf{u}(\mathbf{x}_p, t)$ is the velocity of the carrier flow at the position of the particle. In a continuum approach in which the spatial derivatives of $n\overline{\mathbf{v}}$ are finite, the particle concentration $n(\mathbf{x}, t)$ evolves by (Elperin et al., 1996): $\partial_t n + \nabla \cdot (n\overline{\mathbf{v}}) = 0$. Along the trajectory of a particle which moves with velocity $\overline{\mathbf{v}}$, it is:

$$\frac{\mathrm{d}n}{\mathrm{d}t} = -n\left(\nabla \cdot \overline{\mathbf{v}}\right). \tag{2}$$

where $\nabla \cdot \overline{\mathbf{v}}$ denotes the compressibility of the particle velocity field.

Exploting the FLM, we define a unit deformation tensor as $J_{ij} \equiv \partial x_{p,i}(\mathbf{x}_0, t)/\partial x_{0,j}$ and differentiate Eq. 1 with respect to $\mathbf{x}_0$ in order to obtain:

$$\frac{\mathrm{d}J_{ij}}{\mathrm{d}t} = \dot{J}_{ij}, \qquad \frac{\mathrm{d}}{\mathrm{d}t}\dot{J}_{ij} = \frac{1}{St}\left(J_{kj}\frac{\partial u_i}{\partial x_k} - \dot{J}_{ij}\right). \tag{3}$$

The initial conditions are chosen as $J_{ij}(0) = \delta_{ij}$ and $\dot{J}_{ij}(0) = \partial u_i(\mathbf{x}_0, 0)/\partial x_j$. Along a particle trajectory, the instantaneous value of J corresponds to the inverse of the particle concentration, so that using Eq. 2 and averaging over all particle trajectories gives a relation between J and the compressibility of the particle velocity field $\nabla \cdot \overline{\mathbf{v}}$ (Elperin et al., 1996):

$$\frac{\mathrm{d}}{\mathrm{d}t}\langle \ln|J| \rangle = \langle \nabla \cdot \overline{\mathbf{v}} \rangle. \tag{4}$$

Eq. 4 may result in J becoming equal to zero momentarily, which is equivalent to a singularity in the particle velocity field ($\nabla \cdot \overline{\mathbf{v}} = -\infty$).

According to the MEF, the velocity of particles dispersed in turbulent flows can be seen as the sum of two contributions: a continuous turbulent velocity field shared by all particles called the Mesoscopic Eulerian Particle Velocity Field (MEPVF) and denoted by $\overline{\mathbf{v}}$, and a random velocity component we refer to as Random Uncorrelated Motion (RUM) (Reeks, 2004). The MEF approach provides a way to calculate $\nabla \cdot \overline{\mathbf{v}}$ (F´evrier et al., 2005) and (Simonin et al., 2006), based upon a division of the calculation domain into grid cells. Averaging the velocities of all the particles inside a cell gives $\overline{\mathbf{v}}$, defined in the center of a cell. By taking the spatial derivatives using a finite difference method, one can obtain $\nabla \cdot \overline{\mathbf{v}}$ at each cell center.

Comparison between the methods are presented in a simple two-dimensional synthetic flow field (Babiano et al., 2000) for $St = 0.05$ (Fig. 1a) and for $St = 0.5$ (Fig. 1b), together with the analytical estimate valid for small Stokes $\nabla \cdot \overline{\mathbf{v}} \simeq -\mathrm{St}\nabla \cdot (\mathbf{u} \cdot \nabla \mathbf{u}) = -\mathrm{St}Q$ (Elperin et al., 1996). For a small Stokes number such as $St = 0.05$ (Fig. 1a), the three lines collapse. A different qualitative behaviour is instead observed for $St = 0.5$ (Fig. 1b), as it contains sharp negative peaks in the value of $\langle \nabla \cdot \overline{\mathbf{v}} \rangle$. These intermittent events correspond to

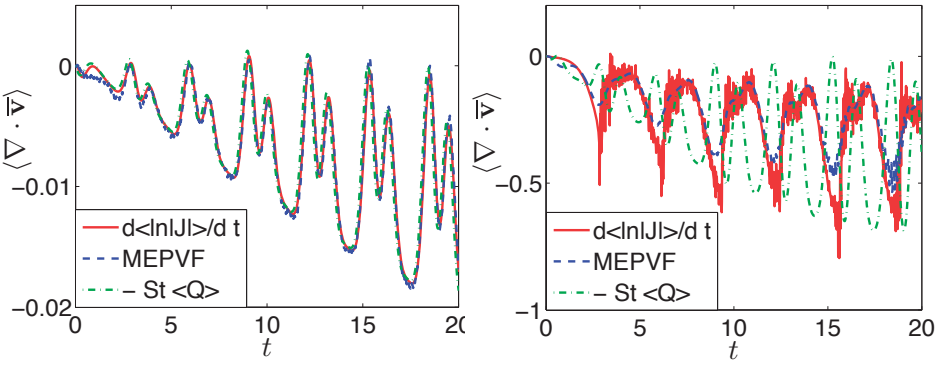

a) b)

Figure 1: (Color online) Compressibility of the particle velocity field $\langle \nabla \cdot \overline{\mathbf{v}} \rangle$ in the synthetic flow as a function of time, measured by the FLM (red solid line), and by the MEF (blue dashed line). a) $\mathrm{St} = 0.05$, b) $\mathrm{St} = 0.2$.

a sudden collapse of the volume occupied by the particles so that $J \sim 0$ and $\langle \nabla \cdot \overline{\mathbf{v}} \rangle \to -\infty$. This phenomenon is due to RUM, i.e. singularities in the flow field where particle trajectories cross and J vanishes. The agreement between the MEF and the FLM is nonetheless very good, although the peaks tend to be a bit steeper in the Lagrangian method, suggesting that the FLM is able to detect singularities in the spatial distribution of particles, in contrast to the MEF which is ultimately based on a difference equation.

References

[1] M. Campolo, A. Cremese, and A. Soldati *Controlling particle dispersion in a transverse jet by synchronized injection*, AIChE J. **54** (2008), 1975-1986

[2] Osiptsov A. N. *Investigation of regions with unbounded growth of the particle concentration in disperse flows*, Fluid Dyn. **19**(1984), 378-384.

[3] F´evrier P., Simonin O., and Squires K. D. *Partitioning of particle velocities in gas-solid turbulent flows into a continuous field and a spatially uncorrelated random distribution; theoretical formalism and numerical study*, J. Fluid Mech. **553** (2005), 1-46.

[4] Simonin O., Zaichik L. I., Alipchenkov V. M., and F´evrier P. *Connection between Two Statistical Approaches for the Modelling of*

Particle Velocity and Concentration Distributions in Turbulent Flow: the Mesoscopic Eulerian Formalism and the Two-Point Probability Density Function Method, Phys. Fluids, **18-12** (2006), 125107-1, 125107-9.

[5] PICCIOTTO M., MARCHIOLI C., REEKS M.W., SOLDATI A. *Statistics of velocity and preferential accumulation of micro-particles in boundary layer turbulence* Nucl.Eng & Des **235** (2005), 1239-1249

[6] IJZERMANS R., REEKS M.W., MENEGUZ E., PICCIOTTO M., SOLDATI A. *Measuring segregation of inertial particles in turbulence by Full Lagrangian Approach* PHYS. REV. E, **80** (2009) 015302.

[7] HEALY D. P. AND YOUNG J. B., *Full lagrangian methods for calculating particle concentration fields in dilute gas-particle flows*, IN *Proc. Roy. Soc. London A: Mathematical, Physical and Engineering Sciences* **461(2059)** (2005), 2197-2225.

[8] MAXEY M. R. AND RILEY J. J., *Equation of motion for a small rigid sphere in a nonuniform flow* PHYS. FLUIDS **26(4)** (1983), 883-889.

[9] ELPERIN T., KLEEORIN N., AND ROGASHEVSKII I. *Turbulent thermal diffusion of small inertial particles*, PHYS. REV. LETT **76(2)** (1996), 224-227.

[10] REEKS M. W. *Simulation of particle diffusion, segregation, and intermittency in turbulent flows*, IN *Proc. of IUTAM Symposium on Computational Modelling of Disperse Multiphase Flow (Edited by S. Balachandar and A. Prosperetti)* (2004), 21-30.

[11] BABIANO A., CARTWRIGHT J. H. E., PIRO O. AND PROVENZALE A. *Dynamics of a small neutrally buoyant sphere in a fluid and targeting in Hamiltonian systems*, PHYS. REV. LETT **84** (2000), 5764-5767.

Small scale anisotropy induced by a spatial variation of the integral scale

DANIELA TORDELLA*, MICHELE IOVIENO*

Abstract. *The main point of this communication is that an onset of anisotropy of the small scale can be observed, even in the presence of a particularly mild turbulence inhomogeneity. We esamine a slight modification of an isotropic field by considering a turbulent field with an initially uniform and isotropic kinetic energy distribution and where the macroscale is then slightly varied in two adjacent regions. Direct numerical simulations show that after a few initial eddy turnover times, the velocity moments, but also the moments of the longitudinal derivatives, become anisotropic. The skewness of the longitudinal derivative in the inhomogeneous direction can in fact become much larger than that of the other directions. Since the boundary conditions used are of an isotropic type, this behavior could be associated to long-range turbulent interaction over very different scales.*

Keywords: small scale, longitudinal derivatives, skewness, anisotropy.

In order to investigate the onset of small scale anisotropy from macroscale inhomogeneity, we consider the time decay of a turbulent flow with initially uniform turbulent kinetic energy, but where the integral scale has been slightly varied in two adjacent regions. The flow is studied by means of direct numerical simulations: Navier-Stokes equations are solved in a parallelepiped domain by means of a Fourier-Galerkin pseudo-spectral method with an explicit fourth order time integration. The initial conditions are obtained by matching two fields, obtained from simulations of homogeneous and isotropic turbulence, over a thin region. The computational domain contains two of such regions placed in a specular way, so that the periodic boundary conditions can be used in the direction of dishomogeneity, direction x, and in the two homogeneous normal directions, see figure 1 and [1, 2, 3].

The different macroscales cause different decay rates of the two turbulent regions [4, 5, 6, 7, 8] and this in turn generates a gradient of turbulent kinetic energy. In fact, the simulations show that the flows with a smaller integral scale decay faster and have higher decay exponents, which range from 1.1 up to 1.65.

*Dipartimento di Ingegneria Aeronautica e spaziale, Politecnico di Torino, Corso Duca degli Abruzzi 24, 10129 Torino, Italy.
E-mail: daniela.tordella@polito.it

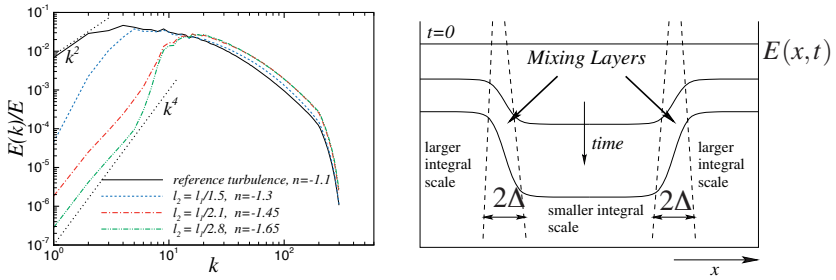

Figure 1: (a) Initial three dimensional energy spectra $E(k)$ of the isotropic turbulent flow matched in the simulations. Continuous line: region ($Re_\lambda = 150$) with the larger scale ℓ_1; other lines: isotropic matched fields with a smaller integral scale $\ell_2 < \ell_1$; n is the decay exponent found in the simulation. (b) Scheme of the flow, the direction x is the inhomogeneous direction [1, 2].

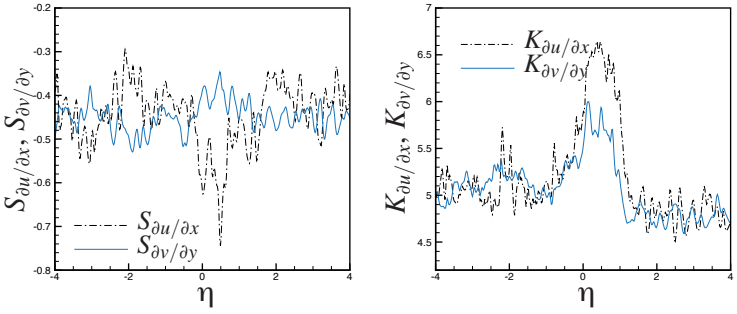

Figure 2: Spatial variation of the longitudinal derivative skewness and kurtosis across the mixing layer, run with $\ell_1/\ell_2 = 2.8$, $Re_\lambda = 150$, $t/\tau = 6.7$; x represents the inhomogeneous direction, $\eta = x/\Delta$ is the normalized coordinate, Δ is the mixing layer thickness, defined on the basis of the mean turbulent kinetic energy distribution, as in [1, 2].

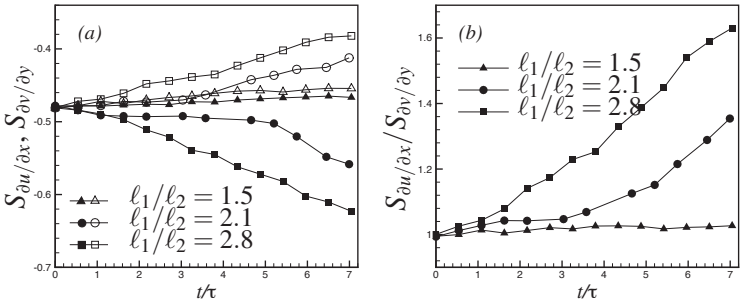

Figure 3: (a) Time evolution of the peak of the longitudinal derivative skewness inside the mixing, simulations at $Re_\lambda = 150$. Filled symbols: skewness of the longitudinal derivative along the inhomogeneous direction x, empty symbols: skewness of the longitudinal derivative along the homogeneous directions y. (b) the ratio between these longitudinal skewnesses (inhomogeneous over homogeneous normal directions) is here proposed as a measure of the small scale anisotropy.

The smaller the macroscale, the higher the exponent value. Due to the different decay, an energy gradient, always concurrent to the integral scale gradient, soon emerges. This gradient is maximum after about one initial eddy-turnover time $\tau = \ell/E^{1/2}$, then it gradually reduces, while the ratio of kinetic energy between the two regions increases [3]. The thickness of the induced kinetic energy layer increases while the two flows interact. The scale and energy mixing layer immediately becomes intermittent and the intermittency level is close to that found in shearless mixings with the imposed initial gradients discussed in [1, 2]. Thus, it is sufficient to introduce an inhomogeneity into the integral scale to induce an inhomogeneity in the kinetic energy during the decay [3].

This inhomogeneity makes the velocity statistics immediately depart from their isotropic values [3]. However, after a few initial eddy turnover times, the derivative moments also become anisotropic, see figure 2. For instance, it can be observed that, with a certain delay of about 6-7 time scales, the ratio between the thickness of the longitudinal derivative in the inhomogeneous direction and those in the normal directions (which are directions along which the field remains homogeneous) increases from 1 to 1.35, when the scale ratio is close to 2, and to 1.64, when the scale ratio is close to 3 (see figure 3). Thus, the large scale inhomogeneity spreads to the small scales. Since the boundary conditions used are conditions of periodicity in all directions, and thus of an isotropic kind, this behavior can be considered in terms of the long-range turbulent interaction among very different scales.

References

[1] TORDELLA, D. AND IOVIENO, M., *Numerical experiments on the intermediate asymptotics of the free shear turbulence mixing.*, J. Fluid Mech. **549** (2006), 441-454.

[2] TORDELLA, D., IOVIENO, M. AND BAILEY, P.R., *Sufficient condition for Gaussian departure in turbulence*, Phys. Rev. E, **77** (2008), 016309.

[3] TORDELLA, D. AND IOVIENO, M., *Step onset from an initial uniform distribution of turbulent kinetic energy*, 12th European Turbulence Conference, Marburg, September 7-10, 2009.

[4] BATCHELOR, G.K., *Energy decay and self-preserving correlation functions in isotropic turbulence,* Q. Appl. Maths **6**, 97-116 (1948).

[5] GEORGE, W.K., *The decay of homogeneous isotropic turbulence.*, Phys. Fluids **4**, 1492-1509 (1992).

[6] GEORGE, W.K., DAVIDSON,L., *Role of initial conditions in establishing asymptotic flow behavior.*, AIAA J. **42**, 438-446 (2004).

[7] LAVOIE, P., DJENIDI L., ANTONIA, R.A., *Effects of initial conditions in decaying turbulence generated by passive grids,* J.Fluid Mech. **585**, 395-420 (2007).

[8] VEERAVALLI, S., WARHAFT, Z., *The shearless turbulence mixing layer,* J. Fluid Mech. **207**, 191-229, (1989).

The Turbulence Problem(s): small-scale non-universality

JOHN CHRISTOS VASSILICOS*

Abstract. *The issues relating to universality and non-universality of small-scale turbulence are, by a wide margin, not just issues to do with varying degrees of anisotropy and with more or less small corrections to Kolmogorov's 1941 and 1962 theories. Fractal-generated turbulence makes the case.*

Keywords: small-scale turbulence, Kolmogorov.

Arguably, the overarching aim of turbulence research is reduced order modelling of turbulent flows. This may be in the form of one-point, two-point (or even multi-point) closures such as $k-\varepsilon$ and EDQNM, filtering closures such as LES or in terms of dynamical systems concepts such as state-space attractors. Arguably, too, such solution(s) to the turbulence problem(s) will not be fully satisfactory if they do not eventually impact industry and/or practical ocean/atmosphere prediction methods. This impact requirement is, however, only a necessary but not a sufficient condition as is clearly exemplied by the $k-\varepsilon$ model which has had, and continuous to have, an enormous impact on industry even though it is not a solution to the turbulence problem(s). The reason why it is not a solution is directly linked to the issue of universality in the context of turbulent flows.

Reduced order models such as $k-\varepsilon$ have been developed for and calibrated against a specific set of well-documented turbulent flows and can return useful results only when applied to conditions close to those particular turbulent flows. These models can fail by a wide margin when widely extrapolated beyond their comfort zone. They can therefore not be relied upon for predicting the behaviour of radically new turbulent flow concepts. Radically new flow concepts are urgently needed for the development of radically new industrial and environmental flow solutions which are to be part of the widespread technological step changes required to avert climate change projections and meet the dramatically evolving energy and environmental constraints. Industry cannot afford to remain within its well-documented comfort zones for long but may also not be able to step out of them significantly without some sort of universal reduced order modelling of turbulence which can be used to invent and investigate new turbulent flow concepts at will and at non-prohibitive cost.

The first question raised is whether universality classes of boundary conditions exist for which solutions of a given non-linear and non-local partial differential equation such as the incompressible Navier-Stokes equations have

*Imperial College London. E-mail: j.c.vassilicos@imperial.ac.uk

statistical properties which are independent of these boundary conditions, perhaps in some limit such as the high Reynolds number limit. Such properties may be statistical in terms of some averaging operation, for example over initial conditions or over time. The second question is whether sufficiently accurate and universal reduced order modelling is possible within these universality classes. Even if reduced order modelling is possible on a case-by-case basis, it may not be possible to develop a reduced order modelling approach which is the same for all the boundary conditions of the universality class. In fact, it might be expected that a negative answer to the first question implies a negative answer to the second. However, in the case where some kind of universal statistical properties of solutions of the incompressible Navier-Stokes equations do exist in some appropriate limit and within an appropriate universality class, the third question will then be to know how to use them to develop some kind of universal reduced order modelling approach to these equations.

These are very difficult questions which may sketch out, at best, broad goals for future generations of researchers. Indeed, it is instructive and also sobering to note that the textbook "Analysis of the Navier-Stokes equations" published in 1995 by C.R. Doering and J.D. Gibbon considers only periodic boundary conditions because of inherent technical difficulties with more realistic boundaries. Many turbulence researchers consider periodic boundary conditions but add a forcing term to the Navier-Stokes equations. It is therefore relevant to ask how such forcing approaches do or do not mimic the way that boundary conditions may drive turbulent flows in reality.

Which turbulence properties are our current best candidates for universality or, at least, for the definition of universal classes? The assumed independence of the turbulence kinetic energy dissipation rate on Reynolds number Re in the high Re limit is a cornerstone assumption on which Kolmogorov's phenomenology is built and on which one-point and two-point closures and LES rely, whether directly or indirectly. This cornerstone assumption is believed to hold universally (at least for weakly strained/sheared turbulent flows). It is also directly related to the universal tendency of turbulent flows to develop sharp velocity gradients, to the apparently universal geometrical statistics of these gradients, and to the apparently universal mix of vortex stretching and compression (described in some detail in the book "An informal introduction to turbulence" published in 2001 by A. Tsinober who introduced the expression "qualitative universality" to describe such ubiquitous qualitative properties). This universal assumption on turbulence dissipation and these apparently universal qualitative properties of turbulent velocity gradients are intimately linked to the mathematical search for finite-time singularities and/or near-singularities of the Navier-Stokes equations.

Evidence against universality has been reported since the 1970s, if not earlier, in works led by Roshko, Lykoudis, Wygnanski and George (see for example the 2008 Freeman Award Lecture of W.K. George: "Is there an asymptotic effect of initial and upstream conditions on turbulence?") and has often

been accounted for by the presence or absence of long-lived coherent structures. Coherent/persistent flow structure can actually appear at all scales and can be the carrier of long-range memory, thus implying long-range effects of boundary/inlet conditions. However, they can also be the reason for reduced order modelling as they introduce the possibilities for significant reductions in number of independent variables (see POD approaches introduced by Lumley). In these respects, it is noteworthy that the stagnation points of fluctuating velocities define persistence in the Eulerian frame (PRE 2005, 71, 015301) whereas low-acceleration regions define persistence in the Lagrangian frame (PRE 2009, 79, 015301), and both have a multiscale spatio-temporal structure. We refer to turbulence problem(s) for two reasons: (i) different universality classes or just boundary/inlet/upstream conditions may require different treatment and (ii) mixing/clustering of fluid/inertial particles in turbulent flows may require different reduced order approaches than the actual velocity field. Stagnation points and zero-acceleration points (different instances of critical points) are very useful in this last respect (see Phys Fluids 2009, 21, 015106; JFM 2006, 553, 143).

All these considerations suggest that kinetic energy dissipation, vortex stretching and compression, geometrical alignments, critical points and the universality or non-universality of each one of these properties are central to turbulent flows with an impact which ranges from fundamental mathematical aspects of the Navier Stokes equations all the way to engineering turbulence modelling and includes, of course, basic Kolmogorov phenomenology and scalings. Reduced order modelling may be too hard to attempt for the turbulent velocity field at the present and for some time to come, but research on the aforementioned properties are a clear prerequisite which can and must be carried out now. Given the current state of knowledge and technical possibilities, turbulence research can and must embark in a thorough experimental and computational investigation of the universality or non-universality of turbulence properties concerning dissipation, vortex stretching/compression, geometrical alignments and multiscale critical point spatio-temporal structure. Is it possible, for example, to tamper with these properties by systematic modications of a flow's boundary and/or upstream conditions?

To investigate such questions, new classes of turbulent flows have recently been proposed which allow for systematic and well-controlled changes in multiscale boundary and/or upstream conditions. These classes of flows fall under the general banner of "fractal-generated turbulence" or "multiscale-generated turbulence" and have such unusual turbulence properties (see Phys Fluids 2007, 19, 035103; 2007, 19, 101518; 2009, 21, 025108) that they may directly serve as new flow concepts for new indutrial flow solutions, for example conceptually new energy-efficient industrial mixers. Turbulence research does not need to come up with reduced order models valid over wide universality classes to impact industry if it can come up with new turbulent flow concepts which can directly offer possibilities for new industrial and/or environmental flow solu-

tions. These same turbulent flow concepts in conjunction with conventional flows such as turbulent jets and regular grid turbulence are also being used for fundamental research into what determines the dissipation rate of turbulent flows and even to demonstrate the possibility of renormalising the dissipation constant so as to make it universal at finite, not only asymptotically infinite, Reynolds numbers (see Phys Fluids 2008, 20, 014102; 2009, 21, 035104). The dissipation rate constant depends on small-scale intermittency, on dissipation range broadening and on the large-scale internal stagnation point structure which itself depends on boundary and/or upstream conditions. In the case of at least one class of fractal-generated homogeneous turbulence, small-scale intermittency does not increase with Reynolds number and the dissipation constant is inversely proportional to turbulence intensity even though the energy spectrum is broad and power-law shaped.

Small Scale Statistics of Turbulence and Inertial Particles in Clouds and in the Laboratory

HOLGER SIEBERT*, SERGIY GERASCHENKO**, KATRIN LEHMANN*,
LANCE R. COLLINS**, RAYMOND A. SHAW***, ZELLMAN WARHAFT**

Abstract. *Small scale turbulence is considered to play a major role in cloud dynamics. Hot-wire measurements in stratocumulus clouds are analyzed in terms of internal intermittency. Good agreement is found with well controlled laboratory experiments. Laboratory measurements of Lagrangian acceleration are then rescaled to cloud conditions, and demonstrate that local accelerations greater than g are expected.*

Keywords: cloud turbulence, inertial particles.

Most clouds are highly turbulent, with characteristic Reynolds numbers in the same range or higher than observed in the boundary layer or clear atmosphere, yet data on their turbulent structure has remained elusive due to the extreme difficulty of the measurements. Without knowing the details of the turbulence, the mechanisms of entrainment, mixing, transport, droplet size distribution and droplet growth in clouds cannot be understood. While laboratory experiments can aid in understanding the turbulence structure and its effect on droplet formation and growth, it is difficult to obtain the high Reynolds numbers but low dissipation rates observed in clouds. Here we describe recent measurements of fine scale turbulence statistics in clouds and relate them to recent laboratory work on inertial particles.

The instruments were part of the Airborne Cloud-Turbulence Observation System (ACTOS), suspended from a helicopter, and moving at a flight speed sufficiently large to be safely outside the rotor downwash [1]. A one-component hot-wire anemometer (CTA, Dantec) was installed on ACTOS with a platinum plated tungsten wire of diameter 5 μm and overall length 3 mm to measure turbulence fluctuations. An elaborate algorithim was used to remove spikes resulting from droplet impacts [2]. At Cornell acceleration statistics of inertial particles were studied by injecting water droplets into a large (1 m x 0.9 m x 20 m) open circuit wind tunnel. The effects of Reynolds, Stokes and Froude number variations were studied in a turbulent boundary layer formed over a flat plate above the tunnel floor. The particles were injected into the flow by means of sprays and humidifiers [3]. The acceleration statistics were determined by moving a high speed camera along the side of the wind tunnel at the flow speed [4].

*Leibniz-Institute for Tropospheric Research, E-mail: siebert@tropos.de
**Cornell University
***Michigan Technological University

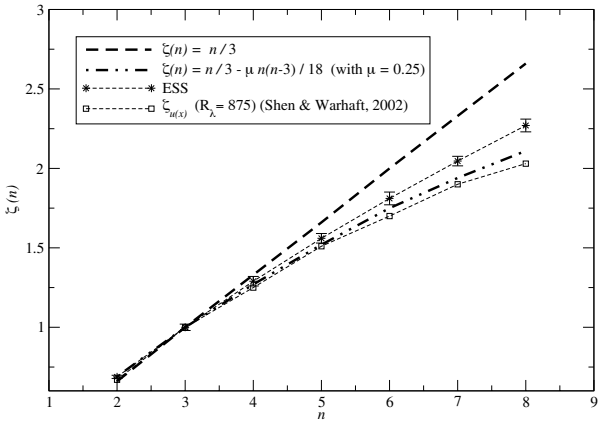

Figure 1: The scaling exponents $\zeta(n)$ of the structure functions in cloud derived by ESS. Theoretical values for K41 and for K62 with an intermittency factor of $\mu = 0.25$ are shown for reference, together with data derived from wind-tunnel experiments by [5].

The hot wire measurements were taken close to cloud top in a 200 m thick cloud layer ($R_\lambda \approx 5{,}000$) over a path of approximately 6 km. Our objective is to see how turbulence statistics in the cloud compare with well controlled laboratory measurements. In particular we are interested in the higher order structure functions, since they reflect small-scale intermittency. Figure 1 shows the scaling exponents of the longitudinal velocity structure function. The n-th order structure function $S^{(n)}(r)$ is defined as $S^{(n)}(r) \equiv \langle(\Delta u(r))^n\rangle_x$. A scaling behavior like $S^{(n)}(r) \sim r^{\zeta_n}$ with a scaling exponent $\zeta_n < n/3$ where n is the structure function order should be observed at higher orders. This anomalous scaling (classical Kolmogorov 1941 scaling predicts $\zeta_n = n/3$) reflects the internal intermittency [6]. The departure from the classic scaling in Figure 1 shows that the nature of the intermittency in the cloud is similar to that obtained in controlled laboratory measurements, which are also shown in the figure. Further analysis of the cloud data [2] determined that the intermittency factor , $\mu \approx 0.25$, in remarkable agreement with laboratory data.

The cloud results show that the fine scales turbulence statistics in a cloud are similar to those observed in the laboratory. In clouds we cannot yet measure the acceleration of the droplets, in particular their probability density function (pdf), and thus we do not know whether there are acceleration events that compete with the gravitational acceleration. But because the intermittency in clouds is similar to that observed in the laboratory, we may deduce from laboratory measurements of inertial particles, the nature of the accelerations in

clouds. We scale the laboratory pdf's in order to elucidate the relative importance of fluid and gravitational accelerations in the cloud.

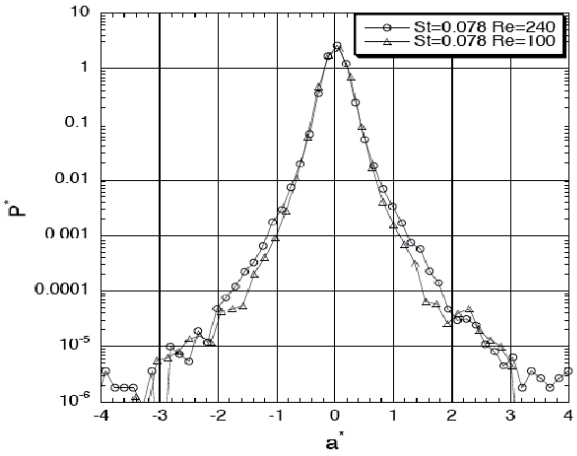

Figure 2: Pdf's of the Lagrangian acceleration of droplets in the Cornell wind tunnel flow [3]. The accelerations have been normalized by the gravitational acceleration and scaled to reflect atmospheric conditions. Stokes and Reynolds numbers (R_λ) are shown in the insert

Figure 2 shows the acceleration pdf's normalized by the acceleration due to gravity, in order to compare the magnitudes of the accelerations that the particles are experiencing with that of gravity. In order to make an approximate comparison with expected atmospheric acceleration statistics we have scaled the pdf with the acceleration ratio $(\mathrm{RMS}_{\mathrm{atmos}})/(\mathrm{RMS}_{\mathrm{lab}})$. The RMS acceleration measured in the laboratory is of the order $10\,\mathrm{m\,s^{-2}}$. In the atmosphere it is of order $1\,\mathrm{m\,s^{-2}}$ in a typical cumulus cloud. We note that the laboratory Stokes and Froude numbers are comparable to those observed in clouds.

The data of Figure 2 suggest the extreme accelerations caused by the turbulent flow field may be having a significant effect on the nature of the inertial particle motion, and may compete with the gravitational acceleration. In particular, roughly one drop in 1000 has an acceleration that is equal to or greater than g. At the much higher Reynolds number of clouds, we would expect the number of drops with accelerations greater than g to be much greater since the tails of the pdf widen with increasing Reynolds number [4].

We have shown that the turbulence fine scale statistics in a stratocumulus cloud are similar to classical laboratory results, exhibiting anomalous scaling for the higher order structure functions and an intermittency factor of approximately 0.25. Due to internal intermittency [7], laboratory experiments show

stretched exponential tails of the probability density functions (pdf's) of the inertial particle acceleration. Because we have demonstrated that the turbulence characteristics in the clouds are similar to those in the laboratory, we have scaled the laboratory pdf's to reflect atmospheric conditions. We have shown that the extreme accelerations that we expect to occur in clouds may compete with the gravitational acceleration. The implications of this for raindrop formation are significant. Traditional cloud models assume droplets fall relative to air at a constant speed, and therefore droplets of different size approach each other primarily as a result of differential gravitational settling. The analysis and experimental work presented here suggests that accelerations caused by the turbulence may compete with gravitational settling, thereby enhancing the rate of raindrop formation due to collision coalescence.

References

[1] SIEBERT, H., FRANKE, H., LEHMANN, K., MASER, R., SAW, E. W., SHAW, R. A., SCHELL, D., AND WENDISCH, M. Probing fine-scale dynamics and microphysics of clouds with helicopter-borne measurements. *Bull. Am. Meteor. Soc. 87* (2006), 1727 – 1738.

[2] SIEBERT, H., SHAW, R. A., AND WARHAFT, Z. Statistics of small-scale velocity fluctuations and internal intermittency in marine stratocumulus clouds. *J. Atmos. Sci.* (2009), in print.

[3] GERASHCHENKO, S., SHARP, N., NEUSCAMMAN, S., AND WARHAFT, Z. Lagrangian measurements of inertial particle accelerations in a turbulent boundary layer. *J. Fluid Mech. 617* (2008), 255 – 281.

[4] AYYALASOMAYAJULA, S., GYLFASON, A., COLLINS, L. R., BODENSCHATZ, E., AND WARHAFT, Z. Lagrangian measurements of inertial particle accelerations in grid generated wind tunnel turbulence. *Phys. Rev. Lett 97* (2006), 144507.

[5] SHEN, X., AND WARHAFT, Z. Longitudinal and transverse structure functions in sheared and unsheared wind-tunnel turbulence. *Phys. Fluids 14* (2002), 370 – 381.

[6] FRISCH, U. *Turbulence - The legacy of A. N. Kolmogorov*. Cambridge University Press, Cambridge, England, 296 pp., 1995.

[7] TOSCHI, F., AND BODENSCHATZ, E. Lagrangian properties of particles in turbulence. *Annu. Rev. Fluid Mech. 41* (2009), 375–404.

Pressure fluctuations and small-scale intermittency in direct numerical simulations at high Reynolds number

PUI-KUEN YEUNG*, DIEGO A. DONZIS**, KATEPALLI R. SREENIVASAN***

Abstract. *We explore statistical relationships among fluctuations of pressure, dissipation and enstrophy in forced isotropic turbulence using a large database generated from direct numerical simulations in the Taylor microscale Reynolds number range approximately 140–1000. Negative pressure fluctuations are related more to strong enstrophy than to strong dissipation, while both dissipation and enstrophy are generally less intense in regions of positive pressure fluctuations.*

Keywords: pressure, intermittency, turbulence simulations.

Pressure fluctuations are important for understanding turbulent flow structure, and, through the gradients, closely related to the acceleration which, in turn, is strongly influenced by the intensity of local straining and rotation. In this short paper we explore statistical relationships among fluctuations of pressure, dissipation and enstrophy in forced isotropic turbulence using a large database generated from direct numerical simulations (DNS). Some major parameters are summarized in Table 1 below. For the largest Reynolds number, we include 95% confidence intervals based on 20 instantaneous 4096^3 snapshots. Statistics for lower Reynolds numbers are derived from a larger number of large-eddy timescales which are more readily available.

In agreement with previous investigations, the data above suggest that as the Reynolds number increases: velocity gradients become more non-Gaussian, the statistics of dissipation and enstrophy (each of which possessing large variability) approach each other, while the statistics of pressure fluctuations, which are dominated by the large scales, show little change. Because of space limitations we focus below on data at the lowest and highest Reynolds number currently analyzed. The highest Reynolds number is sufficient to capture inertial range behavior in both the energy spectrum (Ishihara *etal.* [1]) and pressure spectrum (Tsuji & Ishihara [2]).

Figure 1 shows the probability density function (PDF) of pressure fluctuations, with negative fluctuations sampled up to relatively large amplitudes. Apart from possible statistical error, the effect of Reynolds number is mainly

*School of Aerospace Engineering, Georgia Institute of Technology, Atlanta, GA 30332, USA
**Department of Aerospace Engineering, Texas A&M University, College Station, TX 77843, USA
***International Centre for Theoretical Physics, Trieste, Italy.
E-mails: pk.yeung@ae.gatech.edu; donzis@tamu.edu; krs@ictp.it

N^3	256^3	512^3	1024^3	2048^3	4096^3	
R_λ	135	231	362	595	1003	
μ_3 of $\nabla_\parallel u$	-0.520	-0.540	-0.575	-0.602	-0.630	+/- 0.001
μ_4 of $\nabla_\parallel u$	5.65	6.58	8.11	9.30	10.85	+/- 0.07
$\langle\Omega^3\rangle/\langle\varepsilon^3\rangle$	4.81	4.14	4.21	3.59	2.41	+/- 0.31
$p'/\rho u'^2$	0.923	0.849	0.887	0.870	0.916	+/- 0.039
μ_3 of p	-1.09	-0.95	-1.02	-0.88	-0.87	+/- 0.06
μ_4 of p	6.53	5.90	6.04	5.27	5.32	+/- 0.27

Table 1.1: Selected DNS parameters, including number of grid points, Taylor-scale Reynolds number, and moments of longitudinal velocity gradient ($\nabla_\parallel u$), pressure fluctuation (p), dissipation (ε), and enstrophy (Ω). (Primes, μ_3 and μ_4 denote r.m.s, skewness and flatness respectively.)

to spread the negative tail to increasingly large amplitudes (in some cases beyond 24 standard deviations, though not shown here). The general behavior is consistent with a quasi-Gaussian PDF for positive amplitudes and nearly exponential tails on the negative side.

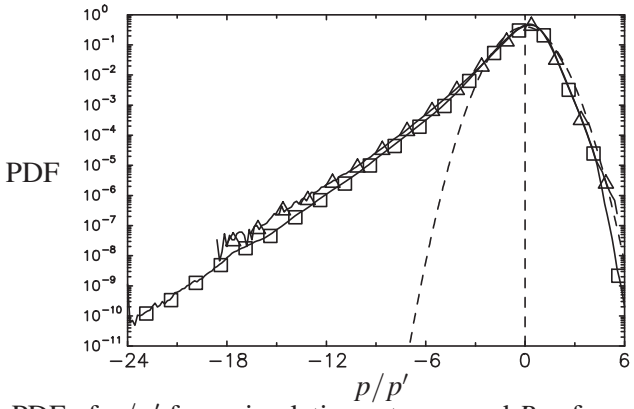

Figure 1: PDF of p/p' from simulations at averaged R_λ of approximately 140 ($\triangle$) and 1000 ($\square$). Dashed parabola is the standard Gaussian, for comparison.

Our main interest here is to understand the nature of local flow conditions that correspond to large, negative p/p'. Homogeneity in space requires that p and $\nabla^2 p$ be negatively correlated. Because of the Poisson equation $\nabla^2(p/\rho) = \frac{1}{2}(\Omega - \varepsilon/\nu)$ we may expect $p < 0$ (low pressure) to be associated with vorticity-dominated regions whereas $p > 0$ (high pressure) is associated with conditions of strong strain rate but little vorticity. In Figure 2 we examine conditional expectations of dissipation and enstrophy given the pressure, in the range $-15 \leq p/p' \leq 4$ which is not greatly affected by sampling difficul-

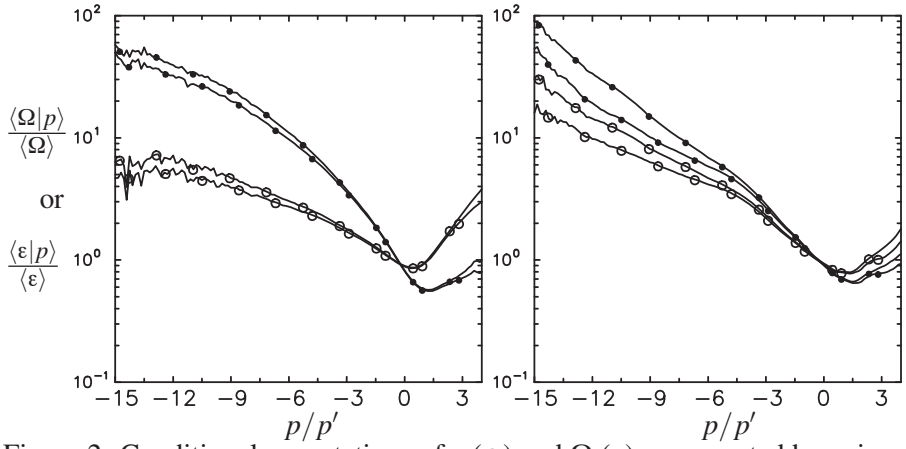

Figure 2: Conditional expectations of ε (○) and Ω (●), represented by pairs of lines bounded by 95% confidence intervals. Left: $R_\lambda \approx 140$; Right: $R_\lambda \approx 1000$.

ties that dominate the far tails. It is indeed seen that negative p usually leads to stronger enstrophy than dissipation, but in general both dissipation and enstrophy are higher in regions of negative p than positive p. As the Reynolds number increases, conditional dissipation is substantially higher but the effect on conditional enstrophy is apparently weaker and less well captured. The difference between dissipation and enstrophy thus becomes weaker, in agreement with recent work (Donzis *et al.* [3]) which showed the PDFs of dissipation and enstrophy become closer while characterized by widening tails of stretched-exponential form corresponding to extreme events in the flow.

This work is supported by the National Science Foundation (NSF), USA. The DNS database has been made possible through the deployment of massive computational resources at several leading-edge supercomputer sites (TACC, NICS, NCCS), and are available to other researchers on request.

References

[1] ISHIHARA, T., GOTOH, T. & KANEDA, Y. *Study of High Reynolds Number Isotropic Turbulence by Direct Numerical Simulation*, Annu. Rev. Fluid Mech. **41** (2009), 165-180.

[2] TSUJI, Y. & ISHIHARA, T. *Similarity scaling of pressure fluctuations in turbulence*, Phys. Rev. E **68** (2003), 026309.

[3] DONZIS, D.A., YEUNG, P.K. & SREENIVASAN, K.R. *Energy dissipation rate and enstrophy in isotropic turbulence: scaling and resolution effects in direct numerical simulations*, Phys. Fluids **20** (2008), 045108.

ABSTRACTS

Abstracts of other communications
arranged in the alphabetical order by first Author

Caustics and Intermittency in Turbulent Suspensions of Heavy Particles

Jeremie Bec
Université de Nice-Sophia Antipolis, CNRS, Observatoire de la Côte d'Azur, Laboratoire Cassiopée, Bd. de l'Observatoire, 06300 Nice, France.
Luca Biferale (A. Scagliarini)
Department of Physics and INFN, Università Tor Vergata, Via della Ricerca Scientifica 1, 00133 Roma, Italy.
Massimo Cencini
INFM-CNR, SMC Dept. of Physics, Università "La Sapienza", Piazzale A. Moro 2 and ISC-CNR, Via dei Taurini 19, 00185 Roma, Italy.
Alessandra S. Lanotte
ISAC-CNR, Via Fosso del Cavaliere 100, 00133 Roma, and INFN, Sezione di Lecce, 73100 Lecce, Italy.
Federico Toschi
J.M. Burgers Centre for Fluid Dynamics, Eindhoven University of Technology, 5600 MB Eindhoven, The Netherlands.

The statistics of velocity differences between very heavy inertial particles suspended in an incompressible turbulent flow is found to be extremely intermittent. When particles are separated by distances within the viscous subrange, the competition between quiet regular regions and multivalued caustics leads to a quasi bi-fractal behavior of the particle velocity structure functions, with high-order moments bringing the statistical signature of caustics. Contrastingly, for particles separated by inertial-range distances, the velocity-difference statistics is characterized in terms of a local Hölder exponent, which is a function of the scale-dependent particle Stokes number only. Results are supported by high-resolution direct numerical simulations. It is argued that these findings might have implications in the early stage of rain droplets formation in warm clouds.

Statistics of two-dimensional Navier-Stokes turbulence

Guido Boffetta
Università di Torino, Torino, Italy.

The existence of a double cascade in two-dimensional turbulences is one of the most interesting phenomena in fluid dynamics. The double cascade were predicted theoretically by Robert Kraichnan in a remarkable paper in 1967, as a consequence of the two conservation laws in the inviscid limit. After 40 years of experimental and numerical investigations, we are finally able to verify

quantitatively Kraichnan's predictions for the double cascade. This is not the end of the story, as two dimensional turbulence is still source of new research and discoveries, such as conformal invariance in the inverse cascade.

Velocity gradients statistics along particle trajectories in turbulent flows

Enrico Calzavarini
Lab. de Physique, École Normale Supérieure de Lyon, CNRS UMR5672, 46 Allée d'Italie, 69007 Lyon, France.

One of the most prominent features of turbulent flows are the strong variations in the energy dissipation field, a phenomenon called intermittency. In an attempt to describe quantitatively intermittent fluctuations in the inertial range of turbulence, Kolmogorov and Oboukhov in 1962 [1, 2] proposed a general relation linking velocity fluctuations, measured at a given spatial increment $\delta_r u = u(x+r,t) - u(x,t)$, with the statistical properties of the coarse grained energy dissipation, $\varepsilon r = r^{-3} \int_{\Lambda(r)} \varepsilon(x) d^3x$ averaged over a volume, $\Lambda(r)$, of typical linear size r : $\delta_r u \sim r^{1/3} \varepsilon_r^{1/3}$, where $\sim$ means "scales as". Equation (1) is known as the Refined Kolmogorov Similarity Hypothesis (RKSH) and it is considered to be one of the most remarkable relations between turbulent velocity fluctuations : many efforts has been devoted in the last decades to its validation. The RKSH relation bridges inertial-range properties with small-scale properties, supporting the existence of an energy cascade mechanism, statistically local in space. So far, a rather strong evidence supports the validity of the RKSH in the Eulerian frame (i.e. the laboratory frame). On the other hand, no investigation has been reported in the literature on the validity of RKSH in the Lagrangian frame. The main difficulty in studying RKSH in a moving reference frame stem from the necessity to make multipoint measurments along particle trajectories, in order to calculate the stress tensor. Also numerical experiments are very demanding, requiring refined computations of velocity differences along particle trajectories, something usually implemented by a heavy use of Fast Fourier Transform combined with off-grid interpolation. Here we report the first of such measurements using state-of-the-art Direct Numerical Simulations (DNS) with resolution up to 2048^3 collocation points, corresponding to $Re_\lambda = 400$. We present an investigation of the statistics of velocity gradients along lagrangian trajectories (i.e. fluid tracers trajectories) in a homogeneous and isotropic turbulent flow. The investigation is also extended to the trajectories of inertial particles : We show that the Lagrangian RKSH is well verified for time lags larger than the typical response time of the particle, τ_p . Implications of these findings for modeling of particle transport in many applied problems are also discussed.

Symmetry, geometry and anomalous scaling in turbulence

Antonio Celani
Institut Pasteur, Paris.

I will discuss the origins of the breakdown of scale-invariance in hydrodynamical turbulence in the light of recent theoretical advances in the study of passive scalar turbulence.

The Bottleneck Effects and the Kolmogorov Constant in Three-Dimensional Turbulence

Diego A. Donzis
Texas A&M University.
Katepalli R. Sreenivasan
ICTP Trieste, Italy.

A large database from direct numerical simulations (DNS) of isotropic turbulence, including recent simulations for box-sizes of up to 4096^3 and Taylor microscale Reynolds numbers of up to about 1000, is used to explore the bottleneck effect in three-dimensional energy spectrum and in second- order structure functions, and to determine the Kolmogorov constant, C_k. The difficulties in estimating C_k at any finite Reynolds number are examined. The data show that the bottleneck effect decreases with the Reynolds number. On this basis, an alternative to the usual procedure for determining C_k is suggested. The proposal does not depend on any particular choice of fitting ranges or power-law behaviors in the inertial range. Within the resolution of the numerical data, C_k thus determined is constant in the Reynolds number. A simple model including non-local transfers is proposed to reproduce the observed scaling. Implications of the findings are discussed.

Extended Self-Similarity works for Burgers and why

Urier Frisch, Sagar Chakraborty, Samriddhi Sankar Ray
CNRS, Lab. Cassiopée, Observatoire del la Côte Azur, 0634 Nice Cedex 4, France.

Extended Self-Similarity (ESS), discovered by Benzi et al in 1993, is the empirical observation that in fully developed turbulence when plotting structure functions of order p vs, say, the structure function of order three, rather than the traditional way where they are plotted vs the separation, then the range over which clean power-law scaling is observed can be substantially increased.

It was believed until recenty that ESS applies to 3D Navier-Stokes but not to the 1D Burgers model. Actually this was due to insufficiently high resolution used in the numerical simulations of the Burgers equation. When using 256K Fourier modes it is found that the ESS way of plotting structure functions gives increased scaling both at the infrared and at the ultraviolet ends of the inertial range.

We provide a full theoretical explanation of this phenomenon which has to do with subdominant corrections to the inertial-range scaling.

We conjecture that a similar explanation applies to the 3D Navier-Stokes case.

Decay exponent of large and small scales in isotropic turbulence

Michele Iovieno, Daniela Tordella
Dipartimento di Ingegneria Aeronautica e Spaziale, Politecnico di Torino, Italy.

The effect of the initial conditions on the decay of homogeneous and isotropic turbulence is still under debate, and there is a substantial body of experimental evidence which would seem to suggest that the initial conditions and the slope of the spectrum, at low wavenumbers, determine the value of the decay exponents. We consider it interesting to verify this hypothesis since, in such a way, it is possible to highlight the possible role played by the smaller scales. To do this, we consider the time decay of a turbulent flow with an initially uniform turbulent kinetic energy, but where the integral scale has been varied slightly in two adjacent regions. The simulations thus follow the temporal decay of two homogeneous and isotropic turbulent flows with uniform initial kinetic energy separated by a thin transition layer in a parallelepiped domain with periodic boundary conditions. The two fields are characterized by different shaped spectra in the low wavenumber range, obtained by applying a high-pass filter to the same homogeneous and isotropic turbulent field, which produces a k^{α} slope with α between 2 and 4. The simulations show that, for flows with an identical kinetic energy, those with smaller integral scales and thus comparatively richer in energy in the small scale range, decay faster and have higher decay exponents, which go from 1.1 up to 1.65 : the smaller the macroscale, the higher the exponent. This is in qualitative agreement with George (1992), who suggests that the energy decay exponent n is a function of the low wavenumber exponent α of the spectrum, $n = (\alpha + 1)/2$, and with the measurements in Antonia et al. (2002). We then focus on the decay rates of the large and the small scale ranges by dividing the spectrum into two parts : the left part – small wave numbers – initially contains 60% of the total energy, the right part – high wave numbers – the remaining 40%.

It can be observed that the decay rate of the full scale range is in-between that of the small scale range and that of the large scale range. It can be also seen that, at the lower values of the integral scale, in fields with the same initial

kinetic energy, the full range exponent comes closer to the arithmetic mean of the two other exponents. This indicates that the actual decay rate of the isotropic turbulence is not only affected by the large scale properties, but also by the small scale properties.

On the intermittency of scalars in atmospheric boundary layer

Irene Mazzitelli
Istituto di Scienze dell'Atmosfera e del Clima, CNR, via del Fosso del Cavaliere 100, 00133 Roma, Italy.

The objective of the present study is to characterize the statistics of large scalar fluctuations in turbulent boundary layer driven by atmospheric convection, and contrast the behaviours of active (temperature ϑ) and passive (humidity q) scalar fields. This issue is assessed by means of a Large Eddy Simulation model for the flow and for the scalar equations, with the subgrid-scale stresses estimated by dynamic modeling. Experimental and numerical studies indicate that, depending on the degree of instability and on surface moisture flux, an entrainment-moistening or drying boundary layer can develop, i.e. humidity, within the mixed layer, may increase or decrease in time. The current analysis is focused on the high order statistics of the humidity field as compared to the temperature field, in those two regimes. The large scalar fluctuations and intermittency are investigated by evaluating the probability density functions of the scalar (q, ϑ) increments $\delta_r q = q(x+r) - q(x)$ at inertial range separations, and by computing the cumulated probability of large fluctuations. In agreement with previous numerical findings in convective boundary layer, temperature statistics presents saturation of intermittency. It is now shown that also humidity statistics displays intermittency saturation, with different characteristics depending on the boundary layer regime. In entrainment-moistening boundary layer, humidity displays the same degree of intermittency as temperature, that is an active scalar. In entrainment-drying boundary layer, results obtained for the humidity field, with respect to intermittency saturation, are consistent with 3D experiments and 2D simulations of passive scalar in homogeneous and isotropic turbulence.

Turbulent dynamics in rapidly rotating Couette flows

Matthew S. Paoletti, Daniel S. Zimmermann, Santiago A. Triana and Daniel P. Lathrop
University of Maryland, College Park, MD 20742, USA.

We present experimental studies of the turbulent flow of water between independently rotating boundaries in two geometries : (1) spherical Couette and

(2) cylindrical Taylor-Couette, which are capable of both strong turbulence ($Re > 10^6$) and rapid rotation ($Ek < 10^{-7}$). The torque required to drive the inner boundary in both cases is precisely measured as a function of the two angular velocities 1 and 2. Of particular interest are three distinct regions of the ω_1 vs. ω_2 parameter space bounded by the inner and outer boundaries having equal : (i) angular velocities (solid-body rotation), (ii) azimuthal velocities and (iii) angular momenta (Rayleigh criterion) with the outer boundary stationary line ($\omega_2 = 0$) serving as the final bound. We supplement the global torque measurements with local wall shear stress measurements and ultrasound velocimetry. We observe distinct phenomena depending upon the particular region of parameter space. For $\omega_1 = \omega_2$, rather than observing solid-body rotation as expected, a spin-over mode is driven by precession produced by the rotation of the Earth. In regions of the parameter space dominated by global rotation we observe Coriolis-restored, linear inertial modes. Lastly, when $\omega_1 \approx 3\omega_2$ the spherical-Couette system intermittently transitions between two turbulent states characterized by disparate torque demands. We model the system as being composed of two interacting, turbulent boundary layers. There are several open questions that we work to answer : (1) Are there any conditions under which angular momentum will flow uphill ? (2) What quantity (angular velocity, azimuthal velocity, or angular momentum) is the system trying to "mix" ?

Topological properties of turbulence in thin films : direct numerical simulations with Ekman friction

Prasad Perlekar
Technische Universiteit Eindhoven, P.O. Box 51, 5600 MB Eindhoven, The Netherlands.

Rahul Pandit *Centre for Condensed Matter Theory, Department of Physics, Indian Institute of Science, Bangalore 560012, India.*

We present a detailed direct numerical simulation (DNS) of the two-dimensional Navier-Stokes equation with the incompressibility constraint and air-drag-induced Ekman friction ; our DNS has been designed to investigate the combined effects of walls and such a friction on turbulence in forced thin films. We concentrate on the forward-cascade regime and study the probability distribution function of the Weiss parameter, which distinguishes between regions with centers and saddles. Our results are is in quantitative agreement with experiments.

Dynamics of vortex filaments in turbulent flows and their impact on particle dispersion

Andrea Scagliarini, Luca Biferale
Università di Roma "Tor Vergata", Roma, Italy.
Federico Toschi
Eindhoven University of Technology, Eindhoven, The Netherlands.

We study, by means of state-of-the-art DNS, the dynamics of pointwise particles passively advected by a turbulent flow. We focus on the connection between preferential concentration of particles and the underlying topological Eulerian structures in general and with vortex filaments in particular. We characterize the latter by tracking particles lighter than the fluid, which tend to accumulate inside vortex filaments and there remaining trapped even for very long time. We study the temporal evolution of the momentum of inertia of bunches of particles. From the time lag during which this quantity remains under a certain threshold, we can estimate the vortex filaments life-times. The preferential concentration of heavy/light particles inside/outside vortex filaments has been also used to investigate the fluctuations of the autocorrelation time of vorticity along particle trajectories. The intense clustering of light particles, due to trapping phenomena inside vortex filaments, has a dramatic impact on their long term pair dispersion. This can be quantified in terms of the evolution of particle pairs distances PDFs and of the finite time Lyapunov exponents for particle trajectories.

Finite-sized particle dynamics in turbulent flows

Romain Volk, Enrico Calzavarini, Emmanuel Levêque, Jean-François Pinton
Laboratoire de Physique de l'Ecole Normale Supérieure de Lyon, 46 Allée d'Italie, 69007 Lyon, France.

Modern experimental techniques allow nowadays to resolve the dynamics of small material particles in highly turbulent flows. This has open a way for a precise comparison, found encouraging, between experimental data and lagrangian data computed from Direct Numerical Simulations of very small - computationally assumed to be pointwise - inertial particles. However, in many realistic experimental situations the size of the particles (its diameter D) is not small as compared the dissipative scale and the agreement between experimental and numerical data falls off. In this contribution, I will focus on the

dynamics of large neutrally buoyant particles with size $D/\eta \in [1,50]$ moving in highly turbulent flows with $R_\lambda \in [100,900]$. I will present a comparison between the lagrangian statistics for both experimental data obtained by Laser Doppler Velocimetry, and numerical data obtained by DNS with a modified equation of movement for the particles that takes into account the size of the particles trough volume and surface averages.

Lagrangian statistical theory of fully-developed hydrodynamic turbulence

Kirill Zybin, Valeria Sirota, Anton Ilyn, Alexander Gurevich
Russian Academy of Science, Moscow, Russia.

In Zybin et al.(2007) we proposed a new statistical theory of turbulence based on the Navier-Stokes equation. The inertial range of scales in incompressible liquid was considered. The idea of the model is that the main role in statistics belongs to the regions where vorticity is very high. We showed that these regions must take the form of vortex filaments, and derived the equation describing the vorticity evolution. It appeared that growth of vortex filament was caused by large-scale pressure pulsations. This large-scale term was used to introduce randomness in the Navier-Stokes equation, instead of adding usually external large-scale random forces.

Applying the theory we find the Lagrangian structure functions. For time much smaller than the correlation time, the structure functions are shown to obey scaling relations. The scaling exponents are calculated analytically without any fitting parameters. A new relation connecting the Lagrangian structure functions of different orders analogously to the extended self-similarity ansatz is found. All the results agree extremely well with the experimental data.

INDEXES

PAPER INDEX

AUTHOR INDEX

PRESENTER INDEX

Pubblicazione realizzata con il contributo del

Ministero per i Beni e le Attività Culturali

«Atti della Accademia delle Scienze di Torino. Classe di Scienze Fisiche, Matematiche e Naturali», Supplement 2009 − Vol. 142, 2008.

Anno di fondazione della rivista 1865

Direttore responsabile Luciano GALLINO

Autorizzazione del Tribunale di Torino n. 1995 del 7-03-1969

Iscrizione al R.O.C. n. 2037 del 30-06-2001

Finito di stampare nel mese di ottobre 2009

Stampato da

Tipografia Bodrato s.n.c. - Torino